NTNU – Trondheim
Norwegian University of
Science and Technology

The Mucin-Alginate Interplay

Investigating the Rheological Impact of
Alginates and Their Influence on Particle
Mobility

Camilla M Reehorst

Biotechnology (5 year)
Submission date: May 2014
Supervisor: Kurt Ingar Draget, IBT
Co-supervisor: Cathrine Taylor Nordgård, IBT

Norwegian University of Science and Technology
Department of Biotechnology

Abstract

Mucus is a hydrogel that covers epithelial cells and acts as an intermediary between the exterior and interior surfaces of the human body. It is complex and diverse, comprised of various compounds and serves as a selective barrier to pathogens, nutrients and administered substances. It is therefore important to circumvent or penetrate this barrier to increase drug bioavailability. The most important constituent of mucus is mucin glycoprotein that enables gel formation. Due to the molecular nature of mucin, it interacts with most substances including polyanionic biopolymers like alginates. Alginate molecules have been extensively used in pharmaceutical and medical industries as mediators because they possess suitable characteristics for a variety of biomedical applications. They have also been shown to influence mucus rheology, and could hold potential to alter other properties of mucus as well, such as particle mobility. In this thesis, the effect of different molecular weight alginates were investigated on the rheology of porcine gastric (PG) mucin, porcine small intestinal mucus (PSIM), porcine tracheobronchial mucus (PTBM) and bio-similar mucus. In addition, the effect of alginate on particle mobility in PG mucin samples were investigated using multiple particle tracking (MPT). The rheological effect of alginate G-block DP_n 12, DP_n 24, DP_n 33 and alginate LFR 5/60 on PG mucin was inconclusive as the sample suffered from pH and mechanical instabilities. Particle mobility was greatest for G-block DP_n 12 and G-block DP_n 33 treated PG mucin at long time scales. In addition, their mean-square displacement (MSD) trajectories were more narrowly distributed than the other samples, which correlates to a higher degree of uniform pore sizes. The rheological behaviour of bio-similar mucus and PSIM after treatment of G-block DP_n 12, G-block DP_n 33 and LFR 5/60 did not coincide, despite bio-similar mucus being a model system for porcine intestinal mucus (PIM). This was ascribed interactions between alginate and polyacrylate in the bio-similar mucus causing phase separation. Alginate G-block DP_n 12 weakened the PSIM and PTBM gel, while G-block DP_n 33 and LFR 5/60 had minor strengthening effects on PSIM.

Sammendrag

Mucus er en vannholdig gel som dekker epitelceller og fungerer som et skille mellom indre og ytre overflater i menneskekroppen. Slimlaget er en særdeles kompleks løsning bestående av mange forskjellige komponenter og virker som en selektiv barriere. Det beskytter kroppen mot potensielle patogener, men også administrerte medisiner. Det er derfor viktig å kartlegge måter å trenge gjennom mucus på slik at biotilgjengeligheten av medisiner øker. Den viktigste bestanddelen av mucus er mucin glykoproteiner som muliggjør gel dannelse. Den kjemiske diversiteten til muciner gjør at de kan vekselvirke med de fleste stoffer, inkludert polyanione biopolymerer slik som alginat. Alginatmolekyler har vært mye brukt i farmaindustrien på grunn av flere ønskelige karakteristikker som gjør dem interessante i medisinsk sammenheng. De har også blitt vist å påvirke reologien til mucus, som kan indikere et potensiale til å endre andre egenskaper ved mucus også, slik som partikkelmobilitet. I denne masteroppgaven har effekten av alginat med forskjellige kjedelengder blitt undersøkt på reologien til renset mucin fra grisemage (PG mucin), tynntarmslim fra gris (PSIM), tracheobronchialt slim fra gris (PTBM) og biolignende slim. I tillegg har effekten av alginat blitt undersøkt på partikkelmobilitet i PG mucin prøver ved hjelp av multiple particle tracking (MPT). Den reologiske effekten av G-blokk DP_n 12, DP_n 24, DP_n 33 og alginat LFR 5/60 på PG mucin var resultatløst på grunn av dårlig pH og mekanisk stabilitet. Partikkelmobilitet var høyest for G-blokk DP_n 12 og G-blokk DP_n 33 behandlet PG mucin ved lengre tidsskala. I tillegg hadde de smalere distribusjon av mean-square displacement (MSD) baner som tyder på at porestørrelsene i prøven ble mer uniform ved tilsats av alginat. Den reologiske adferden til biolignende slim og PSIM ved behandling av G-blokk DP_n 12, G-blokk DP_n 33 og LFR 5/60 var ulik, selv om det biolignende slimet er laget som et modellsystem for tarmslim. Dette tilskrives interaksjoner mellom alginat og polyakrylsyre i det biolignende slimet som fører til faseseparasjon. Alginat G-blokk DP_n 12 svekket gelstyrken til både PSIM og PTBM, mens G-blokk DP_n 33 og LFR 5/60 styrket gelen til PSIM noe.

Preface

Working with this master assignment has been a valuable experience. I have learned much during the last couple of years; not only subject-related, but also in relation to mindset. The work has mostly been joyful and engaging, but also sometimes incredibly challenging and frustrating. The most valuable experience for me has been the tickling of my natural born curiosity. I started this assignment with the naïve thought that the complexity of mucus mimics that of an integral equation; a little reading in a book and a calculator solves the problem. How wrong I have been. I think my perspective on things I used to take for granted has changed, and I can't wait to continue exploring the fascinations of this world further.

I would like to thank my supervisors, Professor Kurt I. Draget and Catherine T. Nordgård, for this unforgettable experience. Professor Kurt I. Draget has guided with a depth of knowledge I can only hope to achieve in the future. Catherine T. Nordgård has been an immense help with everything, and I sorely appreciate her support and encouragement. I could not have hoped for better supervisors. I would also like to thank Morten and Magnus for their help in the lab, Astrid Bjørkøy for instructions on the confocal microscope and the Matlab code, Olav A. Aarstad for HPAEC-PAD analysis, Wenche Strand for NMR analysis and Ann-Sissel T. Ulset for SEC-MALLS analysis. I must also mention Frida, who has worked in the same laboratory as me and shared my joys and failures. I believe that this past year would have been harder if not for Frida's motivational presence.

Lastly I would like to thank my family and my friends for never-ending support and comfort. A special thanks to Nicholas, who has stood by my side every step of the way. You have been my greatest moral support and motivation.

Camilla Marstrander Reehorst

Trondheim, 15.05.2014

Abbreviations

Abbreviation	Meaning
$\langle D_{eff} \rangle$	Ensemble effective diffusivity
δ	Phase angle
ΔG_{mix}	Difference in Gibbs free energy upon mixing two solutions
ΔH_{mix}	Difference in enthalpy upon mixing two solutions
ΔS_{mix}	Difference in entropy upon mixing two solutions
τ	Time scale
A_x	Area under the chromatographic peak
CF	Cystic fibrosis
CLSM	Confocal laser scanning microscope
COMPACT	Collaboration on the Optimization of Macromolecular Pharmaceutical Access to Cellular Targets
C_x	Molar concentration
D_{eff}	Effective diffusivity
DP_n	Degree of polymerization
F_G	Fraction of G-monads
F_M	Fraction of M-monads
F_{GG}	Fraction of G-diads
F_{GM}	Fraction of MG-diads
F_{MM}	Fraction of M-diads
F_{GGG}	Fraction of G-triads
F_{GGM}	Fraction of GGM-traids
F_{MGM}	Fraction of MGM-triads
G	α-L-guluronate
G'	Elastic/storage modulus
G''	Viscous/loss modulus
G*	Complex modulus
G12	Alginate G-block DP_n 12
G24	Alginate G-block DP_n 24
G33	Alginate G-block DP_n 33

HPAEC-PAD	High performance anion exchange chromatography with pulsed amperometric detection
HPLC	High performance liquid chromatography
LFR	Alginate LFR 5/60
M	β-D-mannuronate
M_n	Number-average molecular weight
MPT	Multiple particle tracking
MQ	Milli-Q
MSD	Mean-square displacement
M_w	Weight-average molecular weight
m_x	Concentration of oligomer
$\bar{N}_{G>1}$	Average number of G-units in a G-block containing more than one monomer
NMR	Nuclear magnetic resonance
PG	Porcine gastric
PIM	Porcine intestinal mucus
PSIM	Porcine small intestinal mucus
PT	Particle tracking
PTBM	Porcine tracheobronchial mucus
PTS	Proline-serine-threonine
Rf_x	Response factor
SEC-MALLS	Size exclusion chromatography coupled with multiangle laser light scattering
T	Temperature
TSP	Trimethylsilyl propionate
TTHA	Triethylenetetraminehexacetic acid
W_n	Weight average
X_n	Number average

Table of Contents

1 Introduction

1.1 Background and aim of thesis

The arrival of new drugs into the pharmaceutical market has seen a decline the past few decades compared to the amount of money invested into drug development, characterization and production (Scannell et al., 2012). This is in large part due to safety concerns that warrant extensive clinical trials. Phase 3 of the clinical trial is commonly equally expensive as the other two phases combined, and is usually harder for a drug to pass (Holmgren, 2014). Because of this, research into novel drugs is often based on small changes to existing ones, rather than major alterations that are less likely to pass unopposed through the clinical trials, and is therefore less likely to be funded privately or by the government (Charlton, 2006). Modification of drugs concerns changing the drug formulation or stability, increasing circulation times or decreasing elimination times, increasing bioavailability and absorption rates etc. The major challenge lies in crossing the bodily barriers such as the mucus barrier, made difficult by a high degree of complexity.

Most drugs are administered through the gastrointestinal tract (York, 2013), but drug delivery through the respiratory tract has recent years received some attention mainly due to the large surface area and low enzymatic activity (Patton and Byron, 2007). However, the pulmonary tract is in large part covered in mucus, which is a highly complex barrier. In order to improve drug delivery efficiency, it is important to understand the interactions and properties of the mucus barrier and assess ways of circumventing the restrictions related to absorption and diffusion. Alginates have shown potential to alter mucus flow properties (Taylor et al., 2005b, Taylor Nordgård and Draget, 2011) and has been shown to benefit medical and pharmaceutical sciences (Lee and Mooney, 2012). This is in large part due to the beneficial properties of alginate; they are biological substances, have low toxicity, are relatively inexpensive to manufacture, have high bioavailability and can gel in the presence of divalent cations.

This project is a part of a European collaboration unit called Collaboration on the Optimization of Macromolecular Pharmaceutical Access to Cellular Targets (COMPACT) consisting of both academic and industrial partners focusing on drug development and delivery.

The focus of this thesis is to investigate whether or not it is possible to control mucus barrier properties using alginate. The aim is to facilitate a drug delivery system in healthy human beings, meaning that the effect of alginate should be restricted to increased diffusivity across the mucus

barrier. The idea is therefore to examine various lengths of alginate molecules, in hopes of finding one that conforms to the criteria of increasing permeability without disrupting the normal mucus flow profile, which is important for protection from xenobiotic material. My hypothesis is as follows:

- There exist alginate molecules with specific molecular weights with the ability to affect the barrier properties of mucus without changing mucus flow profile.

Such alginates would have the potential to be used to improve muco-penetration of nanomedicines in situations where modification of mucus flow properties are undesirable.

1.2 Mucus

Mucus covers epithelial surfaces in the body exposed to the external environment and allows nutrient transport across the epithelial surface while protecting against potential pathogens (Cone, 2009). It therefore serves as a selective barrier, and is usually investigated according to its existence in three bodily systems – the pulmonary tract, the gastrointestinal tract and the genitourinary tract. The coherent mucus layer for each system has different gene products and molecular compositions (Khanvilkar et al., 2001). The most important subunits of mucus are the mucin glycoproteins, regardless of where the mucus is produced. These glycoproteins cross-link to form physically entangled gels (Lamont, 1992), and display a multitude of potential interaction sites which non-covalently bind to a variety of particles and pathogens (Woodley, 2001). Each mucus layer is therefore adapted to its environment making it an effective barrier.

1.2.1 Composition

Mucin. Mucin only comprises up to 5 % of mucus (Celli et al., 2005), but is considered the sole contributor to mucus gel formation (Sellers et al., 1988). The mucin subunits are large glycoprotein molecules with a molecular weight ranging from 0.5 up to 40 MDa (Lai et al., 2009, Cu and Saltzman, 2009, Thornton and Sheehan, 2004). They are classified as being either secreted or membrane bound, but only the secreted mucin have gelling capacity (Strous and Dekker, 1992). There are several differences between these two classes of mucin, but some common features are shared between them. Almost all consist of a protein backbone with tandem repeat regions full of proline, threonine and serine residues (PTS regions) constituting 20-55 % of amino acid composition (Van Klinken et al., 1995). The amounts and lengths of the tandem repeats vary between the different mucin gene products – some cell-associated mucin have PTS regions of over 5000 amino acids long (Cone, 2009). Bound through O-glycosylation linkages with the hydroxyl group of serine and threonine residues are carbohydrate molecules of 1-20 monomers. This results in a 'bottle brush' structure with negatively charged glycan side chains protruding from a protein core; the negative charges originate from sialic acid ($pK_a \approx 2.6$), sulfated galactoamines or glucosamines (both with $pK_a \approx 1$). Figure 1 shows a schematic of the structure and function of mucin molecules. The carbohydrate moieties account for up to 80 % of the weight of the mucin molecule (Kornfeld and Kornfeld, 1976) and are partly responsible for the expansion of the mucus gel. The high degree of glycosylation as well as repulsion between negative charges increases the persistence length of the mucin molecules 15-fold (Cone, 2009) to approximately 15 nm (Shogren et al., 1989). The increase in persistence length gives the mucin subunits a more rigid,

wormlike structure instead of full flexibility, which stabilises gel formation. N-acetylgalactosamine is the primary carbohydrate connected to the protein backbone, but others such as N-acetylglucosamine, fucose, galactose, sialic acid and mannose exist to a certain degree (Bansil and Turner, 2006).

The mucin subunits also contain 'naked' regions with little O-glycosylation (or N-glycosylation) and a high proportion (~10 %) of cysteine residues (Bansil and Turner, 2006). These regions have a hydrophobic characteristic and will assume a globular shape stabilised by intramolecular disulphide bond formation. The regions are usually found at the carboxyl and amino terminal of the protein backbone, but may sometimes be interspersed between the glycosylated PTS regions. Cysteine in the terminal areas are responsible for cross binding with other mucin subunits, thus forming a multimeric network (Sheehan et al., 2004). This polymerisation results in mucin aggregates with varying number of monomers and is essential for mucus function. Hence, mucus is polydisperse.

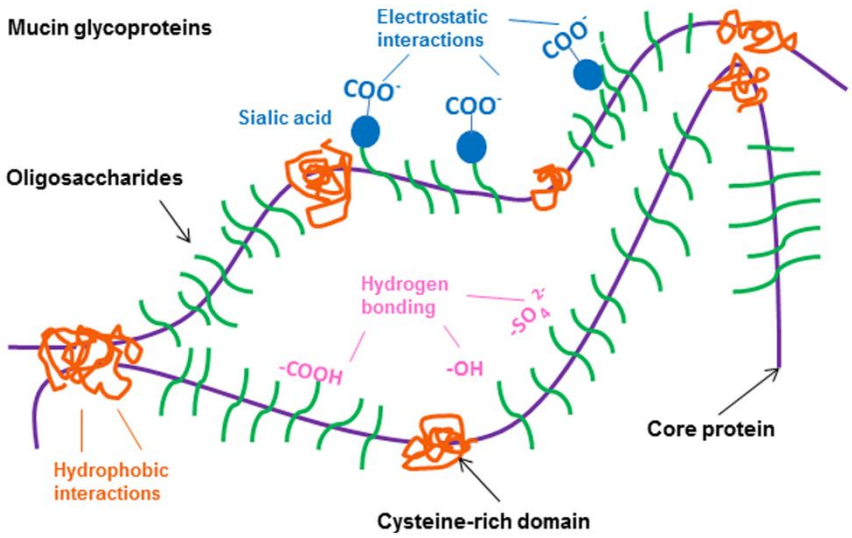

Figure 1. Schematic drawing of mucin glycoproteins. Included in the figure are mucin interaction sites (Yang et al., 2012).

Other components. Approximately 95 % of mucus is water (Khanvilkar et al., 2001). In addition, it contains various amounts of salts (mainly Na^+, K^+, Ca^{2+} and Cl^-), lipids and proteins. The lipids are mainly in the form of free fatty acids, phospholipids and cholesterol (Bansil and Turner, 2006) and their presence contributes to the selectivity of the mucus membrane and protects against radicals (Cone, 2005). They form a lipid layer at the outer edge (furthest away from the epithelial surface) of the mucus blanket and is stabilised by cationic surfactants that bind to the negatively charged mucin molecules. The reduced surface tension caused by the surface-active agents help barrier function by trapping or preventing hydrophobic particles or gases from penetrating the mucus layer (e.g. gastric acid in the

gastrointestinal tract) (Cone, 2009). The protein embedded in the mucus blanket have protective purposes and include immunoglobulins, lysozyme, defensins, hormones and trefoil factors (Cone, 2005).

Not only does the mucus layer contain various amounts of proprietary substances, it also harbors its own microbiota. The microbiota consists principally of bacteria and can be found lining the mucus layer in the oral cavity, the nasopharynx/oropharynx, the urogenital tract and the gastrointestinal canal (Cone, 2005). In the gastrointestinal tract alone almost 500 different species of bacteria has been found (Savage, 2005). Most of the microbes are commensals (most of the time) and do not harm the human vessel. In normal healthy individuals, the microbiota prevents the attachment and penetration of other pathogenic organisms, and help digest xenobiotic compounds humans are unable to do themselves (Savage, 2005).

1.2.2 Properties

Shear-thinning properties. Mucus displays non-Newtonian behaviour under the influence of shear stress (ratio of the applied force and the area of application). With increasing rate of shear stress, the viscosity of mucus decreases and mucus is therefore shear-thinning. The shear rate is the measure of slip velocity over separation distance and has the unit s^{-1}. Viscosity is a fluids resistance to flow and is defined as the shear stress divided by the shear rate (Smidsrød et al., 2008). Cone (Cone, 2005) gathered data from various sources to determine a relationship between viscosity and shear rate in most human mucus (not including ovulatory/cervical mucus). This relationship is given in equation 1. It is clearly depicted by the equation that mucus is a shear-thinning substance, since viscosity is inversely proportional with shear rate.

$$viscosity \propto (shear\ rate)^{-0.85} \quad (1)$$

Due to mucus shear-thinning properties it acts as an excellent lubricant. When mucus is being sheared, the adhesive contact and entanglements between the mucin molecules are pulled apart, which creates a slippage plane (Cone, 2009). The slippage plane is depicted in Figure 2. It has also been shown (Raviv et al., 2003) that negative charges on polymers in general enhance lubrication effects through electrostatic repulsion. In the case of mucus, such repulsion causes the mucin polymers to associate with each other less tightly, greatly reducing close contact between them. This helps reduce the viscosity of mucus under applied shear stress.

Shear thinning properties can either be permanent or temporary. Mucus generally exhibit temporary displacement, and is classified as thixotropic. This is an important property of pulmonary

mucus in relation to coughing (Houtmeyers et al., 1999). Instead of irreversibly breaking bonds, the mucin polymers pull apart when under applied deformation and will partially recoil to its original position (Crystal, 1997). It still maintains gel integrity, meaning that the deformation process is reversible. This separates mucus from most other polymeric gels (e.g. alginate gels) which cannot reform as a gel once the mechanism(s) holding it together ruptures. Mucus depends on both entanglements and interactions in order to gel. The degree of entanglements depends on mucin concentration, length of mucin subunits and the chemical nature of the mucin molecules (Thornton and Sheehan, 2004).

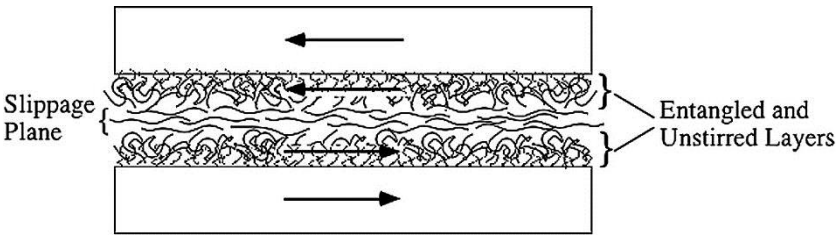

Figure 2. The ability of mucus to form a slippage plane, thus acting as an excellent lubricant. As shear rates increases, the adhesive and entangled mucin molecules pulls apart (Cone, 2009).

Viscoelasticity. Mucus exhibit both liquid and elastic properties and is therefore viscoelastic. Exposing mucus to small displacement forces (i.e. small strain) will cause the mucin polymers to stretch rather than pull apart or disentangle (Cone, 2009). After the applied force is released, the gel will return partly to its original state. This is the elastic characteristic of mucus, but it also displays a viscous character because it flows. The viscoelasticity of mucus is crucial for normal transport of mucus from the respiratory tract. Mucus is transported out of the lung by two main mechanisms – either by mucociliary actions or through coughing. Additionally, a third mechanism called alveolar clearance may also occur for insoluble particles deposited on the respiratory surface of the lung (Houtmeyers et al., 1999). Cough clearance of mucus is considered the secondary clearing mechanism, and usually happens only when mucociliary clearance is insufficient (King, 1998). The effectiveness of cough clearance is highly dependent on mucus viscosity, but is also affected by mucus spinnability and adhesivity (King et al., 1989). The primary clearance mechanism relies on the action of cilia found on ciliated epithelial cells throughout the respiratory tract. The cilia beat independently, although co-ordinated, on the mucus blanket with a shearing force that is small and sufficiently frequent to make the mucus layer respond through elastic forces rather than viscous ones (Cone, 2009). Cilia move in a whipping motion, and will temporarily connect with the mucus blanket only when they are fully extended. In their relaxed state,

when the cilia bend back to their original position, the movement takes place in the periciliary layer. This layer is a densely populated macromolecular solution that surrounds the cilia (Button et al., 2012). The thickness of the periciliary layer is normally slightly less than the length of the cilia, therefore allowing only the tips to touch the mucus blanket when fully extended (Houtmeyers et al., 1999). Because there is a unidirectional contact between the cilia and the mucus layer, the mucus layer is translocated in a cephalic direction – towards the glottis where mucus and trapped particles enter the gastrointestinal tract. Mucociliary clearance in the pulmonary tract depends on the ciliary beat frequency, viscosity and depth of the periciliary layer and the viscoelasticity of the mucus layer (Bates, 1989). Most important is the viscoelastic properties of mucus, and alteration of its normal condition may have adverse effects on human physiology. If mucus becomes too liquid, gravitational forces overcome the ciliary function and the mucus seeps back into the lungs instead of being shuttled through the glottis. This could potentially facilitate bacterial motility, increasing the chance of infections. Similarly, if mucus becomes too viscous, cilia beating becomes insufficient as transportation mechanism. This happens in various pulmonary diseases – e.g. cystic fibrosis. When the mucus becomes too elastic, most particle mobility ceases. This includes the movement of proprietary immunological substances, which decreases the defensive capacity towards bacterial and viral infections (Cone, 2009).

Barrier properties. The barrier functionality of mucus depends on three different characteristics (Sanders et al., 2009):

1. Mucus has dynamic properties. It is constantly secreted, which washes away most particles and bacteria that might cause harm to the parent organism. The rate of secretion depends on location and pathological conditions, but a healthy human adult secretes ~10 L every day, mostly in the gastrointestinal tract (Ensign et al., 2012). This means that pathogens or particles must constantly migrate or diffuse against an outward current in order to reach the epithelial surface for absorption.
2. Mucus is a steric barrier. The mucin polymeric network is entangled and will therefore physically obstruct particles trying to migrate through the mucus layer. The degree of steric hindrance (i.e. pore size) depends on the length of mucin subunits, the extent of cross binding and the chemistry of the mucin molecules which decides the adhesiveness between mucin subunits (Thornton and Sheehan, 2004). The mesh spacing is very heterogeneous in mucus, e.g. mucus lining porcine trachea had mesh sizes ranging from 80 to 1500 nm (Yang et al., 2012).

3. Mucus is interactive. Mucus does not normally covalently attach to particles, but rather exhibit a wide range of different weak interactions that non-specifically bind to foreign matter. It has been shown that the oligosaccharide side chains of mucin are responsible for electrostatic interactions and non-specific hydrogen bonding, while the protein backbone itself allows for hydrophobic interactions (Khanvilkar et al., 2001). In addition, mucus can also adhere to particles by van der Waals interactions (Woodley, 2001). Such low-affinity bonds have short half-lives, and are often broken due to thermal energy within milliseconds. However, mucus exhibit a plethora of these low-affinity bonds at any given time, which keep particles trapped (Cone, 2009). Because of the varied display of interaction modes, mucus is well adapted to trap particles that have hydrophobic or negatively/positively charged surfaces. Hydrophobic surfaces would attract the hydrophobic domain on the mucin protein backbone, and positively charged surfaces would attract the negatively charged glycan side-chains. Negatively charged surfaces are not likely to be attracted, but rather repelled by the glycan side-chains. Studies into virus and protein exterior structure have revealed that particles with a high degree of negative and positive charges, but without any net charge are more likely to partition into the mucus layer unopposed (Cone, 2009).

1.2.3 Porcine gastric mucin

Porcine gastric (PG) mucin has been shown to be structurally related to human gastric mucin (Turner et al., 1999), and is therefore a decent substitute for human gastric mucin because of higher availability and less ethical issues. In addition, MUC5AC is highly expressed in both the stomach and the tracheobronchial tract (Van Klinken et al., 1995), meaning that using porcine gastric mucin as a representation of pulmonary mucin is viable. PG mucin can be acquired in different ways; commercialised crude isolated PG mucin or natural purified PG mucin scraped off a pig stomach. One research group (Kočevar-Nared et al., 1997) showed that Sigma crude PG mucin did not have the same rheological properties as natural PG mucin, thus having limited usage as gastric mucin substitute. The crude PG mucin had very stable rheological values, but did not show the existence of an elastic, stable and strong gel network like the natural PG mucin. This effect has been ascribed to the extensive degradation of the mucin molecules. Degraded mucin appear as separate randomly coiled monomers in solution, instead of a polymeric network, and cannot form an elastic gel (Cone, 2009).

PG mucin undergoes a pH dependent sol-gel transition that is crucial for the mucus layer to remain protective in the gastrointestinal tract due to high variations in pH (Celli et al., 2005). Other factors also contribute to the gastric acid neutralisation such as the lipid layer and outward secretion

of mucus (Cone, 2005). Studies have shown (Cao et al., 1999, Celli et al., 2005) that the phase change threshold is around pH 4 with mucin concentrations greater than 10 mg/mL. The pH affects the conformation of mucin in solution, expanding the structure at lower pH, which increases the persistence length of PG mucin from 8 nm at pH 7 to 43 nm at pH 2 (Cao et al., 1999). Studies have shown that PG mucin aggregates at low pH (Bhaskar et al., 1991, Hong et al., 2005), and that the aggregation is most likely caused by hydrophobic and electrostatic interaction (Cao et al., 1999, Bhaskar et al., 1991, Bansil and Turner, 2006). Exactly how this happens is unclear, but it involves the hydrophobic parts of the protein backbone of mucin molecules (Lee et al., 2005). The pH threshold is around the pKa value of the negatively charged amino acids (aspartic acid and glutamic acid) interspersed on the protein backbone (Cao et al., 1999). The result from lowering pH will be a thicker, more solid dominant gel.

1.3 Alginates

Alginates are a family of linear copolymers, containing blocks of (1→4)-linked β-D-mannuronate (M) and α-L-guluronate (G) residues. The block composition and sequence as well as molecular weight vary according to the organism that produces the alginate (Smidsrød et al., 2008). By 2012 over 200 different alginate molecules were commercially available (Lee and Mooney, 2012). Commercial alginate is typically extracted from brown algae (*Phaeophyceae*), where it is used as structural support. Bacterial species of *Azotobacter* and *Pseudomonas* also produce them, and may provide more defined structural and physical properties than seaweed derived alginate (Lee and Mooney, 2012). Alginates are comprised of three different block structures – consecutive G residues known as G-blocks (e.g. GGGGG), consecutive M residues known as M-blocks (e.g. MMMMM) and alternating M and G residues known as MG-blocks (e.g. MGMGM). The structural characteristics of alginates are shown in Figure 3. G residues are known to be important for gel formation of alginates by binding most divalent cations (especially Ca^{2+}). This is because alginates are polyanions in solution with pH above the pKa (~ 4 pH) value of the carboxylic acid attached to the uronic acids (M and G). In addition, the G residues assume a $^{1}C_{4}$ confirmation and many G residues in succession form cavities, which selectively bind divalent cations. MG-blocks might also participate in gel establishment, but generally leads to weaker gels (Pawar and Edgar, 2012).

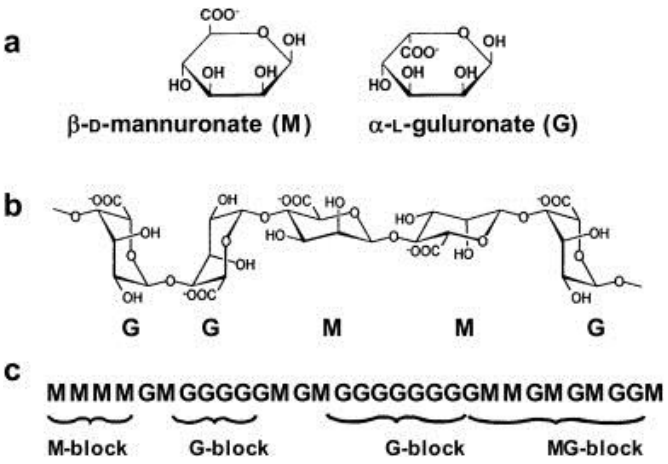

Figure 3. Structural characteristics of alginate: (a) structure of β-D-mannuronate and α-L-guluronate, (b) type of linkind and general confirmation and (c) block distribution (Draget and Taylor, 2011).

Alginates are susceptible to degradation at neutral (by reducing compounds), basic (β-elimination) and acidic (acid hydrolysis) pH. Acid hydrolysis is, however, the most common way of selectively degrading alginates. The mechanism behind the process was described by Timell in 1964 (Timell, 1964) and involves three steps; (1) the glycosidic oxygen between two consecutive monomers protonates; (2) the monomers split by hydrolysis of the glycosidic bond, forming a non-reducing end and a carbonium-oxonium ion; and (3) addition of water changes the carbonium-oxonium ion into a reducing end.

Alginates are interesting candidates in biomedical applications, and have been implemented in pharmaceutical and medical industries (Draget and Taylor, 2011). They are extensively used in wound healing, and have been investigated for use in delivery of drugs, tissue regeneration and *in vitro* cell culturing (Lee and Mooney, 2012). The main reason is their biocompatibility and low toxicity. Alginates are also readily modified to create derivatives with altered physical and chemical properties, which might for instance positively influence drug bioavailability. In addition, alginates gel under relatively mild conditions, which would minimize risk of denaturing the cargo. Alginates have been shown to influence mucus and mucin rheology (Taylor et al., 2005b, Taylor Nordgård and Draget, 2011); high molecular weight alginates increases the mechanical properties of PG mucin, while low molecular weight G-blocks decrease mechanical properties (Draget and Taylor, 2011). Generally, G-blocks are preferred in a drug delivery context since they have been shown to be non-immunogenic (Otterlei et al., 1991).

1.4 Rheology

Rheology is the study of deformation and flow of matter, and is a useful technique for biopolymer solution/gel characterization. The method is efficient at measuring the bulk flow profiles of viscoelastic materials (Deshpande et al., 2010). Most materials have viscoelastic behaviour, meaning they display a combination of both liquid and elastic properties. This is a time dependent behaviour, and even mountains behave as a liquid if studied at an appropriately long time-scale. This means that a material appears elastic either because the time perspective of the deformation process is very fast, or because the material itself has a long characteristic time (Barnes et al., 1989). In order to measure these properties the material in question is subjected to an applied rotational force (torque) quantified as the shear stress which causes the material to deform, called the shear strain. These measurements are stress controlled, but there also exist strain controlled experiments. In strain controlled experiments the strain is held constant, and the induced stress needed to maintain the constant strain is measured.

Usually, the material of interest is deposited between a cone and plate geometry; the plate is stationary and the cone has controllable movement. The cone and plate geometry is often preferred over the double plate geometry because the shear stress will be approximately uniform throughout the sample, provided the angle of the cone is small (Barnes et al., 1989). The cone is moved with a force (shear stress) that mechanically deforms the material. The resultant deformation of the sample – i.e. the degree of displacement from the initial position, is the shear strain and can be measured. The shear stress can be applied linearly or oscillatory. Oscillatory measurements are increasingly used because it allows for observation of material response as a function of frequency, and can therefore be used to describe viscoelastic behaviour over several time-scales (Deshpande et al., 2010). Because of this, it is an efficient mode for investigating the linear viscoelastic region of a material. The linear viscoelastic region of a material is where strain $\propto$ stress and storage modulus (G'), loss modulus (G'') and complex modulus (G*) are independent of strain. Most materials have one or two regions where this is true, but the width of the region(s) varies. In oscillatory experiments the measurements happen during a frequency determined oscillation. The applied stress and resultant strain vary cyclically with the frequency of oscillation, usually in a sinusoidal manner (Deshpande et al., 2010). The relationship between stress and strain during one cycle can be illustrated through sinus plot or Lissajous plot as seen in Figure 4.

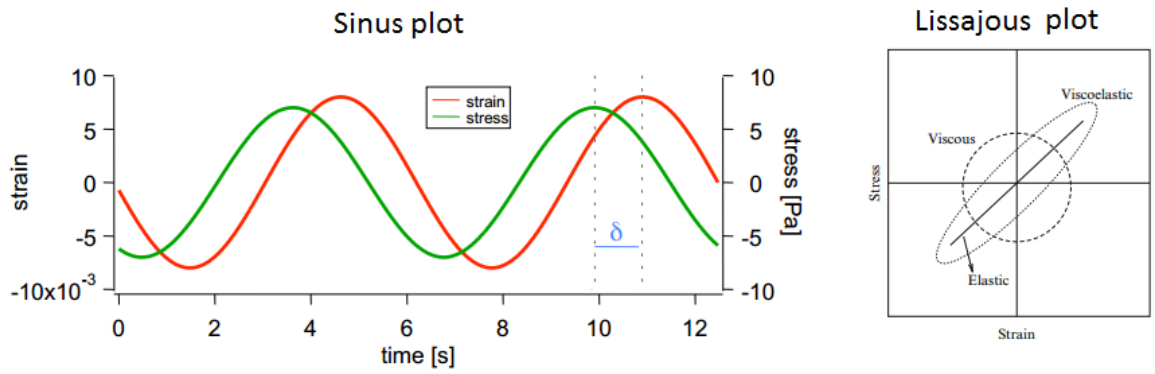

Figure 4. Sinus and Lissajous plot illustrating the relationship between stress and strain. The left image shows how the difference between stress and strain during sinusoidal oscillation relays the phase angle values, which is a measure of the amount of liquid and solid properties in a sample (Vader and Wyss). The right image shows how the Lissajous plot would look for elastic, viscous and viscoelastic materials (Deshpande et al., 2010)

For pure elastic materials both stress and strain are in phase with each other. In other words, the phase angle (δ) between the stress and strain curve equals zero. For pure liquid materials the strain is π/2 out of phase compared to the stress (δ = 90 °). Viscoelastic materials will have phase angle values somewhere between these extremities (0 ° < δ > 90 °). The viscoelastic character at any given frequency of oscillation is characterized by the storage/elastic modulus (G') and the loss/viscous modulus (G"), which quantify the solid-like and liquid-like contribution to the measured stress response respectively (Weitz et al., 2007). The storage modulus correlates with the in-phase behaviour, while the loss modulus correlates with the out-of-phase behaviour of the material, meaning that there is a close relationship between the phase angle (δ) and both moduli. This relationship is presented in Figure 5.

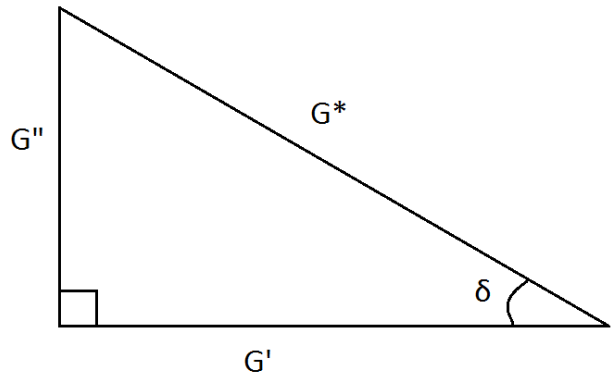

Figure 5. Relationship between the rheological parameters. G is the complex modulus, G' is the storage/elastic modulus, G" is the loss/viscous modulus and δ is the phase angle.*

1.5 Multiple particle tracking

Studying the mobility of particles is important in order to achieve a better understanding of the mechanisms that impede drug diffusion and movement from place of administration to target site. Drug delivery limitations often revolve around inefficient transport through complex bodily fluids such as mucus (Suh et al., 2005), which acts as a highly specialized selective barrier to most particles (Cone, 2009). It is therefore important to investigate how diffusion rates and particle mobility changes under external influence, e.g. by the addition of muco-adhesive agents. For this purpose, particle tracking is a useful technique. It is non-invasive and allows for real-time tracking of single particles on the micrometre scale using video microscopy (Suh et al., 2005). The technique can be extended to track multiple particles simultaneously, and is well equipped to identify particle speed, trajectories and mode of transport in various environments. Particle mobility depends on physical obstacles within the medium and on interactions between particle and medium (Figure 6) (Lieleg et al., 2010). It is therefore possible to determine structural characteristics (e.g. pore size and structural inhomogeneities) and interactive capabilities of the environment (Suh et al., 2005). Because multiple particle tracking (MPT) allows for tracking of many particles simultaneously, particle mobility can be studied at single particle level, subpopulation level or at bulk population level.

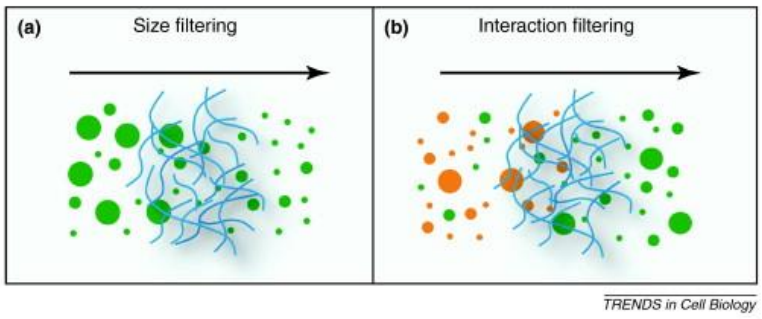

Figure 6. Two modes of particle impediment through mucus/mucin matrices. The hydrogel can impede mobility by physical obstruction, or through interactions (Lieleg and Ribbeck, 2011).

Fluorescent particles can be tracked by the MPT technique using an epifluorescence microscope (e.g. confocal microscope) by registering the spatiotemporal position (x-, y-, z- coordinates and time) of each particle. The particles are usually excited by a light beam originating from a mercury lamp, and the resulting emission spectra is detected and used to determine particle position. The spatiotemporal positions can be used to calculate trajectories for each tracked particle and can further be used to

calculate mean-square displacement (MSD) values. MSD values, which correlate to the distance travelled from the initial position over time (Selvaggi et al., 2010), can then be used to calculate effective diffusivities (D_{eff}) used to determine the mode of particle transport (Suh et al., 2005). The equation used to calculate two-dimensional MSD values and D_{eff} values are given in equation 2 and 3 respectively. Both values are calculated in regards to time scale (τ) which is determined by the speed of the camera capturing images in frames per second (fps). If the camera takes 30 frames every second, each frame will be approximately 33 milliseconds apart, corresponding to an initial time scale of 33 ms. The following time scale values would in this case be 66 ms, 99 ms, 132 ms and so on. The MSD values for a given particle, will be calculated per value of time scale.

$$MSD(\tau) = \langle \Delta x^2 + \Delta y^2 \rangle \quad (2)$$

$$D_{eff} = \frac{MSD(\tau)}{4\tau} \quad (3)$$

Δx^2 and Δy^2 is the difference in x- and y-coordinates respectively between two consecutive frames and τ is the time scale. This means that for a video of 200 frames, the first MSD value that would be calculated at the shortest time scale (33 ms) will be a mean of 199 separate displacement values. The second MSD value, calculated at the second shortest time scale (66 ms), will be a mean of 198 separate displacement values. This continues until the final MSD value is calculated at the longest time scale (6.567 s) with only one displacement value. The calculation principle of MSD values is graphically depicted in Figure 7. Due to the gradually decreasing amount of displacement values as the time scale increases, the contribution of the MSD values based on large time scales to particle movement is statistically inaccurate. This means that MSD values at the longest time scales often can be disregarded during data analysis (Saxton and Jacobson, 1997).

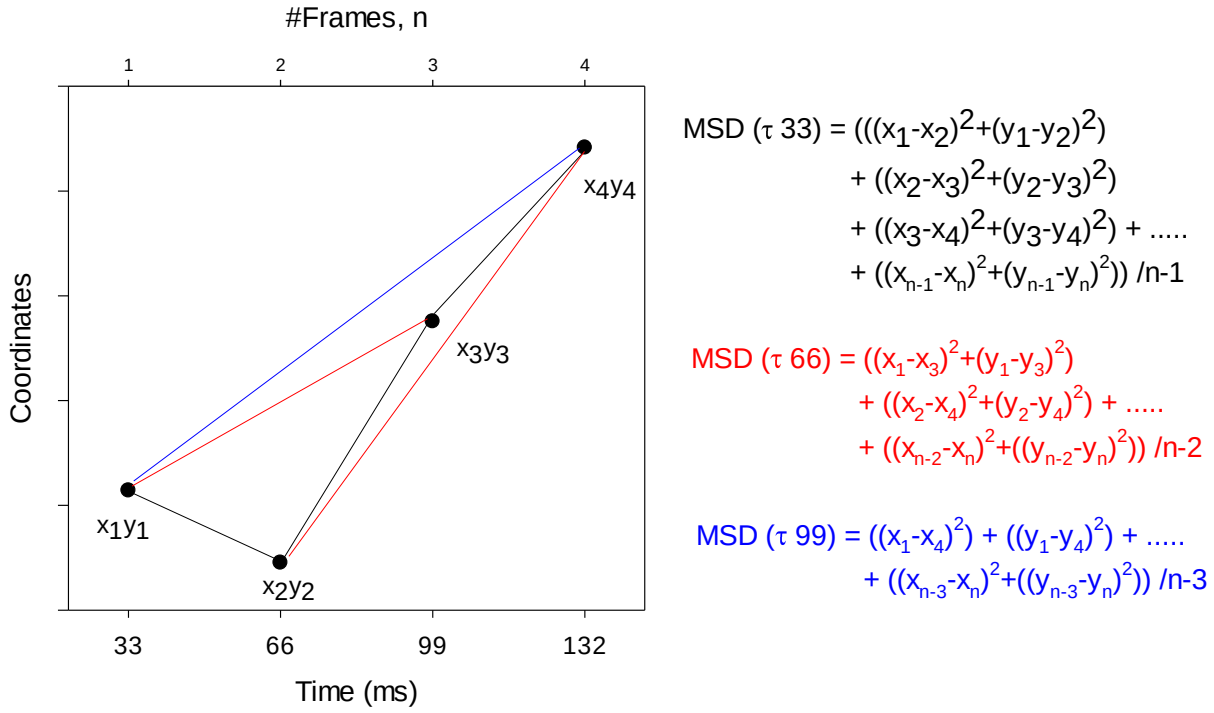

Figure 7. Graphical presentation on how to calculate mean-square displacement (MSD) values. The graph shows a particles trajectory (i.e. position at a given time), and the left shows how MSD values are calculated according to time scale (τ) that does not equal the time, but rather the time in between two frames. n here is the number of frames the particle in question was tracked.

The effective diffusivities (D_{eff}) plotted against time scale can be used to determine the type of movement of the particles embedded within the viscoelastic material. The relationship between the effective diffusivity trajectories and particle movement is shown in Figure 8. Particles are classified as either diffusive (i.e. they move according to Brownian motion), sub-diffusive or active. Diffusive particles can sometimes be immobile because of movement of the viscoelastic material itself that the particles are immersed in, or by physical/chemical entrapment (Suh et al., 2005). Another possibility is that the viscoelastic material contain compartments that restrict the particles to move meso- or macroscopically, but not microscopically.

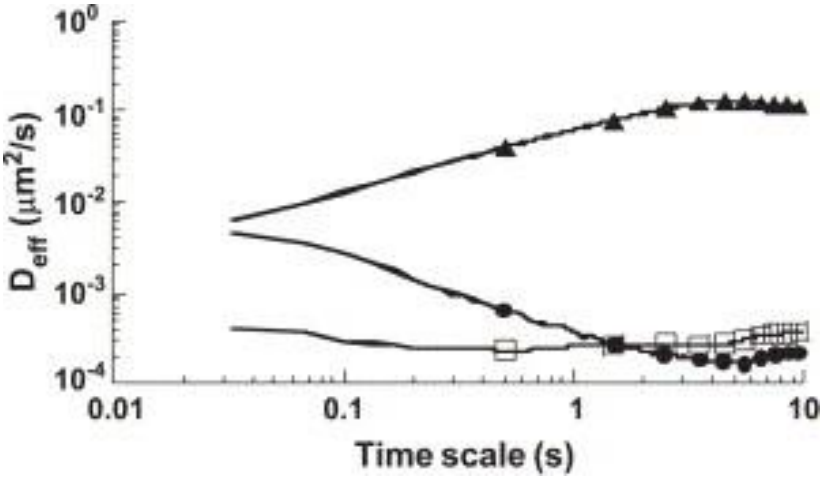

Figure 8. Particle mobility determined through Deff values; active (▲), sub-diffusive (●) and diffusive/immobile (□) (Suh et al., 2005).

1.6 Alginate characterization

The alginate samples that were used in this master thesis were characterized using standard analytical methods. The G-block samples were characterized both by nuclear magnetic resonance (NMR) spectroscopy and high performance anion exchange chromatography with pulsed amperometric detection (HPAEC-PAD), while the alginate LFR 5/60 was characterized by size exclusion chromatography coupled with multiangle laser light scattering (SEC-MALLS).

1.6.1 NMR

NMR is an extensively used analytical method for structure elucidation of compounds. One of the main advantages of NMR is that the method can be used to provide both qualitative and quantitative information. An atom with a magnetically active nucleus will, under an applied magnetic field, give rise to a signal corresponding to the location of that atom. The signal varies according to the positioning of that atom on the molecule, and what kind of physical and chemical environment it is in (Friebolin, 1991). The strength of the signal indicates the amount of atoms present giving rise to those signals, and the position of signals correlates with the molecular arrangement of the compound in question. In this thesis NMR was used to determine the fractions of monads, diads and triads of G and M (F_G, F_M, F_{GG}, F_{MM}, F_{GGG}, F_{GGM} etc.), the degree of polymerization (DP_n) and the average number of G-units in a G-block containing more than one monomer ($\overline{N}_{G>1}$) (Smidsrød et al., 2008).

1.6.2 Chromatography

Chromatography is a collection of various analytical methods, used primarily for the separation and quantification of compounds. The methods usually vary in regards to the separation technique and the mode of detection, but the principle is that a compound with a given characteristic (e.g. size, charge, hydrophilicity etc.) is retained differently within the chromatographic column than compounds that do not have identically matching characteristic (Poole, 2003). HPAEC-PAD separates compounds based on the amount of negative charges, and will therefore efficiently separate different chain lengths of alginate G-blocks (Ballance et al., 2005). The method can be used to determine the degree of polymerization. It also distinctly shows the distribution of various chain lengths, and is therefore a good supplement to the NMR technique. SEC-MALLS is a chromatographic method coupled with light scattering detection, and uses size as separation mechanism. The method is used to determine the molecular weight (M_w) of the compound in question, and can provide information on molecular weight distribution of the sample.

2 Materials and methods

2.1 Materials

2.1.1 Bio-similar mucus

The bio-similar mucus was made according to a protocol designed by COMPACT collaboration partners at the University of Copenhagen, Denmark. The bio-similar mucus was optimized to represent a rheologically comparable substitute for porcine intestinal mucus (PIM). Through having a similar rheological profile to PIM, the bio-similar mucus represents a synthetic model that can be used to assess *in vitro* mucosal influence on drug absorption (Bøgh et al., 2013). The bio-similar mucus was made using $CaCl_2$, $MgSO_4$, NaCl from Merck (Dermstadt, Germany), L-α-phosphatidylcholine, linoleic acid, cholesterol, HEPES, polysorbate tween 80, Sigma mucin type II: crude and bovine albumin from Sigma-Aldrich Co. (St. Louis, USA) and carbopol 934P (polyacrylic acid, batch#DS9068) from Recklitt & Colman Products (Kingston upon Hull, UK). Salts were mixed with HEPES to make one isotonic, and one non-isotonic HEPES buffer to be used in the lipid and polymeric solution respectively. The lipid (L-α-phosphatidylcholine, linoleic acid, cholesterol and polysorbate tween 80) and polymeric (Sigma mucin type II: crude and carbopol 934P) compounds were mixed separately to give homogeneous solutions before the lipid solution was aliquoted to the polymeric solution. Bovine albumin was then added before pH was adjusted to give physiological pH. The protocol that was used to make the bio-similar mucus is given in Appendix A. Several batches of bio-similar mucus were made during the course of the master thesis, with minor variations in lipid composition since the lipid samples were hard to handle, and only small amounts were needed. Adjusted pH was in all batches were in the range of 7.40 ± 0.01.

2.1.2 Native porcine small intestinal mucus and porcine tracheobronchial mucus

Intestines of freshly slaughtered pigs were given to Professor Kurt I. Draget from Gilde slaughterhouse in Steinkjer. The intestines were cut open using a scissor/scalpel and the mucus scraped using spoons. The collected mucus were separated by location (tracheobronchial tract, stomach, small intestine) into beakers and stored at -20 °C.

2.1.3 Porcine gastric mucin

Samples of PG mucin was purchased from Professor J. P. Pearson at Institute of Cell and Molecular Biosciences at the University of Newcastle upon Tyne, UK. The protocol for PG mucin collection and purification is given in Appendix B.

2.1.4 Alginate

Four different alginate samples has been used in this thesis – alginate G-block DP_n 12, alginate G-block DP_n 24, alginate G-block DP_n 33 and alginate LFR 5/60. Alginate LFR 5/60 are guluronate rich molecules (F_G = 0.69) and was purchased from Pronova Biopolymer (Drammen, Norway). The alginate was produced by *Laminaria hyperborea* (kelp) and should have a molecular weight (M_w) of around 30-50 kDa. However, because the sample was from 1993, it was characterized using SEC-MALLS, and found to have a weight- average molecular weight (M_w) of 32.6 kDa and molecular weight distribution of ~10-80 kDa. The SEC-MALLS chromatogram and data analysis is given in Appendix C. The SEC-MALLS characterization found that the alginate LFR 5/60 solution contained some aggregates, so the M_w was calculated by exponential fit of the data.

Alginate G-block DP_n 24 was purified by acid precipitation from alginate sample "G-blokk H3" and alginate G-block DP_n 33 was purified from alginate sample "G-blokk Batch#801-255-02", both a gift to Professor Kurt I. Draget from FMC Biopolymer AS (Drammen, Norway). Alginate DP_n 12 was produced by acid hydrolysis of "G-blokk H3". The protocol for purification of alginate G-block DP_n 24/33 and the production of alginate G-block DP_n 12 is given in Table 1 and Table 2 respectively.

Table 1. Protocol and actual procedure for purification by acid precipitation of "G-blokk H3" and "G-blokk Batch#301-255-02" to give alginate G-block DP_n 24 and G-block DP_n 33.

Step	Protocol	Actual/Comments
1	Mix 2 % alginate solution using MQ-water. Make sure the solution is homogenous by magnetic stirring before continuing.	30.05 g "G-blokk H3" in 1.5 L MQ-water and 9.99 g "G-blokk Batch#801-255-02" in 0.5 L MQ-water.
2	Adjust pH to 2.8.	"G-blokk H3" → 2.803 pH. "G-blokk Batch#301-255-02" → 2.803 pH.
3	Leave solution on stirrer for 2.5 hours. Cover solution with aluminium.	

4	Centrifuge at 1750 rpm for 15 minutes.	The DP_n 24 solution was divided in three beakers, to even out the weight.
5	Discard supernatant, and resuspend sample in 0.25 mL 0.01 M HCl.	Four 250 mL centrifuge bottles were used, and 0.01 M HCl was added to the rim of the bottles. Approximately 175 mL per bottle.
6	Centrifuge as in step 4.	Samples were centrifuged at 1500 rpm for 10 minutes, and further 7 minutes at 1700 rpm. The extra spin was due to improper sedimentation.
7	Discard supernatant, and resuspend sample in 0.25 mL MQ-water.	The centrifuge bottles were filled to the rim with MQ-water. Approximately 175 mL per bottle.
8	Centrifuge as in step 4.	Samples were centrifuged at 1700 rpm for 13 minutes, and further 6 minutes at 2000 rpm. The extra spin was due to improper sedimentation.
9	Discard supernatant, and resuspend sample in 0.25 mL MQ-water. Neutralize solution with 0.5 M NaOH to pH 7.	"G-blokk H3" was resuspended in 500 mL MQ-water, while "G-blokk Batch#301-255-02" was resuspended in 250 mL MQ-water. "G-blokk H3" → 7.021 pH. "G-blokk Batch#301-255-02" → 7.263 pH. Solutions were neutralized using 50 % NaOH and 4 M NaOH.
10	Filter solution.	Both solutions were filtered through a GF/A filter from Whatman PLC (Maidstone, UK) with help of a diaphragm vacuum pump.
11	Freeze dry sample.	The samples were frozen in liquid nitrogen (N_2) from Yara International ASA (Oslo, Norway) while spinning on an evaporator, and then placed on an Alpha 1-4 LD freeze-drying unit from Martin Christ Gefriertrocknungsanlagen GmbH (Osterode am Harz, Germany) freeze-drying unit operating at 0.1 mbar and -60 °C. The samples were left on the freeze-drying unit for two days.
12	Collect and store the sample dark at room temperature.	The powders were stored in separate zip-lock bags. Calculated yield of "G-blokk H3" was 47.69 %, and 56.86 % for "G-blokk Batch#301-255-02".

Table 2. Protocol and actual procedure for acid hydrolysis of newly purified "G-blokk H3" to give alginate G-block DP_n 12.

Step	Protocol	Actual/Comments
1	Mix 1 % alginate solution using MQ-water. Make sure the solution is homogenous by magnetic stirring before continuing.	10.01 g "G-blokk H3" in 1 L MQ-water.
2	Adjust pH to 3.6 using 1 M HCl. Important that nothing precipitates.	"G-blokk H3" → 3.601 pH. Mixture was turbid, but no precipitation could be seen.
3	Bubble through the solution with nitrogen gass for 2-3 minutes.	N_2 (g) from Yara International ASA (Oslo, Norway) was bubbled through the solution for 3 minutes at 0.5 bar.
4	Place solution in 95 °C water bath for exactly 12 hours.	
5	Cool solution quickly in an ice bath.	
6	When solution reaches room temperature, neutralize it with 0.5 M NaOH to pH 7.	"G-blokk H3" → 7.000 pH. Solution was neutralized to using 1 M NaOH.
7	Dialyse solution through a membrane with molecular weight cut-off (MCOW) 12-14,000 until conductivity is <2 µS.	Before dialysis, the sample was concentrated by evaporation (1 L → 0.41 L). Solution was transferred to two Spectra/Por Dialysis Membrane with MWCO 12-14,000 with 29 mm diameter from Spectrum® Laboratories Inc. (Rancho Dominguez, USA). The dialysis bags were left in distilled water the first two days, and MQ-water the third. The conductivity was checked before every water change (after changing to MQ-water). The conductivity jumped up and down, which probably meant that one of the hoses had a leak, and when the samples were removed the conductivity was 5.1 µS.
8	Filter solution.	Solution was filtered through a GF/A filter with help of a diaphragm vacuum pump. Before filtering the solution was concentrated by evaporation (2.1 L → 0.5 L).

9	Freeze dry sample.	The sample was frozen in N_2 (l) while spinning on an evaporator, and then freeze dried at 0.1 mbar and -60 °C. The samples were left on the freeze-drying unit for two days.
10	Collect and store the sample dark at room temperature.	The powder was stored in a zip-lock bag. Calculated yield of the alginate G-block DP_n 12 sample was 44.36 %.

All three alginate G-block samples were characterized using ^{1}H NMR and HPAEC-PAD. The NMR technique was used to determine the number-average degree of polymerization (DP_n), the monad, diad and triad fraction of guluronate and mannuronate (F_G, F_M, F_{GG}, F_{GM}, F_{MM}, F_{GGG} etc.) and the average number of G-units in a G-block containing more than one monomer ($\overline{N}_{G>1}$). The HPAEC-PAD technique was used to determine DP_n for all samples, and provides information on the molecular distribution of the samples. The data collected from both samples are given in

Table 3. The NMR and HPAEC-PAD methods disagreed on the average chain length of the alginate molecules (DP_n), but it was decided to follow the NMR results because the HPAEC-PAD method suffers from poor resolution at long polymer chain lengths of 30-35 (Ballance et al., 2005). This is probably the reason why the discrepancy between DP_n values from the two methods are larger alginate G-block DP_n 33 than for alginate G-block DP_n 12. Spectra and calculations for NMR and HPAEC-PAD values are given in Appendix D and E respectively. The reader may have noticed that the average number of G-units in a G-block containing more than one monomer ($\overline{N}_{G>1}$) is very high for the smallest sample, and show $\overline{N}_{G>1}$ values that are higher than the number average degree of polymerization (DP_n). This is because $\overline{N}_{G>1}$ is calculated under the assumption of infinitely long chain lengths, which in this case is not true. The values should be disregarded.

Table 3. Number-average degree of polymerization (DP_n), monad, diad and triad fraction of mannuronate and guluronate (F_G, F_M, F_{GG}, F_{GM}, F_{MM}, F_{GGG} etc.) and the average number of G-units in a G-block containing more than one monomer ($\overline{N}_{G>1}$) for alginate G-block DP_n 12, alginate G-block DP_n 24 and alginate G-block DP_n 33. Values are determined mostly from ^1H NMR, but HPAEC-PAD was also used to confirm the DP_n value.

	Alginate G-block DP_n 33	**Alginate G-block DP_n 24**	**Alginate G-block DP_n 12**
F_G total	0.868	0.899	0.932
F_G internal	0.837	0.857	0.850
F_G reducing ends	0.031	0.042	0.082
F_M	0.132	0.101	0.068
F_{GG} internal	0.784	0.818	0.826
$F_{GM} = F_{MG}$	0.052	0.040	0.024
F_{MM}	0.080	0.061	0.044
$F_{GGM} = F_{MGG}$	0.032	0.027	0.017
F_{MGM}	0.020	0.013	0.007
F_{GGG} internal	0.752	0.791	0.809
$\overline{N}_{G>1}$	26	33	55
DP_n NMR	33	24	12
DP_n HPAEC-PAD	36	24.5	12

2.2 Methods

2.2.1 Preparation of mucus-alginate solutions

The water used was of Milli-Q water (MQ-water) quality unless otherwise specified. Isotonic alginate solutions of G-block DP_n 12, G-block DP_n 33 and LFR 5/60 (70 mg/mL) was separately added to different samples of bio-similar mucus to a concentration of 4.7 mg/mL. Isotonic saline was used as control to eliminate dilution effects and ionic strength differences (143 µL saline in 2 g bio-similar mucus). The isotonic solutions were added, and the mixture properly stirred using a pipette tip three times with 10 minutes intervals. The same protocol was followed for addition of alginate/saline solutions to the native porcine mucus samples as to the bio-similar mucus sample. However, for the porcine tracheobronchial mucus (PTBM) sample, the concentration of alginate was 3.4 mg/mL, and no control was used due to low sample availability.

2.2.2 Preparation of porcine gastric mucin-alginate solutions

The water used here was of Milli-Q water quality unless otherwise specified. Two different lots of porcine gastric (PG) mucin have been used in this thesis. They are denoted as lot#1 and lot#2 respectively. Freeze-dried PG mucin was dissolved in MQ-water at a concentration of 42.84 mg/mL in order to achieve a final PG mucin concentration after addition of alginate/saline of 40 mg/mL. The solution was left in storage at 3 °C for 48 hours with gentle mechanical stirring. Vigorous stirring was avoided because this could lead to bubble formation in the mucin samples. After completed rehydration, the samples were aliquoted in 0.5 g amounts in Eppendorf tubes and stored at -20 °C. Several different concentrations, hydration media and hydration times were tried for the rehydration of PG mucin. MQ-water was chosen as medium because the resulting hydrated PG mucin solution was visually more viscous and gel-like than using 50 mM NaCl medium or 10 mM HEPES buffer medium. The optimal concentration was determined to be 40 mg/mL. Frequency sweeps of PG mucin at 50 mg/mL and 60 mg/mL concentrations resulted in a high degree of noise, most likely due to suspended PG mucin rather than dissolved PG mucin in the MQ-water medium. After several frequency sweeps of PG mucin with only hydration time as variable, it was found that hydration time influenced PG mucin rheology. All samples were therefore left to hydrate for precisely 48 hours.

Isotonic alginate solutions of G-block DP_n 12, G-block DP_n 24, G-block DP_n 33 and LFR 5/60 (70 mg/mL) was separately added to different Eppendorf tubes containing PG mucin to a final alginate concentration of 4.7 mg/mL. Isotonic saline was used as control to eliminate dilution effects and ionic strength differences (35.5 µL saline in 0.5 g PG mucin). The isotonic solutions were added, and the mixture properly stirred using a pipette tip three times with 10 minutes intervals.

2.2.3 Rheology

All rheological measurements were carried out using a Reologica StressTech rheometer (Lund, Sweden, Serial no. 212-0683) in oscillatory mode. The machine was fitted with a cone-and-plate geometry for small deformation measurements. The cone dimension varied according to material availability, ranging from C 25 1 ETC to C 50 1 ETC. The left number (25/50) relates to the cone diameter, while the right number corresponds to the angle of the cone from the centre outwards (1 = 1 °). All samples were rheologically tested through frequency sweeps. Frequency sweeps were mostly carried out after a strain sweep at 1 Hz frequency in order to determine parameters for the frequency sweep where stress $\propto$ strain and where the moduli are independent on strain (i.e. the linear

viscoelastic area). Every frequency sweep given in this thesis display values that are an average of three measurements. All mucus samples were rheologically tested at 20 °C, while PG mucin samples were tested at 10 °C. All samples applied on the rheometer was covered with low viscosity oil (Dow Corning ® 200/10cS fluid) from VWR International Ltd. (Butterworth, UK) to prevent evaporation. Rheologica software RheoExplorer version 5.0.40.38 was used for instrument control and data analysis.

2.2.4 Particle tracking

Samples for particle tracking were prepared by first measuring out 0.2 g of PG mucin (42.84 mg/mL) into chambers of Lab-Tek ® Chambered #1.0 Borosilicate Coverglass system from Thermo Fisher Scientific Inc. (NY, USA. Lot#1065778 2711). Fluospheres ® Carboxylate-modified microspheres (0.2 µm, yellow-green fluorescent (505/515), 2 % solids) from Invitrogen (Oregon, USA) were mixed with MQ-water, isotonic saline or alginate solutions of G-block DP_n 12, G-block DP_n 24, G-block DP_n 33 and LFR 5/60 respectively at a particle concentration of 0.038 %. This nanoparticle-MQ-water/saline/alginate solution was pipetted into the mucin filled chambers to a final microsphere concentration of 0.0025 %, a final alginate concentration of 4.7 mg/mL and a final PG mucin concentration 40 mg/mL. Each sample was stirred with the pipette tip after addition of particle solution and left overnight in storage at 3 °C. The following day the particles were tracked on a confocal laser scanning microscope (CLSM) Leica SP5 from Leica microsystems (Mannheim, Germany). The parameters the particles were tracked with are given in Appendix F. The microscope image-series were analysed using ImageJ and Matlab. The procedure for image analysis (ImageJ) implements the feature point detection and tracking algorithm described by Sbazarini and Koumoutsakos (Sbalzarini and Koumoutsakos, 2005) and is given in Appendix G, and the Matlab program was developed by Astrid Bjørkøy at the department of physics (NTNU) and is given in Appendix H.

2.2.5 NMR

Alginate G-block DP_n 12, G-block DP_n 24 and G-block DP_n 33 was mixed with 600 µL 99.9 % D_2O from Chiron AS (Trondheim, Norway) to a concentration of 0.01 mg/µL in separate NMR-tubes (178 x x4.95 mm) from Duran® group (Mainz, Germany). To each tube was added 5 µL trimethylsilyl propionate (TSP, 1 % solution in D_2O) from Aldrich (Milwaukee, USA) and 20 µL triethylenetetraminehexacetic acid (TTHA, 0.3 M solution in D_2O) from Sigma (St. Louis, USA). TSP was used as a NMR reference (Grasdalen et al., 1979) and TTHA was added in order to bind Ca^{2+} residues (Gaszner et al., 2001) that might otherwise influence the NMR data by interacting with the alginate molecules (Grasdalen et al., 1979).

The experiments were carried out on a BRUKER Avance DPX 300 equipped with a 5 mm QNP probe. The NMR data was processed and analysed with TopSpin 3.0 software.

2.2.6 HPAEC-PAD

For the quantification of oligomers of alginate high-performance anion-exchange chromatography with pulsed amperometric detection (HPAEC-PAD) was used (Ballance et al., 2005). Alginate G-block DP_n 12, G-block DP_n 24 and G-block DP_n 33 was mixed with MQ-water to a concentration of 2 mg/mL in separate beakers. No internal standard was used since start concentration of alginate G-block was already known. However, an external standard was used in order to make a response curve to determine molecular weight distribution within each sample (alginate G-block DP_n 5.3, produced at NTNU). The measurements were carried out on a high performance liquid chromatography (HPLC) setup with AS-50 auto sampler, ED-40 electrochemical detector and GP-50 gradient pump from Dionex Co. (Sunnyvale, USA). Carbonate free NaOH diluted to 0.1 M from a 50 % (w/v) stock solution was used as mobile phase and 1 M analytical grade sodium acetate (NaAc) from Merck (Dermstadt, Germany) in 0.1 M NaOH as eluent. An AG4A pre column and an IonPac 4x250 AS4A main column was used and linear gradients of NaAc were produced by increasing the concentration of eluent from 0 to 87.5 % over 90 minutes. Elution velocity was 1 mL/min and the pressure showed 650-750 psi. Chromeleon 6.7 software was used for instrument control and data analysis.

2.2.7 SEC-MALLS

The alginate LFR 5/60 sample was mixed with MQ-water to a concentration of 10 mg/mL. The measurements were carried out on a LC-10AD pump and a SCL-10A VP auto injector from Shimadzu Co. (Kyoto, Japan), a Dawn Heleos II LS-detector and a Optilab T-rEx RI-detector from Wyatt Technology Co. (Santa Barbera, USA) and a TSK G-4000 + 3000PWXL column from Toso Haas (Tosoh Bioscience LLC, King of Prussia, USA). The SEC-MALLS data was processed and analysed with Astra 6.0 software.

3 Results and discussion

3.1 The effect of alginate on bio-similar mucus

The bio-similar mucus developed by COMPACT collaboration partners at the University of Copenhagen, Denmark is meant to mimic the rheological properties of porcine intestinal mucus (PIM). It is meant to enable viable drug absorption testing *in vitro* without the need for native PIM (Bøgh et al., 2013). Because the bio-similar mucus consists primarily of commercialized mucin it is not limited to intestine availability. In order to determine how well the bio-similar mucus mimics PIM in the presence of other polymers, the effect of three alginate molecules (alginate G-block DP_n 12, alginate G-block DP_n 33 and alginate LFR 5/60) was investigated on bio-similar mucus and porcine small intestinal mucus (PSIM). Isotonic alginate solutions (70 mg/mL) were mixed with bio-similar mucus to a final concentration of 4.7 mg/mL. The mixture of bio-similar mucus and alginate was properly stirred three times with 10 minutes intervals, before being applied on the rheometer. Isotonic saline was used as control to eliminate changes in ionic strength from adding alginate solution, and to account for any unwanted effects due to dilution.

Bio-similar mucus treated with alginate G-block DP_n 12 (G12), alginate G-block DP_n 33 (G33) and alginate LFR 5/60 (LFR) respectively was rheologically tested through a strain and a frequency sweep. Strain sweeps were done initially to determine the position and range of the linear viscoelastic area(s) where stress and strain are directly proportional and the moduli values are independent of strain (Barnes et al., 1989). Stress and strain values determined from strain sweeps were used as parameters in the oscillatory frequency sweeps. Oscillatory frequency sweeps show the dynamic flow behaviour of mucus at different time scales.

First, the bio-similar mucus was treated with alginate G-block DP_n 12, and the frequency sweep of the treated sample is compared with a frequency sweep of the control sample in Figure 9. Both frequency sweeps were performed on the same day with both samples of bio-similar mucus originating from the same batch. Both samples show expected mucus behaviour – the bio-similar mucus display viscoelastic properties with both solid-like and liquid-like behaviour (Weitz et al., 2007). As the frequency increases, so does both the elastic modulus (G') and the phase angle (δ) values. The elastic modulus increases because the bio-similar mucus is an entangled system. At low frequencies, entangled polymers have enough time to glide apart and reorganize. At high frequencies, the entanglements stretch rather than pull apart causing an increase in elasticity (Sellers et al., 1988). An

increase in phase angle signifies that the bio-similar mucus gel weakens. This can be explained by a larger absolute increase in viscous modulus (G'') values compared to the elastic modulus at higher frequency. This means that the system essentially loses energy, despite the increase in elastic modulus. As frequency increases, the amount of force (stress) needed to uphold the constant strain increases. Increased force entails increased thermal energy inflicted onto the sample. Since the phase angle increases, more of this energy is lost than stored within the sample.

As Figure 9 shows, the frequency sweeps of the G12 treated sample and the control sample seem nearly identical. The small discrepancy towards the end in the elastic modulus values may simply arise from individual differences between the samples. Even though the samples originated from the same batch of bio-similar mucus, there could still have been differences in mixing or application on the rheometer. Literature has established that low molecular weight alginate G-blocks (DP_n 10 and DP_n 20) weaken *ex vivo* cystic fibrosis (CF) sputum and PG mucin (Draget and Taylor, 2011, Draget, 2011, Taylor et al., 2007, Taylor Nordgård and Draget, 2011). The effect of G12 on bio-similar mucus is therefore surprising. This shows that the bio-similar mucus does not interact with alginate G-block DP_n 12 in the same manner as native mucus or purified mucin.

In order to be certain that the results portrayed in Figure 9 were accurate, two more replicates of the bio-similar mucus treated with G12 was tested. The frequency sweeps of the replicates are given in Appendix I, and they show that Figure 9 is representative for G12 treated bio-similar mucus. One of the replicates did show a slight deviation in elastic modulus values compared to the control sample, but the phase angle values remain identical. Since the phase angle corresponds to the ratio of elastic and viscous modulus, it means that even though the values of G' are lower in the treated sample, the relationship between the moduli are identical. The deviation in elastic modulus is therefore deemed not to be significant.

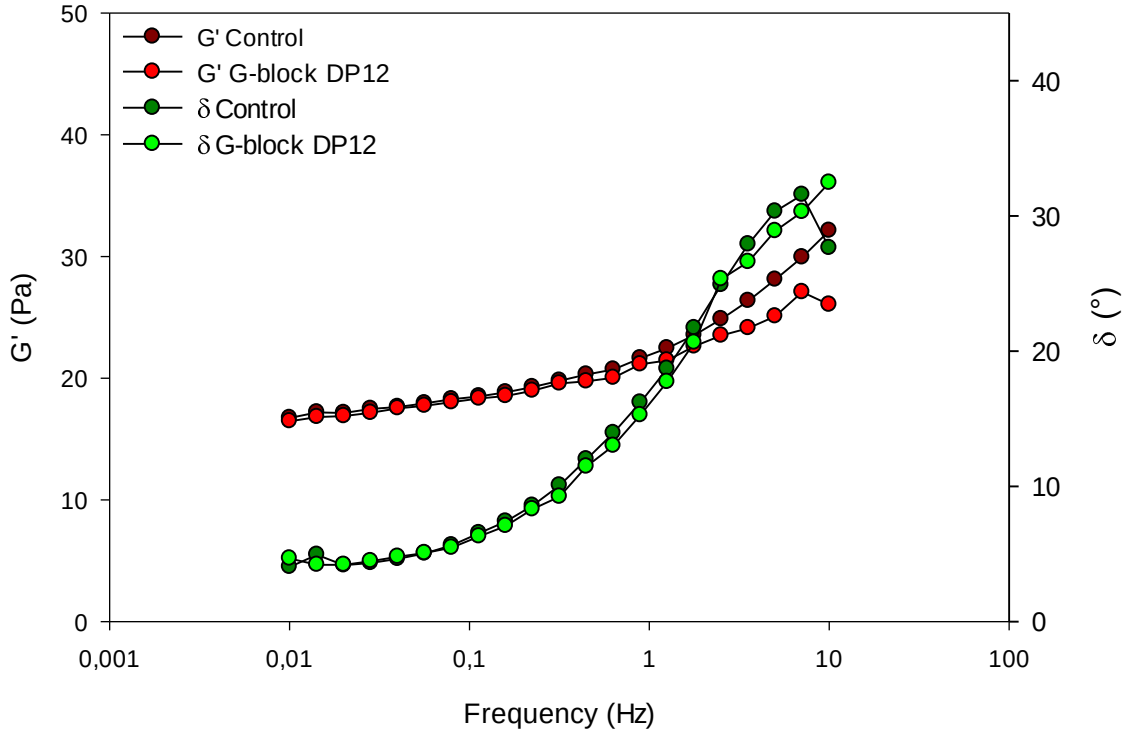

Figure 9. Elastic modulus (G') and phase angle (δ) values for bio-similar mucus control (saline) sample and bio-similar mucus treated with alginate G-block DP_n 12 at a concentration of 4.7 mg/mL. Values were collected from frequency sweeps run at 20 °C from low to high frequency with cone dimension C 40 4 ETC. The parameters of the frequency sweep of the bio-similar mucus control sample was a constant strain of 1E-3 and 2E-2 Pa start stress, while the parameters of the treated bio-similar mucus was a constant strain of 6E-4 and 1E-2 Pa start stress.

The effect of alginate on the bio-similar mucus was then tested using alginate G-block DP_n 33. The G33 treated sample and a control sample were rheologically tested through strain sweeps and consecutive frequency sweeps on the same day. The frequency sweeps are compared in Figure 10 and show that the measured parameters of the bio-similar mucus treated with alginate G-block DP_n 33 deviate from the control sample. This is in contrast to G12 treated bio-similar mucus that did not show any difference from the control (Figure 9). The curve of both the elastic modulus and the phase angle show similar frequency-dependent behaviour as the G12 treated sample, but there is a discrepancy between G33 treated and control sample values. G33 has weakened the bio-similar mucus network as seen by a drop in G' values. In addition, there has been an absolute increase in G'' values leading to higher phase angle values over the entire frequency range.

The bio-similar mucus network does not consist purely of mucin molecules, meaning that this effect cannot definitely be ascribed mucin-G-block interactions. The mucin constituent of the bio-

similar mucus is a commercially available Sigma crude PG mucin that is too heavily degraded to singularly form a gel (Kočevar-Nared et al., 1997). Therefore, in order for the bio-similar mucus to form a stable gel with rheological profile similar to PIM, polyacrylic acid is mixed into the solution (Bøgh et al., 2013). Despite both polymers carrying negative charges, the Sigma crude PG mucin and the polyacrylate stabilize gel formation together. This is possible because of the interactive properties of mucin molecules, which enables mucin to strongly adhere to polyanions such as alginate and polyacrylic acid (Fuongfuchat et al., 1996). Because the bio-similar mucus network is built upon two polymers, the effect of G33 is either with the mucin, the polyacrylate or both. Previous research has shown that low molecular weight alginate G-blocks have a marked weakening effect on purified PG mucin and CF sputum (Taylor Nordgård and Draget, 2011, Draget and Taylor, 2011). Since G12 in this case does not show any effect on the bio-similar mucus, the effect of G-blocks are either a result of G-block-polyacrylate interactions or G-block-polyacrylate/mucin interactions. According to thermodynamic law, binary homopolymer mixtures often lead to phase separation (Bates, 1991). For the mixing of two solutions to occur spontaneously the Gibbs free energy of mixing (ΔG_{mix}) must be negative in value. Gibbs free energy of mixing depends on the entropy (ΔS_{mix}) and the enthalpy (ΔH_{mix}) of mixing shown in equation 4, where T is the temperature.

$$\Delta G_{mix} = \Delta H_{mix} - T\Delta S_{mix} \qquad (4)$$

For two high molecular weight polymers carrying the same charge, the entropy of mixing is very low since the polymers are restricted to particular arrangements defined by molecular interactions, and separation is favoured (Smidsrød et al., 2008). Phase separation is highly dependent on the difference in degree of polymerization between the two polymers (Bates et al., 1988). If the homopolymers are equally large polymers, separation results. However, if the molecular weight of the two molecules is widely different, it is not favourable to separate because the entropy of mixing is large. The polyacrylic acid used in the bio-similar mucus is a high molecular weight polymer, while G12 are low molecular weight molecules in comparison. The difference in M_w between G12 and polyacrylate is thus too large to favour separation. The G33 solution, on the other hand, contains higher molecular weight molecules than the G12 solution. The HPAEC-PAD experiment showed that G33 contains molecules with up to 61 monomers, which could explain why G33 affects the bio-similar mucus and G12 does not. Because the amount of alginate solution in the bio-similar mucus is under 10 % of the mucus volume, it is likely that the G33 solution upon separation will be dispersed throughout the bio-similar mucus without mixing. This will increase the liquid-like properties of the bio-similar mucus, which will cause the appearance of a weaker gel with lowered G' values and higher δ values.

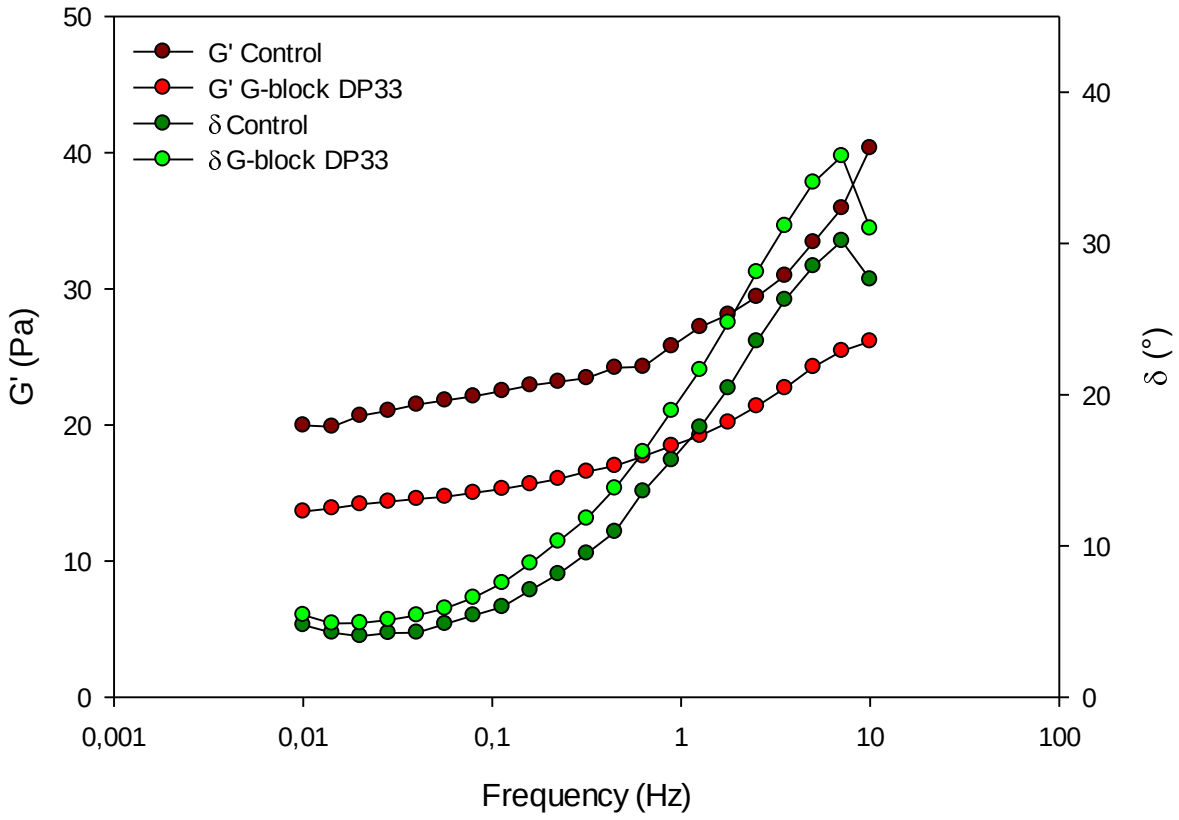

Figure 10. Elastic modulus (G') and phase angle (δ) values for bio-similar mucus control (saline) sample and bio-similar mucus treated with alginate G-block DP_n 33 at a concentration of 4.7 mg/mL. Values were collected from frequency sweeps run at 20 °C from low to high frequency with cone dimension C 40 4 ETC. The parameters of the frequency sweep of the bio-similar mucus control sample was a constant strain of 5E-4 and 1E-2 Pa start stress, while the parameters of the treated bio-similar mucus was a constant strain of 1E-3 and 1E-2 Pa start stress.

The bio-similar mucus was further rheologically tested with alginate LFR 5/60. The frequency sweep of the LFR treated bio-similar mucus is compared with a frequency sweep of a control sample tested on the same day in Figure 11. There is one phase angle value at low frequency for both the treated and the control sample that is out of place. This could be because of slip or air bubbles in the sample, but because the skip in value happens to both the control and the treated sample, it might also be because of batch instability for that particular batch. In any case, it does not influence the rest of the frequency sweep, and can be disregarded.

Apart from this the curves of both the LFR treated sample and the control sample behave as expected and the flow profile matches that of the other alginate treated bio-similar mucus samples. The difference between the LFR treated sample and the control sample is similar to the effect of G33 (Figure 10), but the discrepancy between the treated sample and the control is slightly larger for the

LFR. This supports the idea that alterations in rheology are a result of phase separation. Alginate LFR 5/60 has a higher degree of polymerization (DP_n ~63) than alginate G-block DP_n 33, and should theoretically cause a larger degree of separation (Bates et al., 1988). However, the difference in bio-similar mucus gel weakening between G33 and LFR is not as large as anticipated due to the large difference in DP_n. The reason could be that the alginate solutions were added to the bio-similar mucus per volume, instead of by number of molecules. This means that there are fewer LFR molecules in the bio-similar mucus compared to both G33 and G12, which in extension means that the separation effect would not necessarily be larger. In addition, the mucin constituent of the bio-similar mucus can also interact with the alginate molecules, which means that the effect of alginate cannot fully be ascribed alginate-polyacrylate interactions. Because the effect of LFR is less than anticipated compared to the effect of G33, it could mean that the mucin glycoproteins play an important interactive role as well. This means that the observations are most likely due to interactions between alginate and both mucin and polyacrylate, which makes the bio-similar mucus act differently to the presence of alginate compared with what is expected for natural mucus samples (Draget and Taylor, 2011, Taylor Nordgård and Draget, 2011).

Rheological experiments performed on LFR treated bio-similar mucus were also done in replicates. The replicates show identical response to LFR treatment, and only one of the frequency sweeps are given. Such reproducible results suggest that the bio-similar mucus is a stable gel that behaves consistently under mechanical deformation. The major differences in the bio-similar mucus rheological behaviour arises from batch variations. The reader might have noticed that the control sample values are not identical between Figure 9, 10 and 11. The procedure for every experiment has been identical, the only difference being the batch and the day the experiment was done.

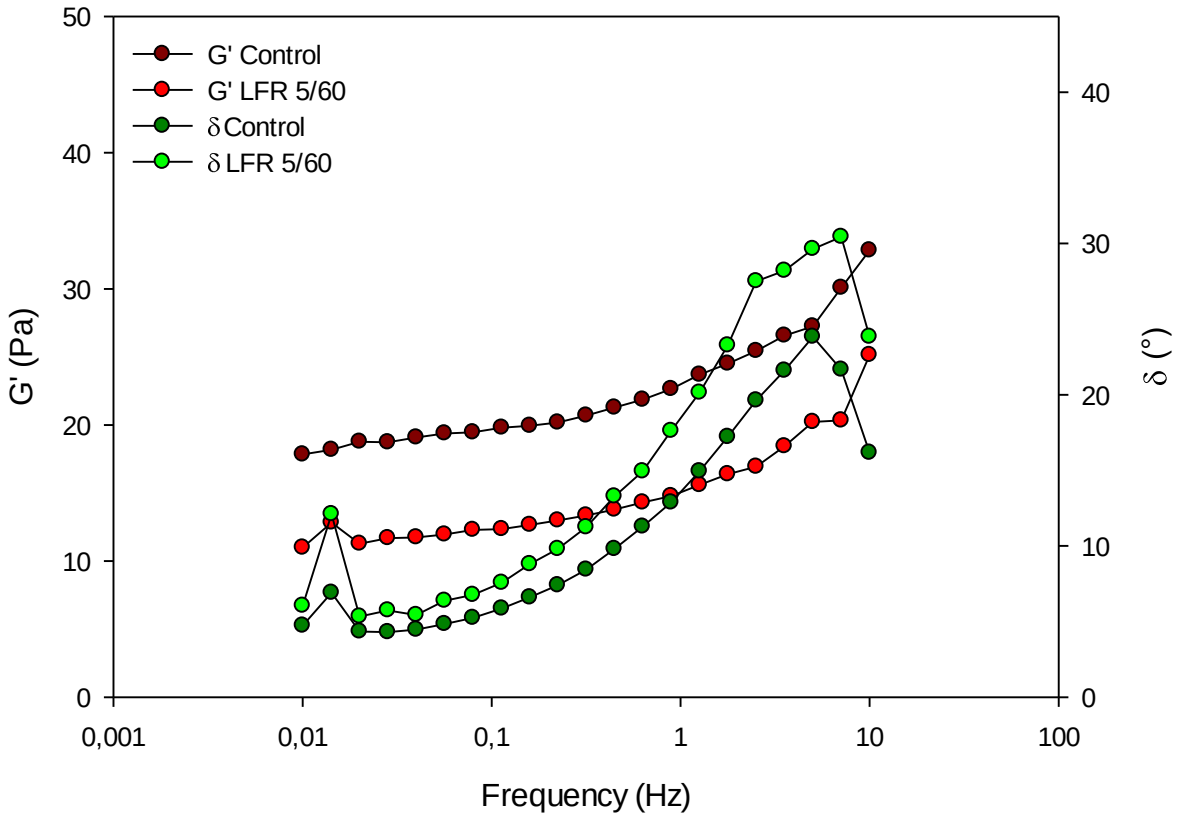

Figure 11. Elastic modulus (G') and phase angle (δ) values for bio-similar mucus control (saline) sample and bio-similar mucus treated with alginate LFR 5/60 at a concentration of 4.7 mg/mL. Values were collected from frequency sweeps run at 20 °C from low to high frequency with cone dimension C 40 4 ETC. The parameters of the frequency sweep of the bio-similar mucus control sample was a constant strain of 6E-4 and 1E-2 Pa start stress, while the parameters of the treated bio-similar mucus was a constant strain of 8E-4 and 1E-2 Pa start stress.

3.2 The effect of alginate on native porcine small intestinal mucus

The effect of alginate on porcine small intestinal mucus (PSIM) was tested using the same three alginate molecules (G12, G33 and LFR) as with the bio-similar mucus to better compare the samples. The rheology of all samples was investigated through strain sweeps and frequency sweeps. The strain sweeps were only performed to find where the values of stress and strain were proportional and where the moduli values are independent of strain. As with the bio-similar mucus, isotonic saline mixed with PSIM was used as control sample to eliminate the change in ionic strength from adding alginate, and

to account for any unwanted effects due to dilution. The mixing regime was identical to the bio-similar mucus, as was the final concentration of alginate (4.7 mg/mL). The PSIM samples treated with alginate solutions were all tested in two replicates, while the control sample was tested in four replicates.

A frequency sweep of both replicates of PSIM treated with G12 compared with separate control samples are given in Figure 12. One of the replicates of treated PSIM had elevated G' values, while the other one had lowered G' values compared to the control samples. Based on previous rheological experiments using low molecular weight alginate G-blocks (DP_n 10 and DP_n 19/20) on both purified PG mucin and *ex vivo* CF sputum (Taylor et al., 2007, Draget, 2011, Taylor Nordgård and Draget, 2011, Draget and Taylor, 2011), the elastic modulus of the treated PSIM was expected to be lower than the control sample. Treatment of G-block on CF sputum and PG mucin were found to weaken the gel, with increased phase angle values and decreased elastic/loss modulus values compared to untreated samples.

In Figure 12, the difference in G' values between the two replicates is most likely due to the inherent variations within the native mucus. Native mucus contains various proteins, ions and lipids/surfactants that creates a chemically diverse and complex solution (Bansil and Turner, 2006). In addition, the PSIM samples are inhomogeneous and the substances native to PSIM can exist in varying amounts throughout the same batch. Because of this, the beaker which contained the frozen PSIM was stirred in order to achieve a more homogeneous mixture before the desired amount of PSIM was measured out. Despite this, food debris and other inhomogeneities could be seen when the PSIM samples were applied on the rheometer. Even though the elastic modulus values are contradictory, the phase angle values in both cases are higher for the treated sample. This means that the amount of energy stored within the gel structure of PSIM differs, but that in both cases G12 has weakened the mucus gel. Thus, introducing alginate G-block DP_n 12 into the PSIM matrix increases the ratio between G'' and G', giving the gel relatively more liquid-like properties.

Literature reports that there exist large inter- and intra-species variations in porcine intestinal mucus elastic properties (Boegh et al.). G' variations have been seen in CF sputum as well, but the ratio between G'' and G' vary little (Sanders et al., 2000), meaning that the phase angle values are generally more representative for mucus rheology in highly complex mixtures such as native mucus. Experimental data from the four control replicates show the same as literature; G' varies between experiments, but the ratio between G'' and G' remains the same giving little variations in phase angle values. The G' and δ values from the four control samples are compared in Figure 13.

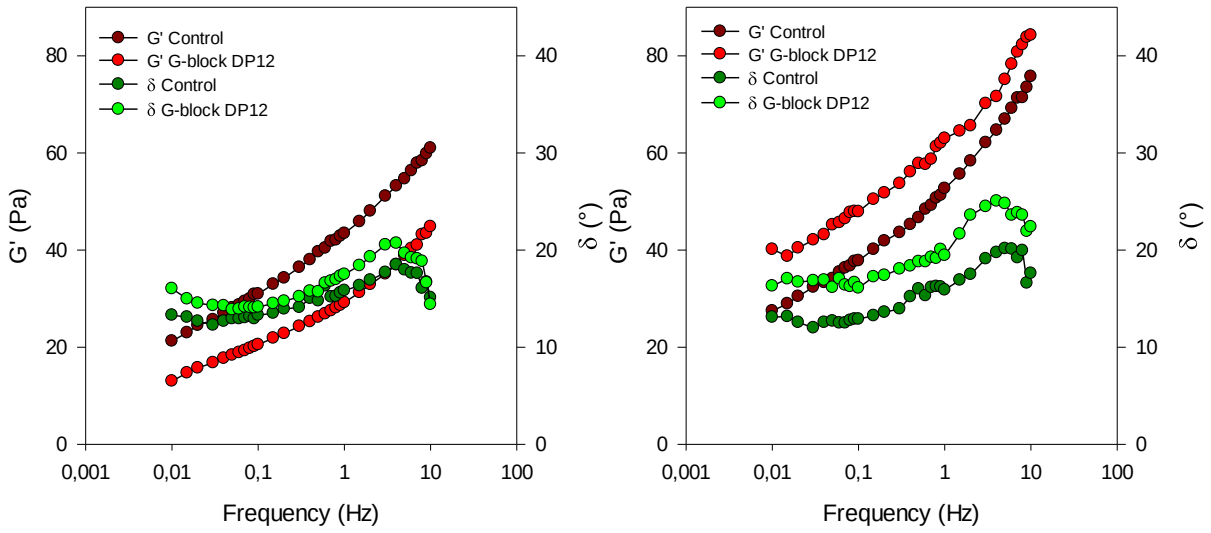

Figure 12. Elastic modulus (G') and phase angle (δ) values of two replicates of porcine small intestinal mucus (PSIM) treated with alginate G-block DPn 12 compared with two replicates of PSIM control (saline). Concentration of alginate was 4.7 mg/mL. Values were collected from frequency sweeps run at 20 °C from low to high frequency with cone dimension C 40 4 ETC. For the left replicate, the parameters of the frequency sweep of the PSIM control was a constant strain of 1E-3 and 1E-2 Pa start stress, while the parameters of the treated PSIM was a constant strain of 1E-3 and 1E-2 Pa start stress. For the right replicate, the parameters of the frequency sweep of the PSIM control was a constant strain of 6E-4 and 2E-2 Pa start stress, while the parameters of the treated PSIM was a constant strain of 6E-4 and 1E-2 Pa start stress.

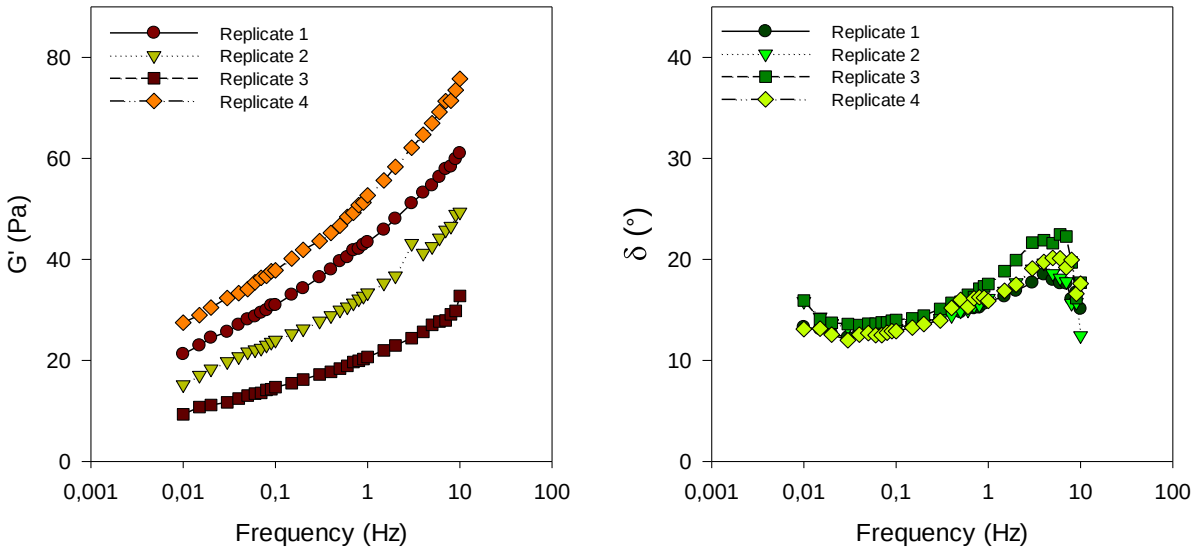

Figure 13. Elastic modulus (G', left graph) and phase angle (δ, right graph) values of four replicates of porcine small intestinal mucus (PSIM) control (saline) sample compared. Values were collected from frequency sweeps run at 20 °C from low to high frequency with cone dimension C 40 4 ETC. The parameters of the frequency sweep of replicate 4 was a constant strain of 6E-4 and 2E-2 Pa start stress, while the parameters of all the other replicates were a constant strain of 1E-3 and 1E-2 Pa start stress.

Figure 14 shows a frequency sweep of the G33 treated PSIM sample compared with a frequency sweep of a control. The parameters of the frequency sweep were based on an initial strain sweep not shown here. Alginate G-block DP_n 33 appears to have strengthened the mucus gel slightly. The values of G' are elevated compared to the control sample, and the values of δ are slightly lower. According to Figure 13 and literature (Sanders et al., 2000, Boegh et al.), the G' values vary too much within mucus to be able to conclude anything, but the δ values are still indicative. Therefore, the slight decrease in phase angle values between the G33 treated sample and the control sample indicates that G33 increase elastic properties more than liquid-like properties. Alginates have been shown to be able to interact with mucin molecules through electrostatic interactions (Taylor et al., 2005b), and that low molecular weight G-blocks weaken the mucin gels by decreasing the cross-linking density between mucin molecules through competitive inhibition (Taylor Nordgård and Draget, 2011). Based on this, it would seem that the chain length distribution in the G33 solution contains alginate G-block molecules long enough with large enough radius of gyration and persistence length to induce a higher cross-linking density compared to PSIM mixed with saline.

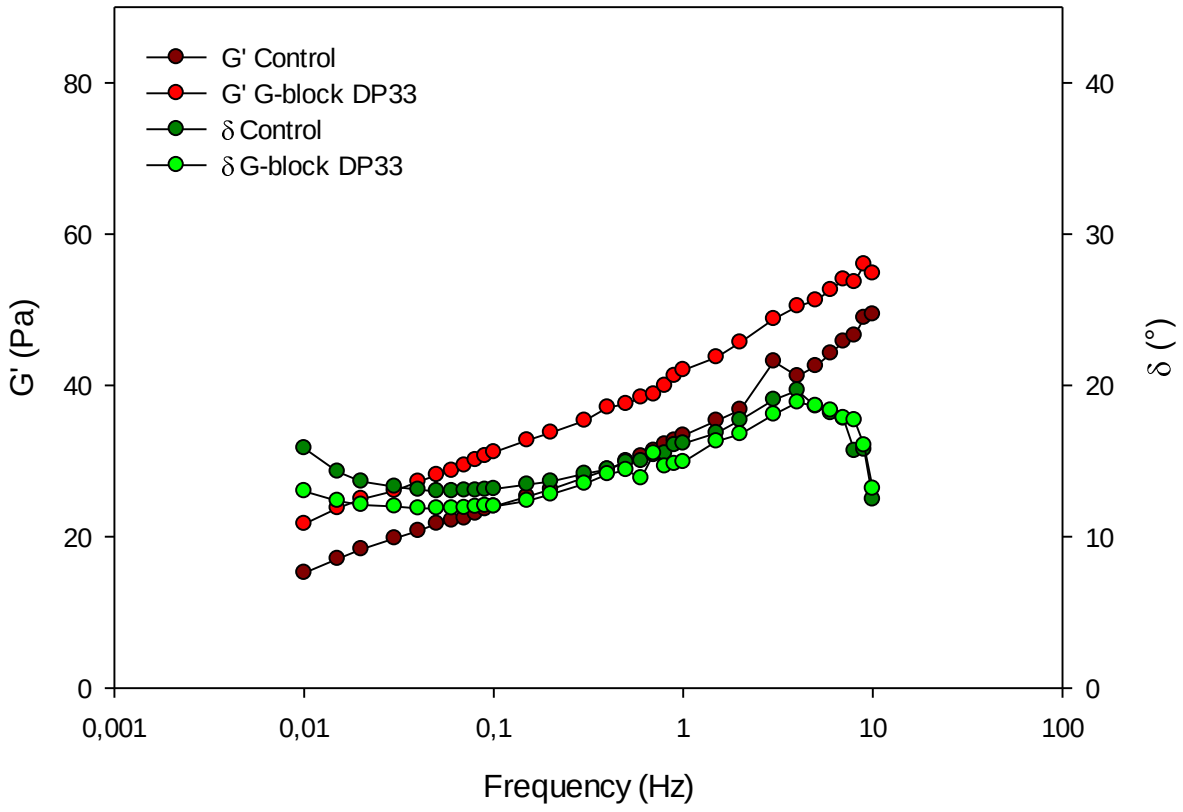

Figure 14. Elastic modulus (G') and phase angle (δ) values for porcine small intestinal mucus (PSIM) treated with alginate G-block DPn 33 compared with PSIM control (saline). The concentration of alginate was 4.7 mg/mL. Values were collected from frequency sweeps run at 20 °C from low to high frequency with cone dimension C 40 4 ETC. The parameters of the frequency sweep for the PSIM control was a constant strain of 1E-3 and 1E-2 Pa start stress, while the parameters for treated PSIM was a constant strain of 1E-3 and 1E-2 Pa start stress.

Figure 15 shows the frequency sweep of PSIM treated with alginate LFR 5/60 and PSIM control compared. Alginate LFR 5/60 have a more defined strengthening effect on PSIM than G33. The elastic modulus values are almost twice as high for LFR treated PSIM, indicating a clear increase in stored energy within the sample. In addition, phase angle values are lower than the control sample, meaning that the elastic properties of PSIM has increased more than the viscous properties upon addition of alginate LFR 5/60. LFR are higher molecular weight (M_w) molecules than any of the G-blocks, which can more readily cross-link to mucin molecules through electrostatic interactions (Taylor et al., 2005b) due to longer chain lengths.

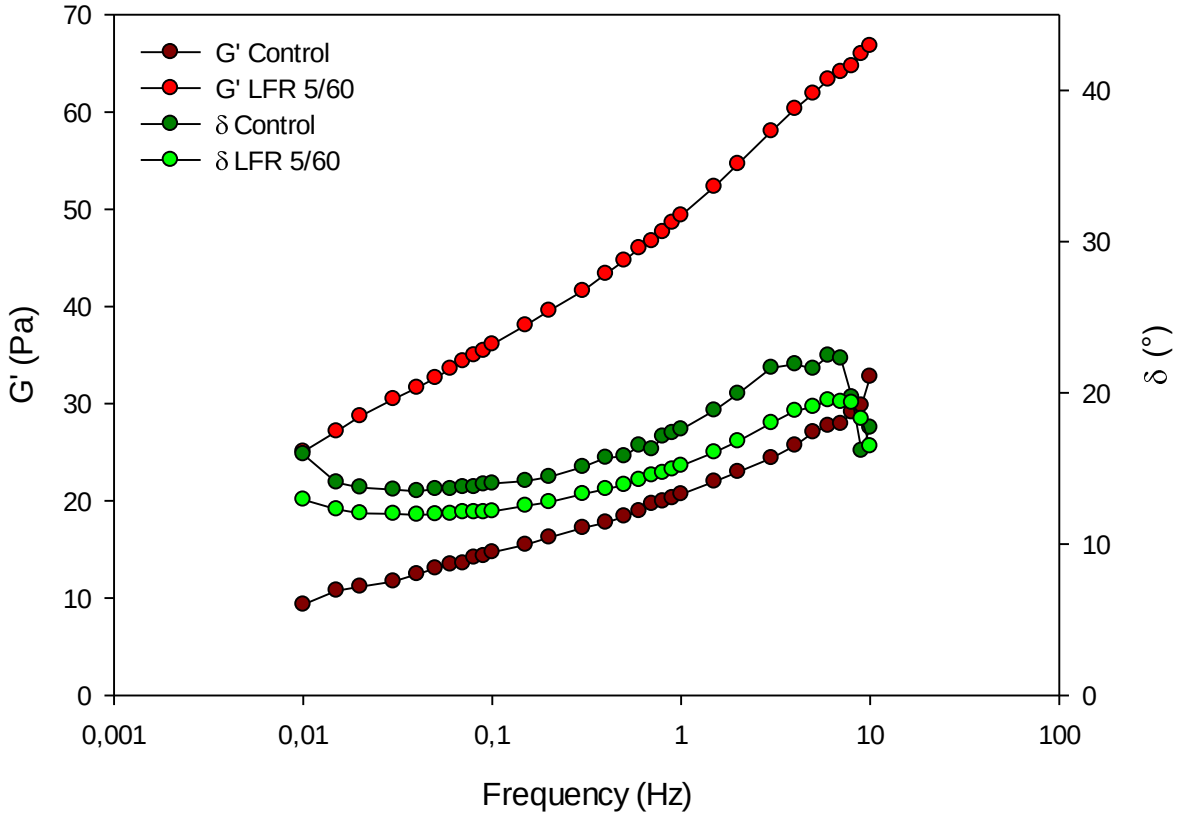

Figure 15. Elastic modulus (G') and phase angle (δ) values for porcine small intestinal mucus (PSIM) treated with alginate LFR 5/60 compared with PSIM control (saline). The concentration of alginate was 4.7 mg/mL. Values were collected from frequency sweeps run at 20 °C from low to high frequency with cone dimension C 40 4 ETC. The parameters of the frequency sweep for the PSIM control was a constant strain of 1E-3 and 1E-2 Pa start stress, while the parameters for treated PSIM was a constant strain of 1E-3 and 1E-2 Pa start stress.

Compared to the bio-similar mucus experiments, the elastic modulus values of PSIM generally have a steeper slope, and the phase angle values vary less with frequency. The elastic modulus curves are steeper most likely because PSIM is more complex and diverse than the bio-similar mucus. Mortazavi et al. (Mortazavi et al., 1993) investigated the properties of mucin-polyacrylate gels and found evidence that it is both an entangled and a weakly cross-linked system. Cross-linking happens mainly through hydrogen bonding between the polyacrylate molecules and the mucin carbohydrate moieties (Patel et al., 2003). For a purely chemically cross-linked gel, the elastic and viscous modulus would be independent of frequency of oscillation, while the slope for G' and G'' values would increase with increased frequency for physically entangled systems (Ross-Murphy and McEvoy, 1986). This is because the physically entangled subunits glide apart at low frequencies, but as frequency increases the entangled polymer chains are not given time to gently glide apart and will instead stretch which increases elasticity. Both PSIM and the bio-similar mucus are both entangled and cross-linked gels, but the reason that the G' curve is steeper for native PSIM over the range of frequency could be that there exist a more extensive entangled network of mucin polymers than of mucin-polyacrylate or because the bio-similar mucus is less cross-linked. The degree of entanglements depend on the concentration of mucin, the length of mucin subunits and the chemical nature of the mucin molecules (Thornton and Sheehan, 2004). Less than 1 % of the bio-similar mucus consisted of polyacrylic acid and 5 % were Sigma crude mucin. The concentration of mucin in PSIM was not tested, but it could potentially have been higher. In addition, the length of mucin subunits in the native mucus sample would be expected to be longer since the commercial mucin is heavily degraded (Kočevar-Nared et al., 1997). The native mucus is also expected to exhibit a more diverse chemical nature because of other inherent substances in mucus. The native mucus sample might also possess several more interaction sites on its mucin constituents due to the purification method of Sigma mucin which often causes cleavage of hydrophobic domains on the protein backbone (Davies and Viney, 1998), but also because of the polyacrylate that only interact through electrostatic interactions and hydrogen bonding.

The phase angle values for PSIM are more stable than the bio-similar mucus ones. This means that the viscous modulus of the bio-similar mucus increases more relative to the elastic modulus as frequency increases. In other words, more energy is lost in the bio-similar mucus than in the PSIM. This could be a consequence of the lubricating ability of mucus. Under increasing shear rate, the mucus creates a slippage plane (Cone, 2009), which causes very little of the energy introduced into the sample to be lost through frictional forces. However, even though the Sigma mucin molecules are degraded, the bottle brush structure of the mucin molecules remain mostly intact (Davies and Viney, 1998), and the experiments are performed within the linear viscoelastic area, meaning the shear rate that could cause a slippage plane should not increase. The behaviour of bio-similar mucus was investigated by

Frida (Våset, 2014), who found that the behaviour was independent of stress and strain (i.e. the phase angle increased abruptly at higher frequencies in both stress-controlled and strain-controlled experiments). It is unclear what could have caused this.

Even though the bio-similar mucus forms a rheologically stable gel with similar profile to PSIM, it does not mimic the dynamic behaviour of PSIM in the presence of other polymers with negative charge. Only alginate has been investigated here, but based on thermodynamic laws, the observed effect is expected in other binary homopolymer mixtures as well (Smidsrød et al., 2008). The difference between the effects of alginate on PSIM and the bio-similar mucus is most likely because of the differences in structure between mucin and polyacrylate. Granted, both mucus samples form entangled gels with some degree of weak cross-linking, but the mucin molecules display a larger pool of different interactions and shows signs of being more extensively entangled. The polyacrylate is negatively charged, and interact by electrostatic interactions and hydrogen bonding, whereas mucin molecules interact by hydrophobic and Van der Waals interactions in addition to the aforementioned interactions for polyacrylic acid (Woodley, 2001). In addition, the mucin molecules contain positively charged regions in addition to negative ones (close to the cysteine-rich domains which are cleaved in the commercialized mucin sample), arising from amino acids on the protein backbone of mucin molecules (lysine, arginine and histidine) (Taylor Nordgård and Draget, 2011). These charges might cause the alginate molecules to stay in the solution and bind to mucin through electrostatic adhesion instead of separating into another phase as is the case in the bio-similar mucus.

3.3 The effect of alginate on purified porcine gastric mucin

Purified porcine gastric (PG) mucin can be used as a model system for human tracheobronchial mucus, because of similar gene products in the gastrointestinal mucus compared with the tracheobronchial mucus (Van Klinken et al., 1995), and because porcine and human mucus are structurally related (Turner et al., 1999). It is therefore interesting to investigate the effect of alginate on PG mucin. Here, the effect of four different alginate molecules are studied – alginate G-block DP_n 12 (G12), alginate G-block DP_n 24 (G24), alginate G-block DP_n 33 (G33) and alginate LFR 5/60 (LFR). Two different lots of PG mucin has been used in this thesis. The samples are denoted lot#1 and lot#2 respectively.

PG mucin lot#1 was rehydrated in MQ-water at a concentration of 40 mg/mL, and was stored at 3 °C for 48 hours with gentle stirring. Because the aim of this thesis is to translate the findings into human benefit, the desired pH was physiological pH 7.4. The rehydrated PG mucin had ambient pH 4.6, and 10 mM HEPES buffer (buffer range 6.8-8.2) was added to the solution to prevent the pH from getting too high during titration. After HEPES addition, the pH was 5.2 and the PG mucin solution was visibly thinner. A small part of the sample was transferred to a separate beaker and pH reduced to 3.7, which visibly thickened the solution. A sample from each solution of pH 3.7, 4.7 and 5.2 was applied on the rheometer and their flow properties studied. The sample at pH 3.7 and 4.7 was tested through frequency sweeps with stress and strain values determined via initial strain sweeps. The sample at pH 5.2 was only tested through one frequency sweep due to noticeably lower viscosity than the other samples. Flow properties of very liquid samples are hard to measure using oscillatory rheology, which are best suited at measuring viscoelastic solids (gels) (Barnes et al., 1989). Liquid samples often generate a high degree of noise because of low material response, which is why predetermined stress and strain values were used for the sample at pH 5.2.

Values from the three frequency sweeps of PG mucin at pH 3.7, 4.7 and 5.2 are depicted in Figure 16. Three of the graphs show the elastic (G') and viscous (G'') modulus of each sample separately, while the fourth graph shows the phase angle values from all samples compared. The PG mucin sample at pH 3.7 has a flow profile close to what is expected of a viscoelastic solid. Elastic modulus is higher than the viscous modulus over the entire frequency range. This leads to phase angle values between 0 ° and 45 °. The other two samples display liquid-dominant properties, with G'' being higher than G' most of the frequency sweep and phase angle values mostly above 45 °. These signs indicate that PG mucin at pH 4.7 and 5.2 behave like an elastic liquid rather than a viscoelastic solid (Weitz et al., 2007). However, even though the PG mucin at 4.7 and 5.2 are elastic liquids, they are still entangled systems and the G' and G'' increase with increasing frequency of oscillation. At low frequencies, the liquid character of the sample is apparent, and there is no resistance to the deformation. At higher frequency more of the thermal energy used to induce the constant strain is being stored than lost because the entangled molecules resist the deformation, leading to a decrease in phase angle values. This is opposite to viscoelastic solids where more energy dissipates than is being stored at high frequency.

The results from Figure 16 indicate that PG mucin rheology is pH dependent. This behaviour has not been seen for PG mucin received at the Rheodor laboratory before (Nordgård, 2014), and the behaviour suggests some structural change between pH 3.7-4.7. Based on literature, mucin molecules are negatively charged glycoproteins (Cone, 2009). Some of these negative charges arise from negatively charged amino acids (glutamic acid and aspartic acid) located on the protein backbone with

pK_a values around 4 (Cao et al., 1999). At pH under 4 these carboxyl groups protonate, which leads to a reduction in electrostatic interactions between mucin molecules and an increase in hydrogen bonding. In addition, the conformational change is thought to expose hydrophobic regions located on the protein backbone of mucin (Lee et al., 2005). These regions were previously unable to interact due to electrostatic repulsion, but as some repulsion ceases there will be an increase in hydrophobic interactions between such exposed regions. The resulting conformational changes strengthens the gel under pH 4, which is imperative for gastric mucus to prevent acid from reaching the epithelial surface (Celli et al., 2005).

According to the observations, the PG mucin sample is not a gel at pH over 4. This is contradictory to native mucus, where it is a gel at physiological pH as well as pH under 4. Another influential factor could therefore be that ionic strength affected PG mucin rheology, since HCl/NaOH was added to lower/elevate pH. However, if the observations were a consequence of ionic strength, the PG mucin sample should not have gelled when the pH was reverted to 3.7 after being 5.2, since it has been reported that high ionic strength decreases PG mucin viscosity (Bhaskar et al., 1991). The ionic effect could still have been a factor, but it was not the sole reason for the sol-gel transition.

As a result of low material response of the PG mucin sample at pH 5.2, the frequency sweep is crowded by noise. Noise appears due to low mechanical resistance in the sample (i.e. low material response), which leads to minimal rotational forces (torque values). Low material response causes inaccuracies in the measured values, which is why some values of G’ and G’’ at low frequencies from the frequency sweep of the PG mucin sample at pH 5.2 were omitted from Figure 16.

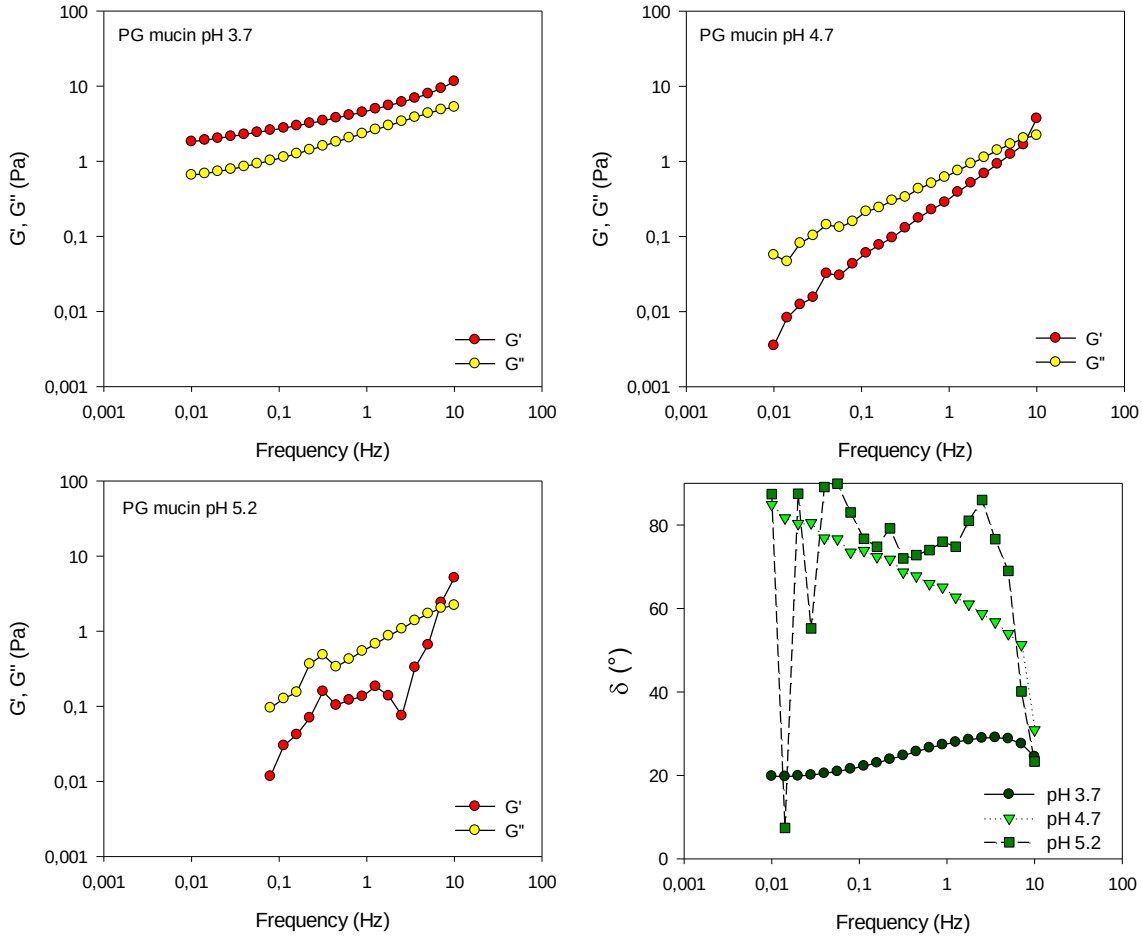

Figure 16. Elastic modulus (G'), viscous modulus (G'') and phase angle (δ) values of untreated porcine gastric (PG) mucin at three different pH values. The concentration of PG mucin was in all cases 40 mg/mL. All values depicted were collected from frequency sweeps at 20 °C from low to high frequency. Upper left graph shows G' and G'' values of PG mucin at pH 3.7 measured at constant strain 2E-1 and 1 Pa start stress with cone dimension C 40 1 ETC. Upper right graph shows G' and G'' values of PG mucin at pH 4.7 measured at constant strain 2E-1 and 1.7E-1 Pa start stress with cone dimension C 40 1 ETC. Lower left graph shows G' and G'' values of PG mucin at pH 5.2 measured at constant strain 5E-2 and 3E-3 Pa start stress with cone dimension C 50 1 ETC. Lower right graph show the δ values of the three samples compared.

The pH dependence was a minor setback for further experimentation, partly because physiological pH is 7.4, but also because alginate protonates at low pH and would precipitate out of the solution (Stanford, 1886). There are always considerations to make regarding translation of results from animal material experimentations to human use (Watkins et al., 2010), and even if the experiments were performed at low pH, the results could still be used as a foundation for further tests. However, if alginate does not maintain its structure and function, then realizing the aim of this thesis will not be feasible. PG mucin lot#2 did not show pH instabilities to the same degree as lot#1, but because there were minor variations, the PG mucin solution was left at ambient pH of 4.5. Since temperature also proved to influence rheology, all frequency sweeps of PG mucin samples were done

at 10 °C. PG mucin lot#2 was rehydrated in MQ-water in the same manner as lot#1 (48 hours, 3 °C, gentle stirring) at a concentration of 42.84 mg/mL (to achieve a final concentration of 40 mg/mL after addition of alginate/saline). Isotonic saline was used as control as with PSIM and the bio-similar mucus in order to prevent ionic strength differences between treated and untreated PG mucin, and to account for dilution effects. Freshly made samples were quickly measured into small Eppendorf tubes and frozen because hydration time proved to be a significant factor for PG mucin rheology.

The effect of alginate on PG mucin lot#2 was tested using G12, G24, G33 and LFR at a concentration of 4.7 mg/mL. Each sample was subjected to four frequency sweeps at four different strains (5E-4, 1E-3, 5E-3 and 1E-2) and one strain sweep. Exposing the samples to four different strains was thought to show the dynamic properties of PG mucin better than just one frequency sweep; it shows how the treated samples behave under increasing deformation. Unlike the previous experiments with PSIM and the bio-similar mucus, the strain sweep was done last in the series of sweeps. This was to prevent the samples from being subjected to unnecessary high deformation prior to the frequency sweeps.

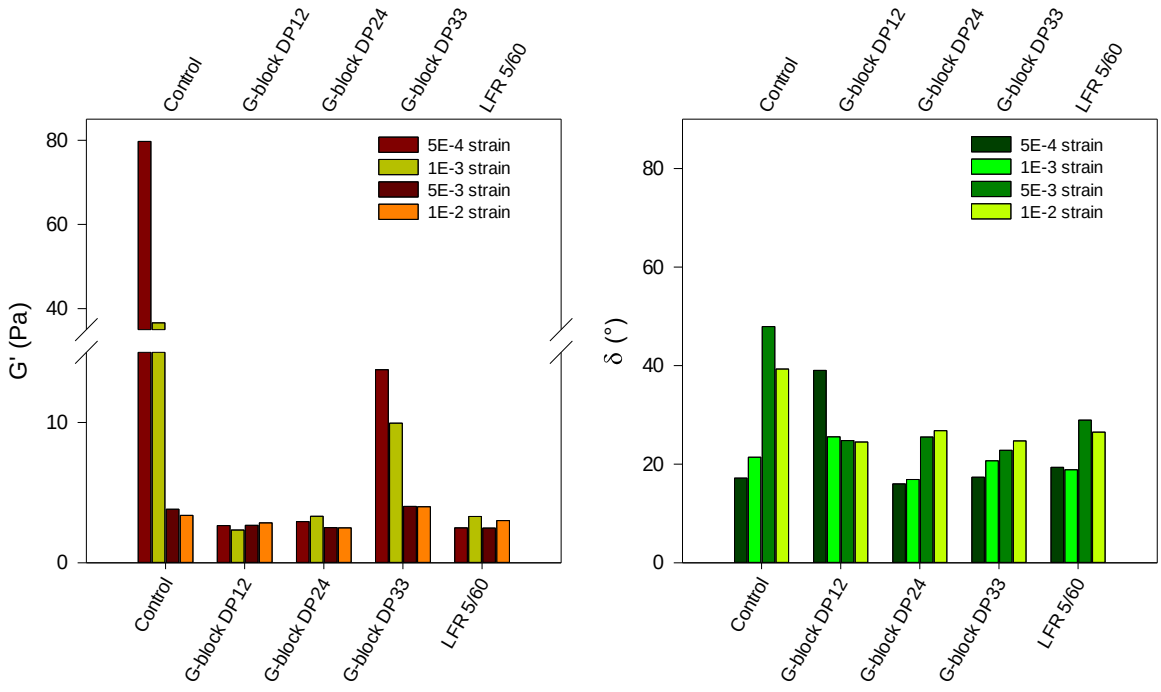

Figure 17. Elastic modulus (G' and phase angle (δ) values of porcine gastric (PG) mucin control (saline) and PG mucin treated with alginate G-block DP_n 12, alginate G-block DP_n 24, alginate G-block DP_n 33 and alginate LFR 5/60 at 1Hz frequency over four different values of strain. Concentration of alginate was 4.7 mg/mL and concentration of PG mucin was 40 mg/mL. All values were collected from frequency sweeps run at 10 °C from low to high frequency with cone dimension C 40 1 ETC.

Complete frequency sweeps for all samples at 5E-4 and 1E-3 strain is given in Figure 18 and Figure 19 respectively, and complete frequency sweeps for all samples at 5E-3 and 1E-2 strain is given in Appendix J.

Figure 17 shows elastic modulus and phase angle values for all samples over all strains at 1 Hz frequency compared. PG mucin control sample has the highest G' values at 5E-4 and 1E-3 strain followed by G33 treated PG mucin. The other mucin samples have very low values of G' at 1 Hz frequency over all four strains. This suggests that G12, G24, G33 and LFR treatment of PG mucin decreased amount of stored energy within the mucin matrix, indicating that the gel weakened. As mentioned earlier, the effect of low molecular weight alginate G-blocks (DP_n 10 and DP_n 19/20) have been tested on *ex vivo* CF sputum and PG mucin (Draget and Taylor, 2011, Taylor et al., 2007, Taylor Nordgård and Draget, 2011). Both were found to have a weakening effect, and it is therefore not surprising that G12 and G24 show a high degree of gel weakening. It was found that G-block DP_n 10 had a more profound weakening effect on mucus structure than G-block DP_n 19 (Taylor Nordgård and Draget, 2011), and that the effect of G-block DP_n 19 on CF sputum samples varied compared to the control (saline). In this case, G12 and G24 treatment seems to have exactly the same effect. However, according to Figure 18 and 19 showing the full frequency sweeps of all the samples compared at 5E-4 and 1E-3 strain respectively, the G12 treated sample suffered from a high degree of noise (frequency sweeps at 5E-3 and 1E-2 strain is given in Appendix J). The similarities between G12 and G24 treatment may therefore not be significant. The G33 treated PG mucin exhibit a stronger gel than G12 and G24, which is logical based on the previous findings regarding G-block DP_n 10 and G-block DP_n 19 (Taylor Nordgård and Draget, 2011). G33 molecules have a higher degree of polymerization in general with larger radius of gyration and persistence length, meaning that the G33 cross-link between mucin subunits more than the lower molecular weight counterparts.

The phase angle values for all the alginate treated samples seem to be similar in Figure 17 (disregard the δ values for G12 treated PG mucin at 5E-4 and 1E-3 strain due to noise). This means that even though the G' values indicate a gel weakening, the phase angle values does not. Apparently, all PG mucin samples seem to have almost equal amounts of liquid-like and solid-like properties at 5E-4 and 1E-3 strain. This is because G'' decrease by a factor equal to the decrease in G', causing the phase angle values to remain the same in both alginate and saline treated samples. At higher strain, the δ values for the control sample increases, but the alginate treated values remain similar. This is surprising compared to literature documenting different rheological effects of different molecular weight alginates on PG mucin (Draget and Taylor, 2011, Taylor et al., 2005a, Taylor et al., 2007, Taylor et al., 2005b, Taylor Nordgård and Draget, 2011). However, torque values from each experiment was very low (data not shown), indicating low mechanical response which could explain some of these surprising findings.

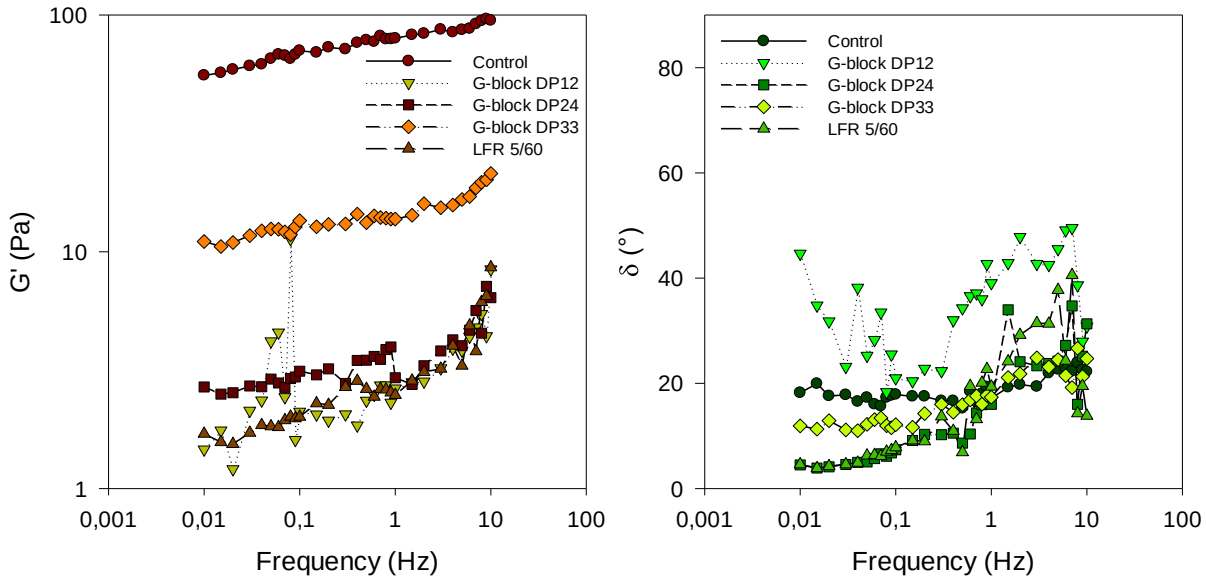

Figure 18. Elastic modulus (G', left graph) and phase angle (δ, right graph) values for porcine gastric (PG) mucin control (saline) and PG mucin treated with alginate G-block DP_n 12, alginate G-block DP_n 24, alginate G-block DP_n 33 and alginate LFR 5/60 compared. All values are from frequency sweeps at 10 °C from low to high frequency with constant strain 5E-4 and 1E-2 Pa start stress. Cone dimension was C 40 1 ETC. Concentration of PG mucin in MQ-water was 40 mg/mL and concentration of alginate was 4.7 mg/mL.

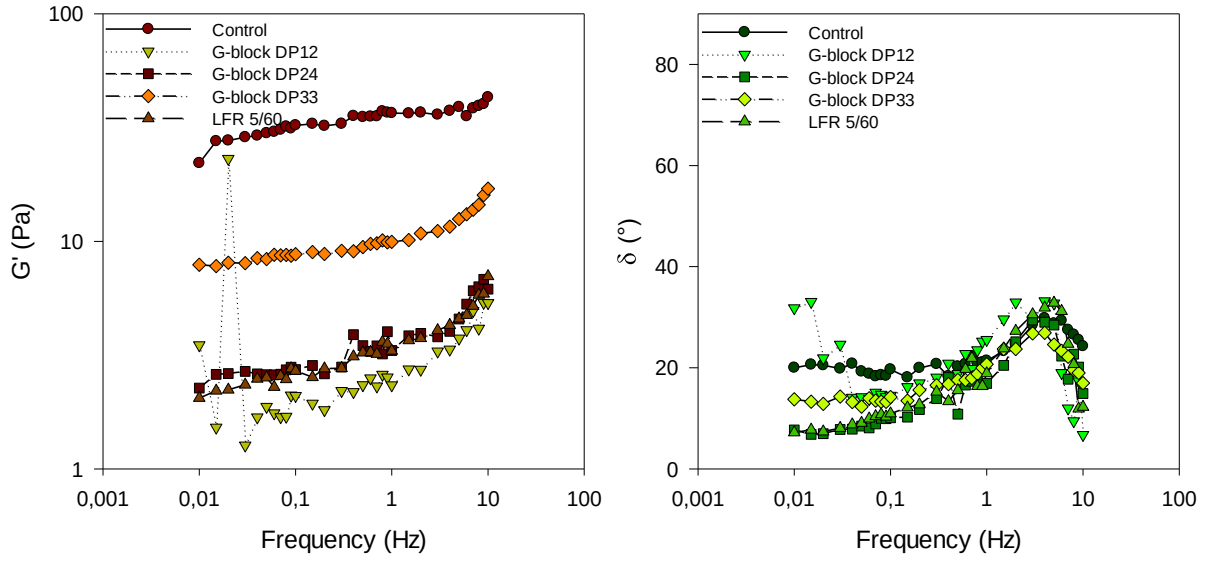

Figure 19. Elastic modulus (G', left graph) and phase angle (δ, right graph) values for porcine gastric (PG) mucin control (saline) and PG mucin treated with alginate G-block DP_n 12, alginate G-block DP_n 24, alginate G-block DP_n 33 and alginate LFR 5/60 compared. All values are from frequency sweeps at 10 °C from low to high frequency with constant strain 1E-3 and 1E-2 Pa start stress. Cone dimension was C 40 1 ETC. Concentration of PG mucin in MQ-water was 40 mg/mL and concentration of alginate was 4.7 mg/mL.

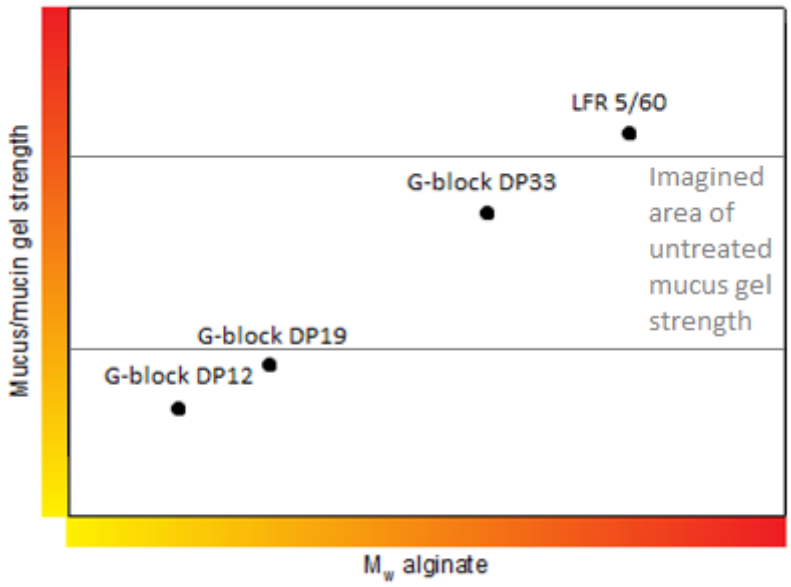

Figure 20. The effect of differently sized G-rich alginate molecules on mucus/mucin gel strength based on experiments with porcine small intestinal mucus (PSIM) and literature (Taylor et al., 2005a, Taylor Nordgård and Draget, 2011). An area where the gel strength of untreated mucin/mucus is thought to be is also given.

Assuming that the elastic modulus values in Figure 17 are correct despite the low torque values, LFR treatment causes equal amounts of lost energy as G12 and G24 treatment compared to the control. Based on literature (Taylor et al., 2005a, Taylor Nordgård and Draget, 2011) and on the results obtained from the PSIM experiments, the relationship between gel strength and molecular weight of G-rich alginates follows the graph in Figure 20. The concentration of alginate solution in PG mucin is exactly the same as in PSIM, and alginate should consequently have a similar effect on PG mucin. A possible explanation could be that some of the inherent substances of PSIM associated with LFR molecules, which increased gel strength. For instance, mucus secretions contain divalent calcium ions (Ca^{2+}), seemingly an important feature for mucin interactions (Perez-Vilar, 2007). Alginates high in guluronate gel in the presence of divalent cations, and they have an especially high affinity for Ca^{2+} (Pawar and Edgar, 2012). It is therefore possible that LFR gels within PSIM due to residual Ca^{2+} or even mucin bound Ca^{2+}, which strengthens the gel (Fuongfuchat et al., 1996). Low molecular weight G-blocks on the other hand would react differently because they consist almost entirely of G-residues. This means that if the G-residues bind calcium there would be nothing to keep the molecules in solution, and the G-blocks would precipitate out (Skják-Bræk et al., 1986). The effect of G12 on PSIM could therefore be due to G12 precipitation which increases liquid-like properties or because of G12 incorporation into the mucin network which decreases the cross-linking density. Based on the

observed effect of G33, the most likely scenario is that the G-block molecules incorporate into the mucin structure because precipitation of G33 would not cause a strengthening effect seen in Figure 14Figure. However, the LFR molecules has a fraction of M-residues (F_M) equal to 0.31 and will stay in solution after gelling. In the PG mucin sample there does not exist a significant population of calcium ions, meaning that alginate gelling is not a factor when considering the effect of alginate. The observed effect will purely depend on alginate-mucin interactions, which could explain the large difference in LFR effect. However, LFR should still be able to increase cross-linking density in PG mucin samples due to a high degree of polymerization, and the results are therefore unexpected. Another possibility is that the dilution effect could have been more profound for the LFR sample. All alginate solutions were added per volume to a final concentration of 4.7 mg/mL, but because of differences in molecular weight, there would be more molecules of the shorter G-blocks in the mucus/mucin solution compared to LFR.

According to Figure 17, the samples mostly show expected behaviour as deformation increases. As the deformation increases, the increased strain on the sample causes the non-covalent, low-affinity bonds keeping the mucin gel together to break. This leads to lower elastic modulus values because the energy contained within the bonds dissipates. The phase angle values similarly increase because the ratio of G'' and G' increase, meaning the samples show relatively more liquid-like properties. The G' values for the G12, G24 and LFR treated sample do not follow the expectations. It is likely that the response of the samples are too low to achieve high enough signal to noise ratios for accurate measurements. However, the phase angle values conform to the theory more than the G' values. In every sample except for the G12 treated one, the phase angle values increase with increasing strain. Both G' and G'' decrease at higher strain, but G'' values decrease less relative to G' giving rise to higher phase angle values.

Another interesting point to make is that PG mucin control sample seems to be less resistant to deformation. According to the strain sweeps that were done with all samples, the control showed a steeper downward slope than all the treated samples as the strain increased. Although the data from the strain sweeps are not given here, it still becomes apparent from Figure 17 where the G' and δ values for the control sample change more drastically between the frequency sweeps at different strains. Studies has shown that muco-adhesive polymers generally stabilize the mucus gel, increasing the resistance to deformation through an act of synergism (Madsen et al., 1998b). This has been ascribed interactions between mucin and the muco-adhesive polymer in the form of non-covalent bonding (hydrogen bonds, electrostatic interactions) (Madsen et al., 1998a).

As mentioned, the effect of alginate LFR 5/60 on PG mucin was surprising compared to the observed effect of LFR on PSIM (depicted in Figure 20). It was therefore decided to perform another frequency sweep with a new sample of PG mucin treated with LFR. The replicate showed even lower values of G' than before (data not shown). In order to validate that the results were not a consequence of the duration of freezing, two PG mucin control samples were rheologically tested since the control showed higher response than the other treated samples. One of the samples were from the original rehydrated batch of PG mucin, while the other were from a second batch that had been frozen for a shorter period of time. The frequency sweeps of both replicates are given in Figure 21 at constant strain 1E-3. There is a clear discrepancy between the initial control sample and these replicates. Both replicates in Figure 21, although not equal, have values of G' under 10 Pa, while the initial control sample had G' values between 20 and 40 Pa (Figure 19). Based on these findings it was hypothesized that the act of freezing might disrupt the PG mucin network, not the length of subzero storage. If this were to be true, the only possible explanation would be that water upon solidification forms ice crystals that could physically damage the mucin latticework in different degrees depending on the amount of crystals formed. There are disagreements in literature regarding the effect of freezing on mucus samples. One research group determined that freezing of CF sputum samples did not have any significant effect ($p < 0.05$) on G' and G'' values (Sanders et al., 2000), while other groups have found that freezing markedly lowered G' values for gastrointestinal mucus (Bøgh et al., 2013, Bell et al., 1984, Boegh et al.) presumably due to ice crystal formation. Here, the effect of freezing could have been more profound because the PG mucin was frozen in small Eppendorf tubes, which could have been a contributing factor to increased disruption due to ice crystal formation.

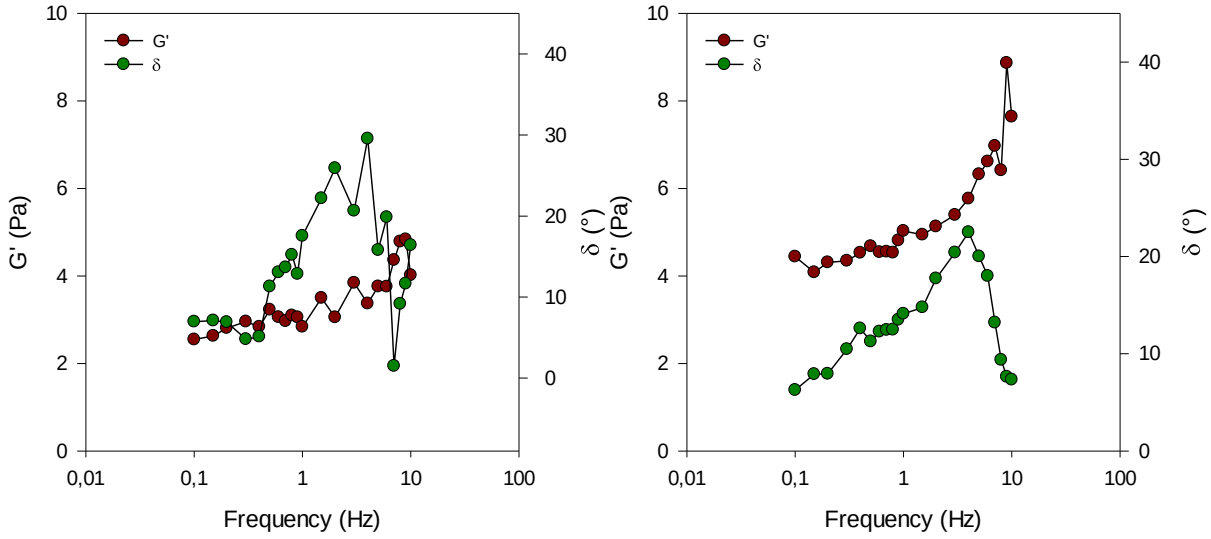

Figure 21. Elastic modulus (G') and phase angle (δ) values of two replicates of porcine gastric (PG) mucin control (saline) sample. Concentration of PG mucin in MQ-water was 40 mg/mL. Values for both graphs are from frequency sweeps at 10°C from low to high frequency with constant strain 1E-3 and 1E-2 Pa start stress. Cone dimension was C 40 1 ETC. The sample to the left is from the first batch of rehydrated PG mucin that had been frozen 55 days, while the sample to the right is from the second batch of rehydrated PG mucin that had been frozen for 24 days.

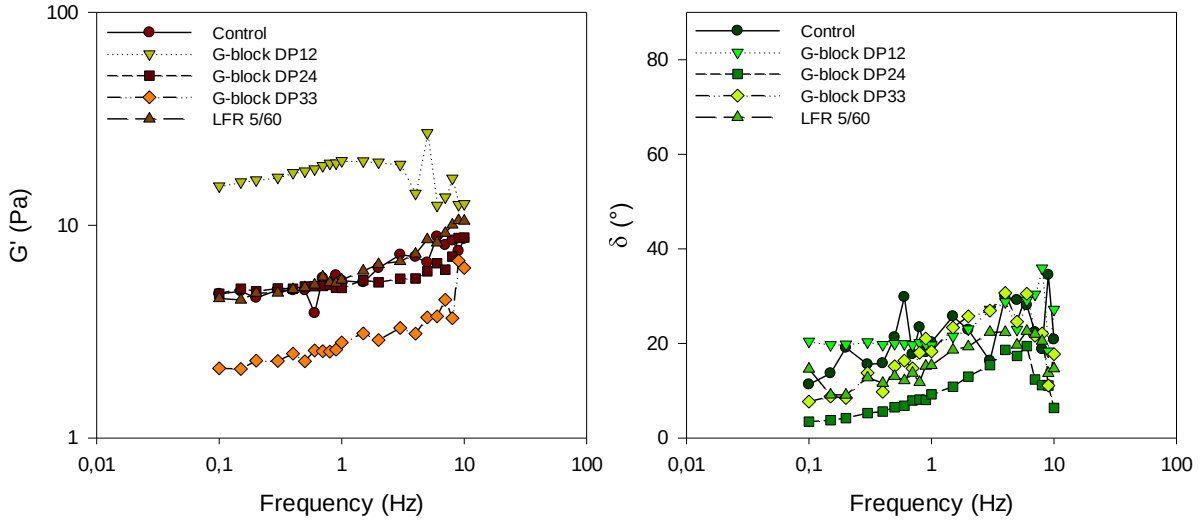

Figure 22. Elastic modulus (G') and phase angle (δ) values of porcine gastric (PG) mucin control (saline) and PG mucin treated with alginate G-block DP_n 12, alginate G-block DP_n 24, alginate G-block DP_n 33 and alginate LFR 5/60 compared. The concentration of PG mucin in MQ-water was 40 mg/mL and the concentration of alginate was 4.7 mg/mL. All values are collected from frequency sweeps at 10 °C from low to high frequency at constant strain 1E-3 and 1E-2 Pa start stress. Cone dimension was C 40 1 ETC.

In order to eliminate the potential freezing issue, it was decided to redo frequency sweeps at 1E-3 strain on freshly rehydrated PG mucin control sample and PG mucin treated with alginates. The new batch of PG mucin was hydrated for 72 hours in storage at 3 °C with gentle stirring. Concentration of PG-mucin in MQ-water was 42.84 mg/mL (to achieve a final concentration of 40 mg/mL after addition of alginate/saline). This batch was left to hydrate for a longer period of time under the assumption that the observed rheological impact of hydration time on PG mucin rheology would diminish over time. Therefore, because the samples were going to be tested on the same day, with 5 hours separating the first and last experiment, the new batch of PG mucin was left to hydrate 24 hours longer than before.

Figure 22 shows elastic modulus and phase angle values from frequency sweeps of the freshly rehydrated PG mucin treated with various alginate molecules and the PG mucin control sample compared. This time, the G12 treated PG mucin has the highest elastic modulus values. The G33 treated sample has the lowest, while the remaining samples are bundled together in between the extremes. These results are puzzling, and do not coincide with previous findings or literature (Draget and Taylor, 2011, Draget, 2011, Taylor et al., 2007, Taylor et al., 2005b, Taylor Nordgård and Draget, 2011). The phase angle values for all samples do not provide more clarity. The graph is crowded with noise, and there is a larger difference between the samples than before (Figure 19). As mentioned earlier the elastic modulus values of mucus samples can vary greatly between replicates of mucus (Boegh et al., Sanders et al., 2000). However, this sample contains only mucin molecules without the other inherent substances of mucus. PG mucin is therefore not as inhomogeneous as native mucus, and should in theory have more stable values of G'. A possible explanation for the observed inconsistencies is that the PG mucin lot#2 suffered from instabilities greater than first anticipated. The response from the sample was low in every experiment with torque values between 1E-7 and 1E-8 Nm. These were very low values compared to the other native mucus samples which had torque values between one and two decades higher, meaning that in every experiment with PG mucin the signal to noise ratio was extremely low. This could have led to the observed differences in elastic modulus and phase angle values between replicates. The reason might be that the purification method of PG mucin unintentionally degraded the mucin molecules. Another reason could be the small observed changes in pH between batches.

Supporting information that the signal to noise ratio in PG mucin samples was very low, is given by comparing Lissajous data from PG mucin and PSIM in Figure 23. Lissajous plot shows the relationship between stress and strain, which should follow an elliptic curve since PG mucin is a viscoelastic material (Deshpande et al., 2010). Figure 23 shows the Lissajous plot of a control sample at 1 Hz frequency from a frequency sweep of frozen PG mucin and from a frequency sweep of PSIM. Lissajous data from the

other PG mucin samples are not given, but they show a similar degree of noise as the PG mucin control sample. The Lissajous data from the PSIM control sample follows an even elliptical curve. Also, the three iterations are similar, which suggest that the measurements are stable. The PG mucin control sample, on the other hand, show a high degree of noise. The data does not follow any defined curve, and the iterations are in disagreement. These are clear signs that the PG mucin sample is unstable and that the response is low. Please note that these two graphs cannot be directly compared data point to data point because they are collected from different frequency sweeps run with different parameters. The right graph (PSIM) is included only to serve as a reference to how Lissajous plot should look in rheologically stable samples.

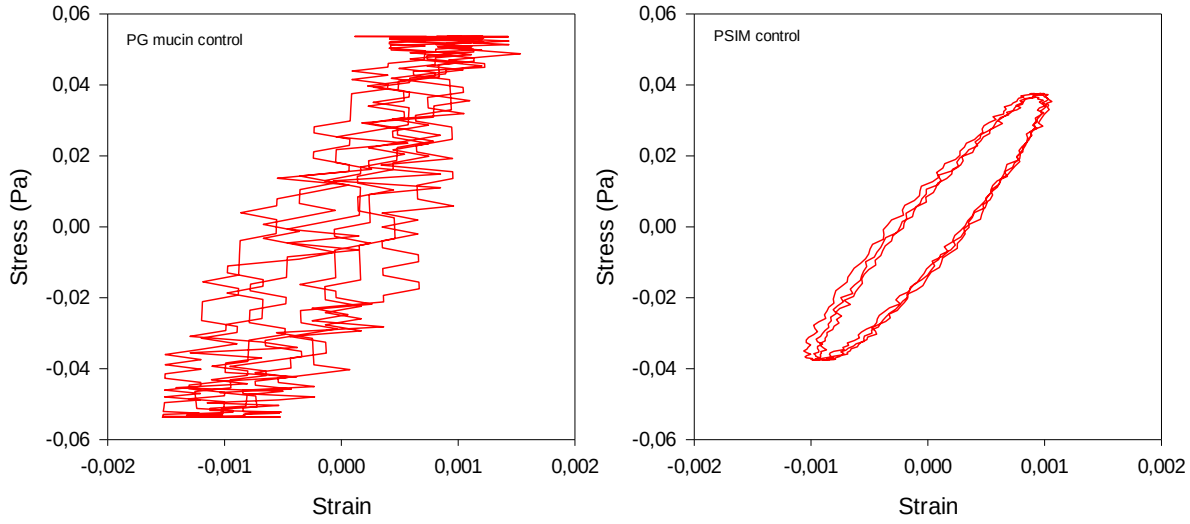

Figure 23. Stress plotted against strain (Lissajous plot) at 1 Hz frequency for porcine gastric (PG) mucin control to the left and porcine small intestinal mucus (PSIM) control to the right. The Lissajous data for PG mucin were collected from a frequency sweep at 10 °C from low to high frequency with constant strain 1E-3 and 1E-2 Pa start stress, while the Lissajous data for PSIM were collected from a frequency sweep at 20 °C from low to high frequency with constant strain 1E-3 and 1E-2 Pa start stress. Cone dimension for PG mucin was C 40 1 ETC and C 40 4 ETC for PSIM. Three iterations per data point.

Even though the mechanical response of PG mucin entails that the rheological effect of alginate is inconclusive, it should still be possible to investigate the mobility in treated PG mucin samples using multiple particle tracking. Particle tracking is a non-invasive technique (Selvaggi et al., 2010), and the results should therefore be viable. Carboxylated polystyrene nanoparticles (200 nm) were mixed with isotonic saline (control), alginate G-block DP_n 12, alginate G-block DP_n 24, alginate G-block DP_n 33 and alginate LFR 5/60 solutions respectively. The resulting nanoparticle solutions were added to PG mucin at a concentration of nanoparticles of 0.0025 %. The final concentration of PG mucin was 40 mg/mL, and the final concentration of alginate was 4.7 mg/mL. Mobility was investigated

by taking images every 70 ms for 20.09 seconds. The mean-square displacement (MSD) and effective diffusivities (D_{eff}) values were calculated based on a video microscopy series of every PG mucin-nanoparticle sample. MUC5AC is a key constituent of tracheobronchial, cervical and gastric mucus (Gendler and Spicer, 1995), and is the main determinant of the mucus gel-like properties (Lieleg et al., 2010). Since PG mucin consists of MUC5AC and is structurally related to human mucin (Turner et al., 1999), it should be a reasonable substitute to mucus for investigating particle mobility. Particle mobility depends on the steric and interactive filtering abilities of mucus (Lieleg et al., 2010).

Figure 24 shows MSD values for PG mucin control sample and PG mucin treated with the four different alginates plotted against time scale (τ). The figure also shows the MSD values of the carboxylated nanoparticles in water depicted in the bottom right graph. The graph is given as perspective on how mobility in a low viscosity liquid lacking latticework looks. The movement of particles in water is very uniform because water does not contain any restricting matrix and carries no charge, and the velocities are high because the viscosity of water is much lower than that of PG mucin. PG mucin control and PG mucin treated with G24 and LFR show a wide distribution of MSD trajectories. This indicates that particles in the solution move with different speed which is common behaviour for particles immersed in an inhomogeneous medium (Crater and Carrier, 2010). Heterogeneity in particle velocities arise from variations in pore sizes; particles will have increased mobility as they traverse through larger pores, and decreased mobility as they traverse through tighter pores (Dawson et al., 2003). Research has shown that particles with sizes up to 500 nm can move through mucus (Lai et al., 2009), but that with larger particle sizes the MSD trajectories becomes more uniform (Dawson et al., 2003). This is because the larger particles do not have free passage to move through pores, and must therefore follow restricted pathways (where the pore sizes are largest) resulting in uniform movement of particles. As can be seen in Figure 24, both the G12 treated and the G33 treated PG mucin sample have narrower distributions of MSD trajectories. The fastest and the slowest populations seen in the control sample, are not recognizable in the G12 or the G33 treated sample. This suggests that G12 and G33 treatment, not only open the smaller pores, but also diminishes the larger pores within the mucin structure. Possibly, the alginate G-blocks could cause large PG mucin pores to collapse due to alginate-mucin interactions, while increasing the smaller pore sizes by competitive inhibition of mucin-mucin interactions. A similar scenario has been seen in CF mucus with treatment of rhDNase (Dawson et al., 2003), where the authors proposed pore collapse due to entanglements. In the G12 and G33 samples there still exists some larger pores indicated by a small population of particles with high velocity. It was expected that the various alginate molecules would all show a narrower distribution, because alginate is a muco-adhesive that interacts with mucin molecules (Taylor Nordgård and Draget, 2011), which potentially changes mucin structural orientation. Granted, there are a lot of inconsistencies in the bulk

rheological measurements, but under the assumption that the observed rheological effect portray some truth, all alginate samples weakened the gel. It is therefore odd that especially G24 treatment of PG mucin did not cause a narrower distribution, since G24 has a molecular weight between G12 and G33 that both showed more uniform movement of particles through the sample. One explanation could be that G12 and G33 molecules are better distributed in the sample, and the effect is therefore observed in general for the particle population. As for the G24 and the LFR treated PG mucin samples, the effect might be localized, which leads to subpopulations with large differences in velocities.

Another important aspect of mobility to take into effect is the interactive part. At ambient PG mucin pH (~4.5) the nanoparticles should be able to interact by electrostatic interactions through negative charges from carboxyl croups, hydrogen bonding through protonated carboxyl groups (due to acidic pH) and hydrophobic interactions through hydrophobic polystyrene beads (depending on the density of the coating). This means that the impediment of movement through PG mucin is influenced by several different interaction mechanisms. Most likely, mucin and particles would interact though all three types of interactions mentioned. However, the addition of alginate potentially changes the interactions between mucin and nanoparticles. Alginate is thought to bind to mucin molecules through electrostatic interactions with positively charged amino acids (Taylor Nordgård and Draget, 2011). Such binding would hide these interaction sites from the nanoparticles, causing less restrictive movement. In addition, because alginates also interact through hydrogen bonds due to some degree of protonation, they could potentially also hide hydrogen-binding sites from the nanoparticles.

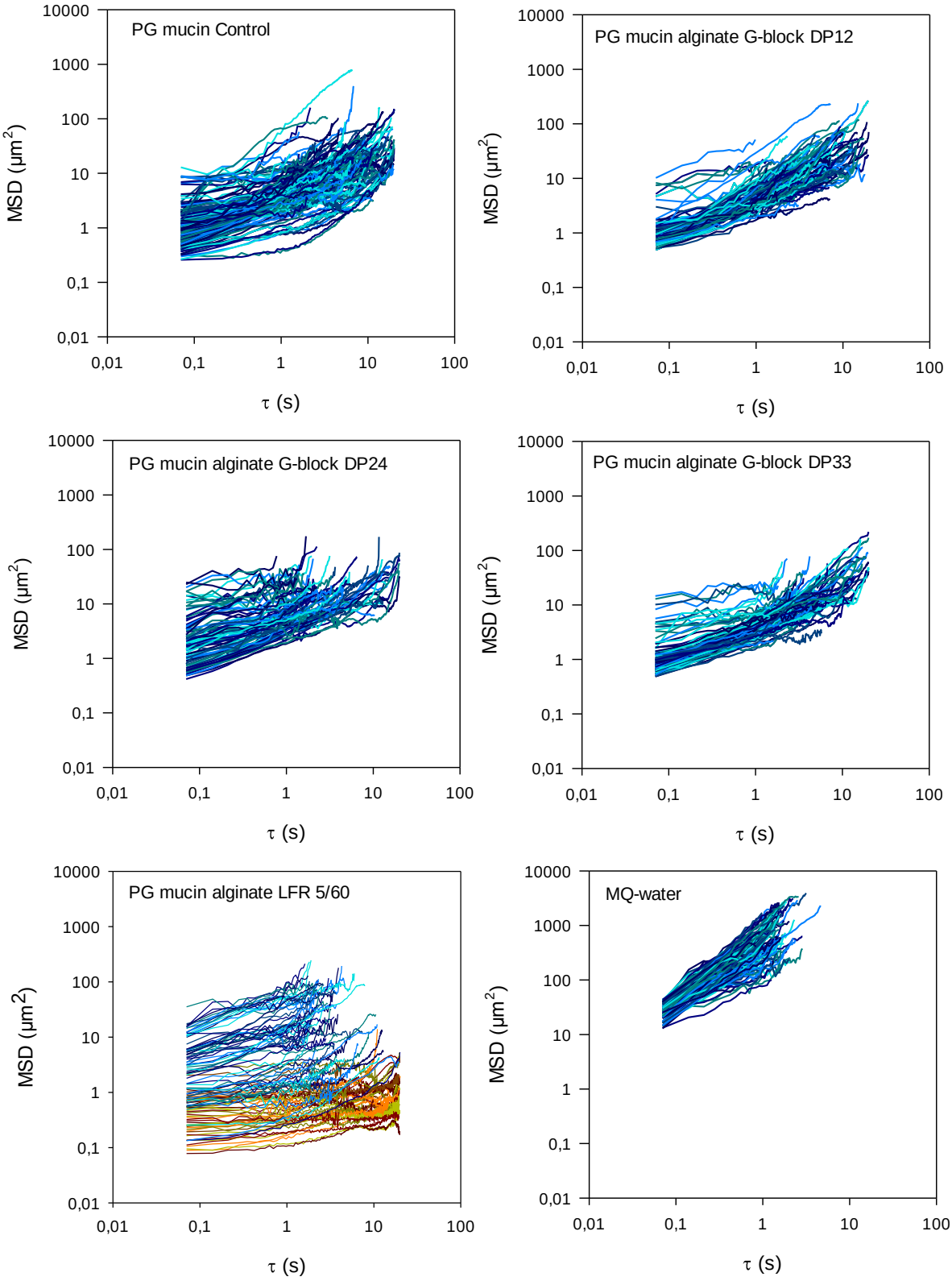

Figure 24. Mean-square displacement (MSD) values for MQ-water, porcine gastric (PG) mucin control and PG mucin treated with alginate G-block DP_n 12, alginate G-block DP_n 24, alginate G-block DP_n 33 and alginate LFR 5/60 plotted against time scale (τ). Fluorescent carboxylated nanoparticles (200 nm) were tracked by multiple particle tracking at a concentration of 0.0025 %. The particles were tracked for 20.09 s. Concentration of PG mucin was 40 mg/mL and concentration of alginate 4.7 mg/mL. The number of particle trajectories in each case in approximately 100.

An interesting point to make is that the velocity of particles immersed in PG mucin seem to scale with time scale. This is in contrast to particle movement through water where the particles have straight trajectories, which is typical for pure liquid materials (Selvaggi et al., 2010). This suggests that the behaviour must be caused by the mucin molecules. Indeed, such behaviour is typical for viscoelastic materials (Selvaggi et al., 2010), and it has been hypothesized that it arise from particles being trapped in mucin cages. At higher time scales the particle escape from these cages is more noticeable and the MSD values subsequently increase (Dawson et al., 2003, Crater and Carrier, 2010). The caging is most likely due to both steric hindrance and mucin-particle interactions.

The MSD values depicted in Figure 24 show some degree of noise, especially towards the later time scales. Some of it might be caused by the resolution of the confocal microscopy used to track the particles (i.e. signal-to-noise ratio), but it is mainly caused by inaccuracies in MSD values at long time scales (Saxton and Jacobson, 1997). The most obvious noise towards the ends of the MSD trajectories have been removed prior to being plotted, because it was crowding the graphs.

When tracking particles using multiple particle tracking, it is possible that the tracked trajectories follow the movements of the medium they are suspended in (Suh et al., 2005). Two randomly chosen trajectories for G12 treated PG mucin are given in Figure 25 and show that this is not the case here. The trajectories follow a randomized path, independent of each other. The trajectories also look like the start of a beads-on-a-string type of trajectory which is typical for sub-diffusive particles. This behaviour often arise from interactions holding a particle in place before it breaks free and moves on (Suh et al., 2005), and in the case of PG mucin, it could also symbol the pores. This means that each “bead” is an illustration of a particle trapped physically or by interactions, while the string is the transition between pores or the particle breaking free from their interactive prison. This is the type of movement that creates the time scale dependent increase in MSD values mentioned earlier. Note that not all the trajectories in all the samples are similar to the ones portrayed in Figure 25, but it illustrates that the measured movement of particles do not arise from movement of the mucin matrix.

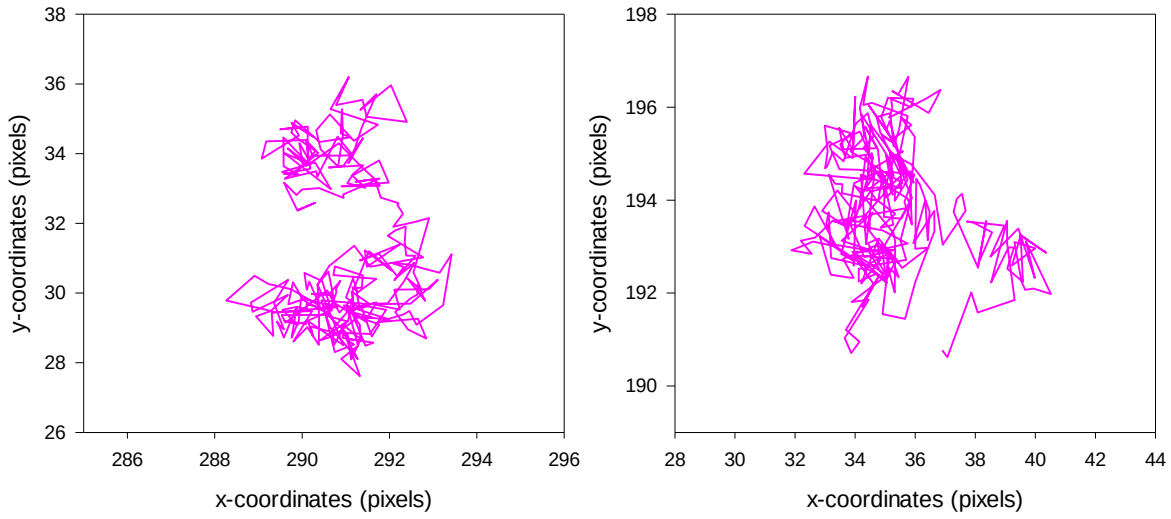

Figure 25. Particle movement in x- and y- direction for fluorescent carboxylated polystyrene nanoparticles (200 nm) in porcine gastric (PG) mucin treated with alginate G-block DPn 12. The concentration of nanoparticles was 0.0025 %, the concentration of PG mucin was 40 mg/mL and the concentration of alginate was 4.7 mg/mL. The particles were tracked using a CLSM Leica SP5 confocal microscope for 20.09 seconds.

The exception to the aforementioned explanation of particle mobility is the LFR treated sample. LFR treated PG mucin show many MSD trajectories with very low mobility, which distinguishes the LFR treated sample from the other alginate treated samples. The LFR treated sample seems to have two subpopulations of particles (shown with different colours in Figure 24). One is extremely immobile, with very low velocities, while the other population has similar trajectories to the G24 treated PG mucin sample. When tracking particles in the LFR treated PG mucin sample, aggregates of particles were observed. Figure 26 shows an image of LFR treated PG mucin compared with an image of PG mucin control, where the aggregates of nanoparticles can be seen as large green spots in the image to the left. It is hard to say what might have caused the aggregation, but it definitely has something to do with alginate LFR 5/60. The alginate-nanoparticle solutions and the control-nanoparticle solution were added to two different batches of mucin (one that had been frozen, and one unfrozen). In both cases, only the sample treated with LFR showed aggregates. SEC-MALLS characterization of the LFR sample showed that the sample contained some aggregates, however, the volume of aggregates was negligible. In any case, the aggregates could not consist entirely of LFR molecules, because the negatively charged alginate molecules would repel the carboxylated nanoparticles due to electrostatic repulsion. A more reasonable explanation would be that the aggregates consist mainly of mucin molecules because mucin can trap and immobilize the nanoparticles through electrostatic adhesiveness (and possibly hydrogen bonding and hydrophobic

interactions), and that these mucin aggregates were caused by the LFR molecules. Whether this is because of impurities in the LFR sample or simply due to LFR-mucin interactions is impossible to say.

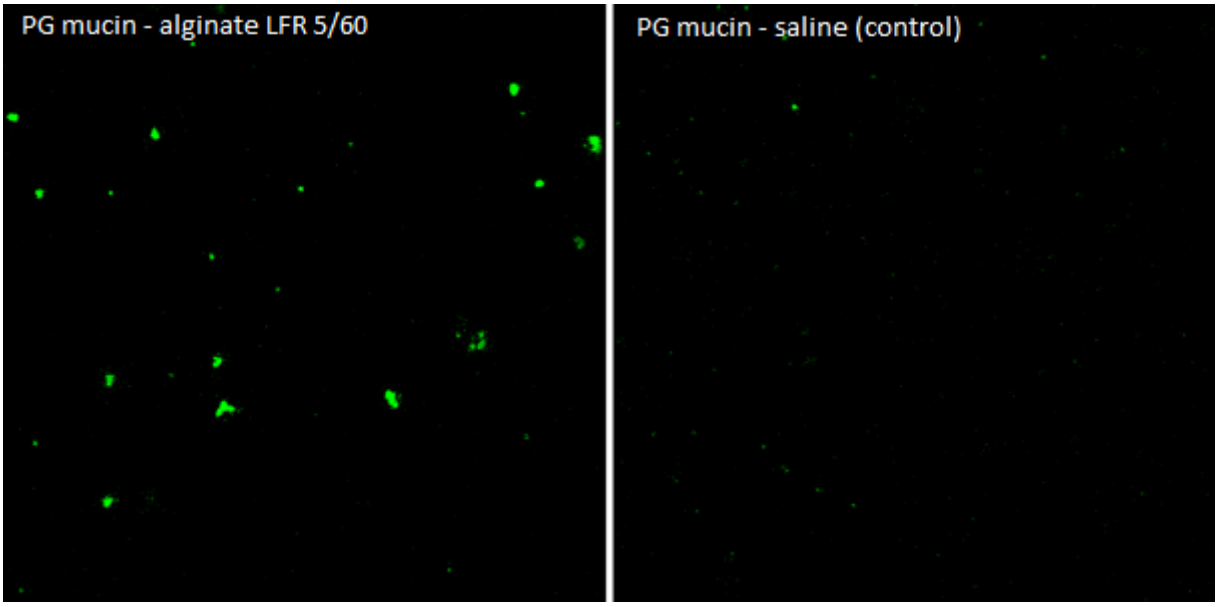

Figure 26. Image of PG mucin treated with alginate LFR 5/60 to the left, and PG mucin with physiological saline (control) to the right. The images show fluorescent carboxylated particles (200 nm) distributed in each respective sample tracked by a CLSM Leica SP5 confocal microscope. Particle concentration was 0.0025 %. Concentration of PG mucin was 40 mg/mL and concentration of alginate 4.7 mg/mL. The zoom of the microscope is the same in both cases, and they were tracked with the same parameters.

The carboxylated polystyrene nanoparticles were only tracked in x- and y- direction (xyt acquisition mode). Naturally there would be particle movement in z- direction as well as in x- and y- direction. In order to have an idea on how the particles move in all directions, the percentage of tracked particles was plotted against time scale (τ) in Figure 27. The figure shows how many of the original number of tracked particles that are still visible at any given time scale. Particle movement in MQ-water is again given as a perspective on how quickly the particles move out of camera focus or out of tracking parameters. As before, because water does not react or physically impede the particles, the high velocities make them only traceable to $\tau = 5$ seconds. In all the PG mucin samples, some particles are tracked over the entire time scale. This supports the fact that PG mucin is a porous network of cross-linked mucin monomers, because the movement of these particles are restricted to stay in x- and y-direction. It also restricts the particles to move too long in x- and y- direction, which would cause the software program to identify them as two separate particles. Based on the longest MSD trajectories in Figure 24 it is apparent that the particles does not lack mobility (apart from one subpopulation of LFR

treated PG mucin), so they are either held in xy-plane through interactions with mucin (and possibly alginate) molecules, by steric hindrance, or simply because of statistics (only traceable particles will remain towards the end no matter the cause).

All alginate treated samples appear to have a steeper initial drop in value from 100 % tracked particles than PG mucin control. This means that the movement within the alginate treated PG mucin is greater than the movement within PG mucin control in all directions. However, the value of tracked particles for the LFR treated sample levels out after the initial drop, which refers to the immobile subpopulation in the LFR treated PG mucin sample. G12 and G33 treated PG mucin display similar trends in Figure 27. The amount of tracked particles steadily decrease over time scale. This is in agreement with the results depicted in Figure 24 that suggested more uniform movement of the carboxylated particles compared to the control sample. PG mucin treated with G24 seems to have the steepest downward slope, and displays higher movement than any other mucin sample. This is somewhat surprising, because G24 treated PG mucin seems to have a large part of its matrix intact according to Figure 24. As mentioned earlier, a localized effect of G24 could explain these results.

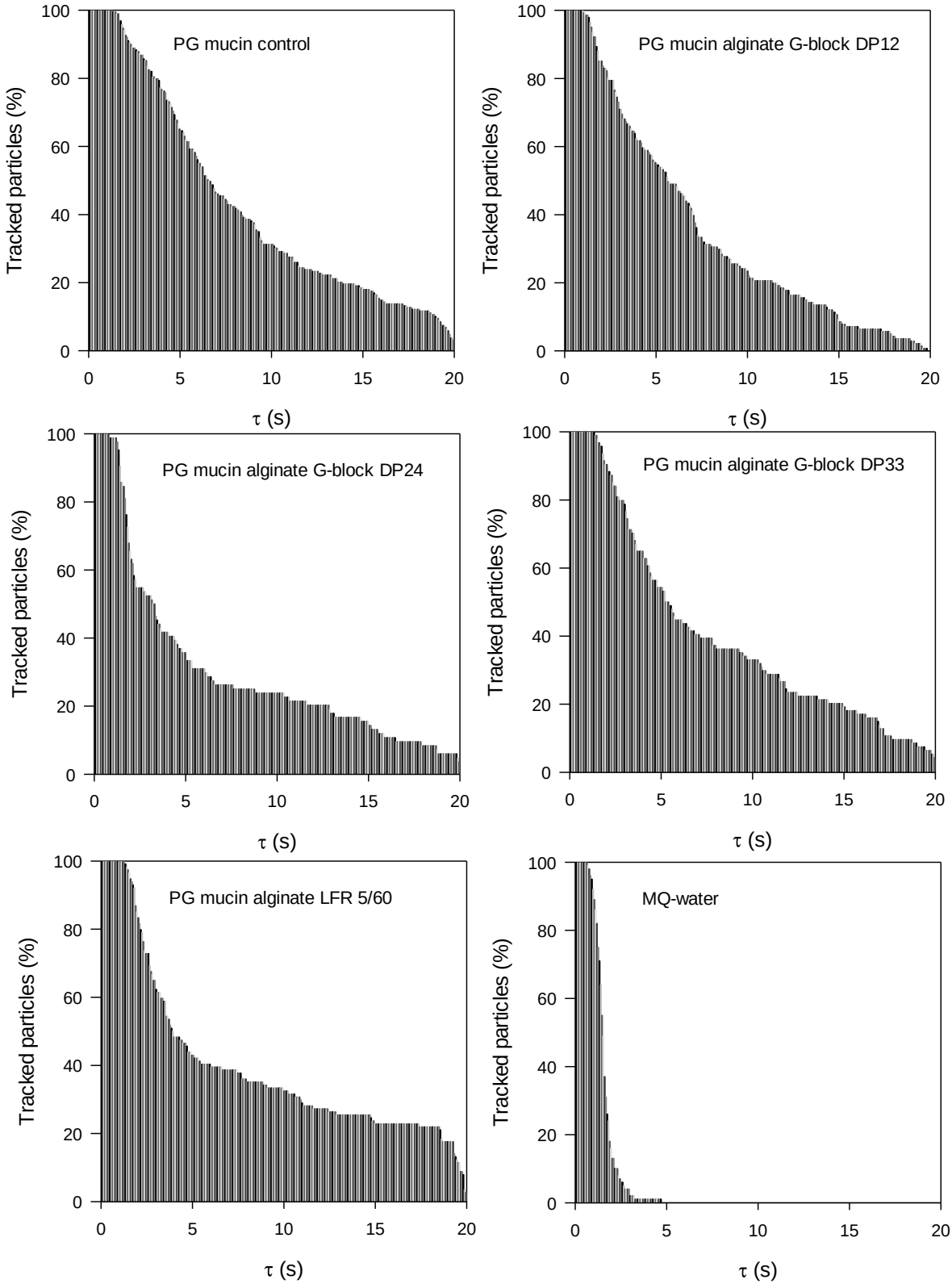

Figure 27. Percentage of tracked particles in porcine gastric (PG) mucin control and PG mucin treated with alginate G-block DP_n 12, alginate G-block DP_n 24, alginate G-block DP_n 33 and alginate LFR 5/60 plotted against time scale (τ). The values are based on the MSD values in Figure 24. Fluorescent carboxylated nanoparticles (200 nm) were tracked by multiple particle

tracking at a concentration of 0.0025 %. The particles were tracked for 20.09 s. Concentration of PG mucin was 40 mg/mL and concentration of alginate 4.7 mg/mL.

Investigating effective diffusivities (D_{eff}) is a good way of determining whether particle movement is active, diffusive or sub-diffusive (Suh et al., 2005). Ensemble effective diffusivity ($<D_{eff}>$) values for PG mucin control and PG mucin treated with G12, G24, G33 and LFR is plotted against time scale (τ) in Figure 28. The vertical lines in the graph corresponds to 80 % of the tracked particles remaining in camera focus or within tracking parameters. The figure shows that the carboxylated polystyrene nanoparticles in all samples are sub-diffusive, and that the mobility is greatest for LFR and G24 treated PG mucin at short time scales. However, when 80 % of the tracked particles have disappeared out of camera focus or out of tracking parameter, the two samples become less mobile. The LFR treated PG mucin sample has immobile subpopulations as mentioned before, which is why the ensemble effective diffusivities drops quickly. At longer time scales the G12 and G33 treated PG mucin samples show highest particle mobility. This supports the MSD data suggesting a more uniform movement through G12 and G33 treated PG mucin. The even $<D_{eff}>$ slopes indicate that the samples does not contain any marked subpopulations.

Interestingly, the diffusivity through PG mucin control sample is very similar to the diffusivity through G12 and G33 treated PG mucin, at least up until 7 seconds. This is probably because the sample displayed a wide distribution of MSD trajectories (Figure 24), with many particles exhibiting high velocities. The reason that PG mucin control has a population of particles with high speed could be the amount of ions in the solution. The control sample consist of isotonic saline, and even though the ionic strength is equal between the control and the alginate treated samples, there still exists more ions in the control solution compared to the alginate solution. This is because alginate are multivalent ions, which contribute more to the ionic strength than monovalent ones (Smidsrød et al., 2008). Because saline consists only of monovalent ions, more ions need to be added to match the ionic strength of the alginate solution. The positively charged monovalent ions are thought to be able to shield the negatively charged surface of the carboxylated polystyrene nanoparticles, which decreases the electrostatic interactions between the nanoparticles and the mucin molecules (Lieleg et al., 2010). Such decrease in interactions between mucin molecules and nanoparticles means the particles are shielded from interactive impediment, and the particles will only be hindered physically. This might cause a general increase in particle mobility (Lieleg et al., 2010).

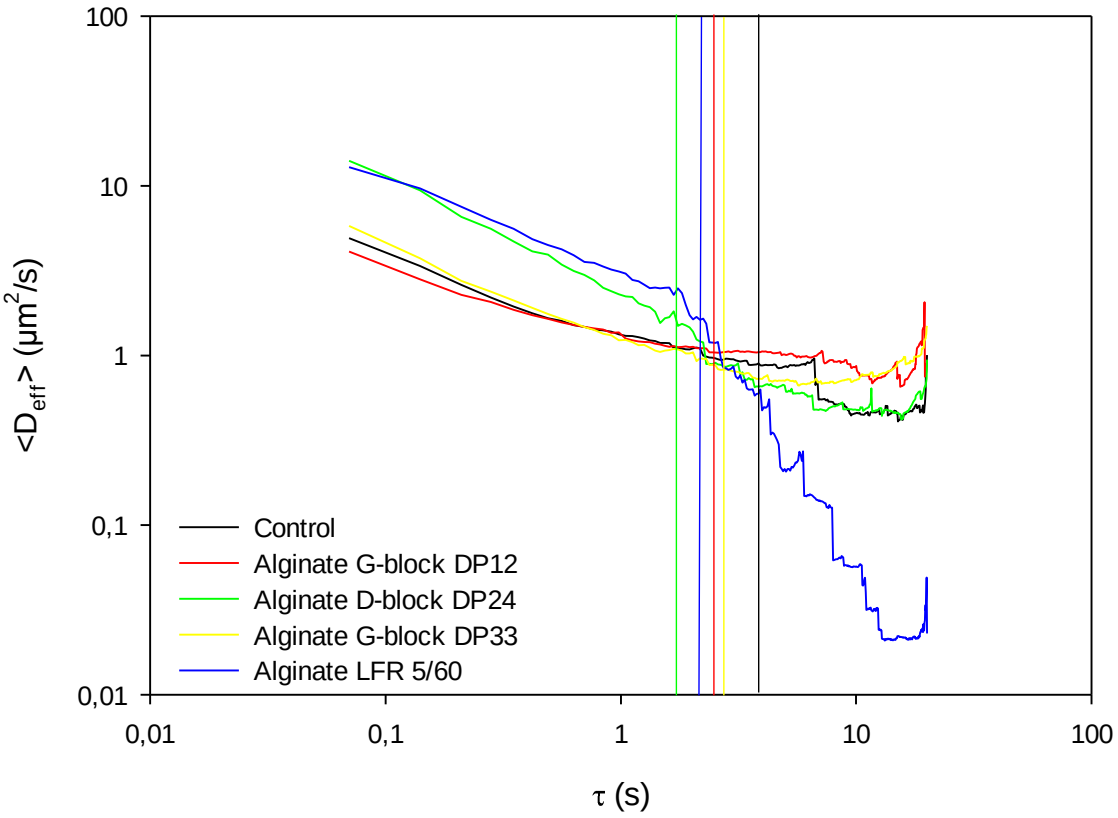

Figure 28. Ensemble effective diffusivities (<Deff>) of porcine gastric (PG) mucin control and PG mucin treated with alginate G-block DP_n 12, alginate G-block DP_n 24, alginate G-block DP_n 33 and alginate LFR 5/60 plotted against time scale (τ). The trajectories are based on the MSD values in Figure 24. Fluorescent carboxylated nanoparticles (200 nm) were tracked by multiple particle tracking at a concentration of 0.0025 %. The particles were tracked for 20.09 s. Concentration of PG mucin was 40 mg/mL and concentration of alginate 4.7 mg/mL.

3.4 The effect of alginate on native porcine tracheobronchial mucus

The continuance of the results in this thesis is aimed at human tracheobronchial mucus. It is therefore interesting to investigate the effect of alginate on porcine tracheobronchial mucus (PTBM) directly, because the results should be more comparable than the effect of alginate on bio-similar mucus, PSIM or PG mucin due to more similarities in gene products and general molecular composition. The trachea of newly slaughtered pig were opened, and the mucus scraped using a metal spoon. The mucus was collected in Eppendorf tubes and stored at -20 °C. Only the effect of alginate G-block DP_n 12 was investigated due to small amounts of PTBM available. Most of the mucus collected

was tainted with blood, which could have unfortunate impact on PTBM rheology. G12 was mixed with the PTBM at a concentration of 3.4 mg/mL. Preferably, the concentration of alginate should have mimicked that of the other mucus/mucin systems, but the quantity of PTBM did not allow for that. In addition, the G12 treated sample was rheologically tested at different values of stress and strain than the other systems, but assuming all values were measured within each respective samples linear viscoelastic area, they can still be compared.

Elastic modulus and phase angle values of the G12 treated PTBM and PTBM untreated are compared and plotted against frequency in Figure 29. There was unfortunately not enough sample to make a control with isotonic saline for the treated PTBM, and some of the dissimilarities between the samples in Figure 29 might arise from differences in ionic strength. It is also probable that some of the differences arise from the dilution that has happened with the addition of alginate G-block DP_n 12. Studies have shown that an increase in ionic strength can lead to a significant lowering of PG mucin viscosity (gel weakening) (Bhaskar et al., 1991). However, based on literature (Taylor Nordgård and Draget, 2011, Draget and Taylor, 2011, Taylor et al., 2007, Draget, 2011) and the observed effect of G12 on PSIM, the effect of G12 on PTBM seems legitimate. It is therefore safe to conclude that alginate G-block DP_n 12 weakens mucus gel. The effect of G12 on PTBM seems to be larger than on PSIM even after taking some differences due to dilution and ionic strength into account. The elastic modulus values of the PSIM samples were very varying, and drawing any conclusions from G' values cannot be supported. The phase angle values, however, are more comparable, because they have been shown to be more stable throughout this thesis and literature (Sanders et al., 2000). One reason for the increased effect of G12 on PTBM compared to PSIM could be because of different alginate concentration. Alginate G-block DP_n 12 was added to PTBM at a lower concentration than to PSIM. However, had the observed differences been because of concentration, it would have been expected that alginate had a bigger weakening effect on PSIM instead of PTBM. A more sound explanation would relate to differences in mucus composition and mucin gene products. PSIM and PTBM both contain many different inherent substances. The quantity of these compounds would naturally differ from the two samples because the mucus have different responsibilities regarding particulate transport and protective capabilities. PSIM is more used to harsher environments in general, and could have an increased tolerance towards potential threats. Purely based on the results gathered here, it is not possible to pinpoint why the effect of G12 is more pronounced on PTBM than on PSIM.

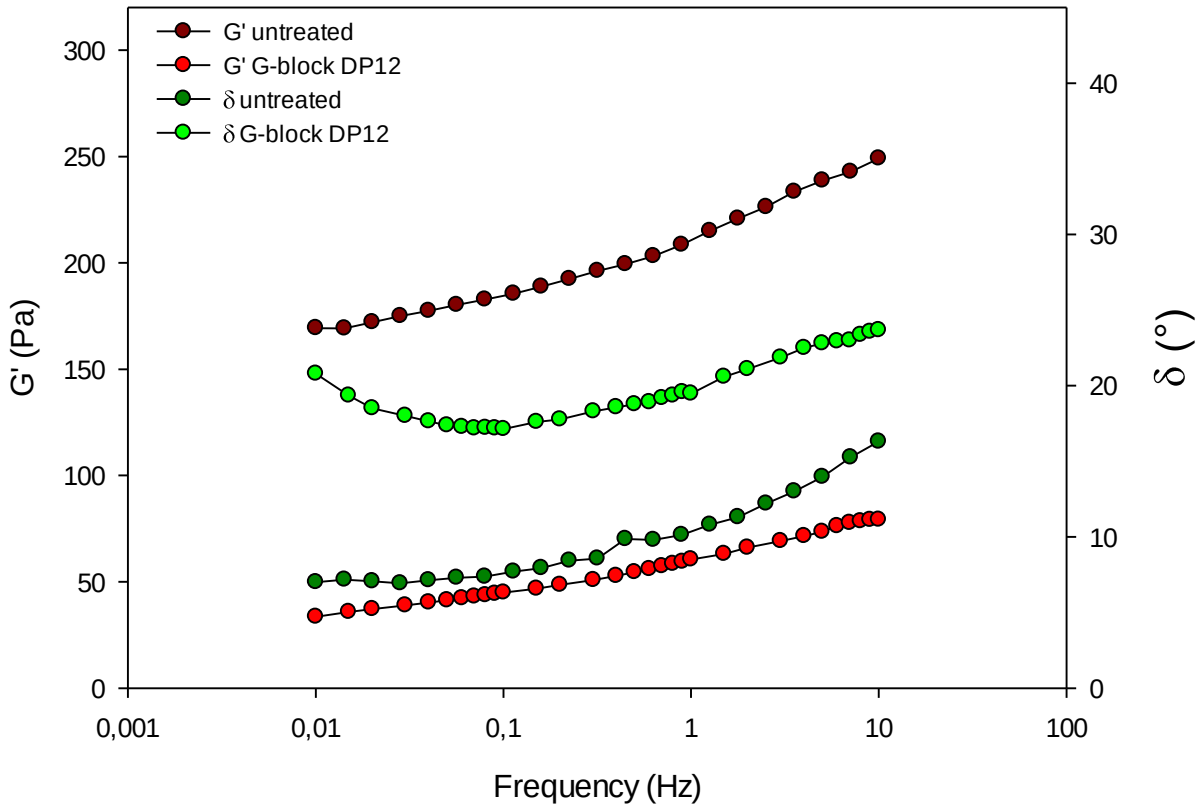

Figure 29. Elastic modulus (G') and phase angle (δ) values for untreated porcine tracheobronchial mucus (PTBM) and PTBM treated with alginate G-block DPn 12 compared. Concentration of alginate was 3.4 mg/mL. Values are from frequency sweeps at 20 °C from low to high frequency at constant strain 5E-2 and 1 Pa start stress. Cone dimension was C 25 1 ETC.

4 Conclusion

The effect of alginate G-blocks and LFR 5/60 have been investigated on bio-similar mucus, PSIM, PTBM and PG mucin throughout this thesis. The bio-similar mucus reacted very differently to the presence of alginate compared to PSIM, even though it is meant to represent a model system of PIM. This is because of the structural differences. The bio-similar mucus gel is stabilized by both polyacrylic acid and commercialized mucin, which means that both polymers have potential to interact with the alginate molecules. It is therefore likely that polyacrylate-alginate electrostatic repulsion led to phase separation, causing the G-block DP_n 33 and LFR 5/60 treated bio-similar mucus samples to have weaker gel profiles than G-block DP_n 12 treated bio-similar mucus and control. The bio-similar mucus is therefore not viable as a model system for PIM behaviour under influence of other muco-adhesive molecules – at least other negatively charged polymers.

Both lot#1 and lot#2 of PG mucin suffered from instabilities. PG mucin rheology was heavily influenced by pH, temperature, hydration time and low mechanical response. The rheological effect of alginate on PG mucin is therefore inconclusive and the experiments should be redone with a more mechanically stable PG mucin sample. Based on PSIM and PTBM, alginate G-block DP_n 12 has a weakening effect on mucus gel structure. Alginate G-block DP_n 33 and LFR 5/60 have a minor strengthening effect on PSIM. The difference between PSIM control and PSIM treated with G-block DP_n 33 was minimal, and there may therefore exist alginate molecules with molecular weights close to that of G-block DP_n 33 that does not influence mucus rheology. G33 treated PG mucin, in addition to G12 treated PG mucin, had highest mobility at long time scales. The MSD trajectories were also narrower, which is indicative of uniform pore sizes. The effect is possibly a consequence of alginate-mucin interactions through electrostatic forces and hydrogen bonding causing the smaller pores to open up, while collapsing some of the larger pores. G24 and LFR treated PG mucin showed a wide distribution of MSD trajectories indicative of large subpopulations. This also became apparent by expressing the highest particle mobility at short time scales, and lowest mobility at long time scales. Aggregates were observed in the LFR treated PG mucin sample, most definitely caused by the addition of LFR, but the underlying reason is unknown.

The rheological effect of alginate G-block DP_n 33 on PSIM and the effect on PG mucin particle mobility supports the hypothesis that there exists a specific molecular weight alginate molecule that increases particle mobility without influencing mucus rheology, but further experiments should be performed to verify this.

5 Future work

Molecular weight alginate G-blocks with chain lengths close to DP_n 33 could according to the results obtained in this thesis have potential to influence particle mobility without affecting mucus rheology. However, more work is needed to ascertain that this is true for native tracheobronchial mucus. The rheological impact of alginate G-block DP_n 33 has only been investigated on porcine small intestinal mucus here, which contains different gene products and molecular composition compared to tracheobronchial mucus. Porcine gastric mucin is a viable substitute, and the rheological effect of alginate on porcine gastric mucin should therefore be investigated further, with a sample that is mechanically stable. In addition, particle mobility should be studied in native mucus samples since they are more complex than porcine gastric mucin. The ideal scenario would be to investigate the effect of alginate on both particle mobility and rheology on native tracheobronchial mucus. For this purpose it might be a good idea to measure the microrheology, instead of the bulk rheology as is done in this thesis, because tracheobronchial mucus is hard to acquire in large quantities. In addition, particle tracking should be performed with particles with different sizes and surface characteristics to get a more dynamic view of what happens to the structure and function after addition of alginate. Future work should also include diffusion and permeability studies on mucus treated with alginate, and not just particle mobility.

References

BALLANCE, S., HOLTAN, S., AARSTAD, O. A., SIKORSKI, P., SKJAK-BRAEK, G. & CHRISTENSEN, B. E. 2005. Application of high-performance anion-exchange chromatography with pulsed amperometric detection and statistical analysis to study oligosaccharide distributions--a complementary method to investigate the structure and some properties of alginates. *J Chromatogr A,* 1093**,** 59-68.

BANSIL, R. & TURNER, B. S. 2006. Mucin structure, aggregation, physiological functions and biomedical applications. *Current Opinion in Colloid & Interface Science,* 11**,** 164-170.

BARNES, H. A., HUTTON, J. F. & WALTERS, K. 1989. *An introduction to rheology*, Elsevier.

BATES, D. V. 1989. *Respiratory function in disease,* Philadelphia, Saunders.

BATES, F. S. 1991. Polymer-Polymer Phase Behavior. *Science,* 251**,** 898-905.

BATES, F. S., MUTHUKUMAR, M., WIGNALL, G. D. & FETTERS, L. J. 1988. Thermodynamics of isotopic polymer mixtures: Significance of local structural symmetry. *The Journal of Chemical Physics,* 89**,** 535-544.

BELL, A. E., ALLEN, A., MORRIS, E. R. & ROSS-MURPHY, S. B. 1984. Functional interactions of gastric mucus glycoprotein. *International Journal of Biological Macromolecules,* 6**,** 309-315.

BHASKAR, K. R., GONG, D. H., BANSIL, R., PAJEVIC, S., HAMILTON, J. A., TURNER, B. S. & LAMONT, J. T. 1991. Profound increase in viscosity and aggregation of pig gastric mucin at low pH. *American Journal of Physiology - Gastrointestinal and Liver Physiology,* 261**,** G827-G832.

BOEGH, M., BALDURSDÓTTIR, S. G., MÜLLERTZ, A. & NIELSEN, H. M. Property profiling of biosimilar mucus in a novel mucus-containing in vitro model for assessment of intestinal drug absorption. *European Journal of Pharmaceutics and Biopharmaceutics*.

BUTTON, B., CAI, L.-H., EHRE, C., KESIMER, M., HILL, D. B., SHEEHAN, J. K., BOUCHER, R. C. & RUBINSTEIN, M. 2012. A Periciliary Brush Promotes the Lung Health by Separating the Mucus Layer from Airway Epithelia. *Science,* 337**,** 937-941.

BØGH, M., BALDURSDOTTIR, S. G., NIELSEN, M. H., MÜLLERTZ, A. & NIELSEN, H. M. 2013. Development and rheological profiling of biosimilar mucus. *Nordic Rheology Society. Annual Transactions,* 21**,** 233-240.

CAO, X., BANSIL, R., BHASKAR, K. R., TURNER, B. S., LAMONT, J. T., NIU, N. & AFDHAL, N. H. 1999. pH-dependent conformational change of gastric mucin leads to sol-gel transition. *Biophys J,* 76**,** 1250-8.

CELLI, J., GREGOR, B., TURNER, B., AFDHAL, N. H., BANSIL, R. & ERRAMILLI, S. 2005. Viscoelastic Properties and Dynamics of Porcine Gastric Mucin. *Biomacromolecules,* 6**,** 1329-1333.

CHARLTON, B. G. 2006. Why medical research needs a new specialty of 'pure medical science'. *Clinical Medicine,* 6**,** 163-165.

CONE, R. A. 2005. Chapter 4 - Mucus. *In:* JIRI, M., MICHAEL, E. L., JERRY, R. M., JOHN, B., LLOYD, M., WARREN STROBERA2 - JIRI MESTECKY, M. E. L. J. R. M. J. B. L. M. & WARREN, S. (eds.) *Mucosal Immunology (Third Edition).* Burlington: Academic Press.

CONE, R. A. 2009. Barrier properties of mucus. *Adv. Drug Delivery Rev.,* 61**,** 75-85.

CRATER, J. S. & CARRIER, R. L. 2010. Barrier Properties of Gastrointestinal Mucus to Nanoparticle Transport. *Macromolecular Bioscience,* 10**,** 1473-1483.

CRYSTAL, R. G. 1997. *The Lung: scientific foundations,* Philadelphia, Lippincott - Raven.

CU, Y. & SALTZMAN, W. M. 2009. Mathematical modeling of molecular diffusion through mucus. *Advanced Drug Delivery Reviews,* 61**,** 101-114.

DAVIES, J. M. & VINEY, C. 1998. Water–mucin phases: conditions for mucus liquid crystallinity. *Thermochimica Acta,* 315**,** 39-49.

DAWSON, M., WIRTZ, D. & HANES, J. 2003. Enhanced Viscoelasticity of Human Cystic Fibrotic Sputum Correlates with Increasing Microheterogeneity in Particle Transport. *Journal of Biological Chemistry,* 278**,** 50393-50401.

DESHPANDE, A. P., KRISHNAN, J. M. & KUMAR, S. 2010. *Rheology of complex fluids*, Springer.

DRAGET, K. I. 2011. Oligomers: Just background noise or as functional elements in structured biopolymer systems? *Food Hydrocolloids,* 25**,** 1963-1965.

DRAGET, K. I. & TAYLOR, C. 2011. Chemical, physical and biological properties of alginates and their biomedical implications. *Food Hydrocolloids,* 25**,** 251-256.

ENSIGN, L. M., CONE, R. & HANES, J. 2012. Oral drug delivery with polymeric nanoparticles: The gastrointestinal mucus barriers. *Advanced Drug Delivery Reviews,* 64**,** 557-570.

FRIEBOLIN, H. 1991. Basic one-and two-dimensional NMR spectroscopy.

FUONGFUCHAT, A., JAMIESON, A. M., BLACKWELL, J. & GERKEN, T. A. 1996. Rheological studies of the interaction of mucins with alginate and polyacrylate. *Carbohydrate Research,* 284**,** 85-99.

GASZNER, B., SIMOR, T., HILD, G. & ELGAVISH, G. A. 2001. The effects of the NMR shift-reagents Dy(PPP)2, Dy(TTHA) and Tm(DOTP) on developed pressure in isolated perfused rat hearts. The role of shift-reagent calcium complexes. *J Mol Cell Cardiol,* 33**,** 1945-56.

GENDLER, S. J. & SPICER, A. P. 1995. Epithelial Mucin Genes. *Annual Review of Physiology,* 57**,** 607-634.

GRASDALEN, H. 1983. High-field, 1H-n.m.r. spectroscopy of alginate: sequential structure and linkage conformations. *Carbohydrate Research,* 118**,** 255-260.

GRASDALEN, H., LARSEN, B. & SMIDSRØD, O. 1979. A p.m.r. study of the composition and sequence of uronate residues in alginates. *Carbohydrate Research,* 68**,** 23-31.

HOLMGREN, E. B. 2014. *Theory of drug development,* Boca Raton, Taylor & Francis.

HONG, Z., CHASAN, B., BANSIL, R., TURNER, B. S., BHASKAR, K. R. & AFDHAL, N. H. 2005. Atomic Force Microscopy Reveals Aggregation of Gastric Mucin at Low pH. *Biomacromolecules,* 6**,** 3458-3466.

HOUTMEYERS, E., GOSSELINK, R., GAYAN-RAMIREZ, G. & DECRAMER, M. 1999. Regulation of mucociliary clearance in health and disease. *European Respiratory Journal,* 13**,** 1177-1188.

KHANVILKAR, K., DONOVAN, M. D. & FLANAGAN, D. R. 2001. Drug transfer through mucus. *Advanced Drug Delivery Reviews,* 48**,** 173-193.

KING, M. 1998. Experimental models for studying mucociliary clearance. *European Respiratory Journal,* 11**,** 222-228.

KING, M., ZAHM, J. M., PIERROT, D., VAQUEZ-GIROD, S. & PUCHELLE, E. 1989. The role of mucus gel viscosity, spinnability, and adhesive properties in clearance by simulated cough. *Biorheology,* 26**,** 737-45.

KOČEVAR-NARED, J., KRISTL, J. & ŠMID-KORBAR, J. 1997. Comparative rheological investigation of crude gastric mucin and natural gastric mucus. *Biomaterials,* 18**,** 677-681.

KORNFELD, R. & KORNFELD, S. 1976. Comparative aspects of glycoprotein structure. *Annual Review of Biochemistry,* 45**,** 217-237.

KRISTIANSEN, A. Sequential parameters of alginate from ^{1}H NMR data. NTNU.

LAI, S. K., WANG, Y. Y. & HANES, J. 2009. Mucus-penetrating nanoparticles for drug and gene delivery to mucosal tissues. *Adv Drug Deliv Rev,* 61**,** 158-71.

LAMONT, J. T. 1992. Mucus: the front line of intestinal mucosal defense. *Annals of the New York Academy of Sciences,* 664**,** 190-201.

LEE, K. Y. & MOONEY, D. J. 2012. Alginate: Properties and biomedical applications. *Progress in Polymer Science,* 37**,** 106-126.

LEE, S., MÜLLER, M., REZWAN, K. & SPENCER, N. D. 2005. Porcine Gastric Mucin (PGM) at the Water/Poly(Dimethylsiloxane) (PDMS) Interface: Influence of pH and Ionic Strength on Its Conformation, Adsorption, and Aqueous Lubrication Properties. *Langmuir,* 21**,** 8344-8353.

LEVY, G. *Particle Detector and Tracker - User Manual* [Online]. Mosaic Group Web page. Available: http://mosaic.mpi-cbg.de/ParticleTracker/doc/ParticleTrackerUserManual.pdf [Accessed 07.05 2014].

LIELEG, O. & RIBBECK, K. 2011. Biological hydrogels as selective diffusion barriers. *Trends in Cell Biology,* 21**,** 543-551.

LIELEG, O., VLADESCU, I. & RIBBECK, K. 2010. Characterization of Particle Translocation through Mucin Hydrogels. *Biophysical Journal,* 98**,** 1782-1789.

MADSEN, F., EBERTH, K. & SMART, J. D. 1998a. A rheological assessment of the nature of interactions between mucoadhesive polymers and a homogenised mucus gel. *Biomaterials,* 19**,** 1083-1092.

MADSEN, F., EBERTH, K. & SMART, J. D. 1998b. A rheological examination of the mucoadhesive/mucus interaction: the effect of mucoadhesive type and concentration. *Journal of Controlled Release,* 50**,** 167-178.

MORTAZAVI, S. A., CARPENTER, B. G. & SMART, J. D. 1993. A comparative study on the role played by mucus glycoproteins in the rheological behaviour of the mucoadhesive/mucosal interface. *International Journal of Pharmaceutics,* 94**,** 195-201.

NORDGÅRD, C. T. 2014.

OTTERLEI, M., ØSTGAARD, K., SKJÅK-BRÆK, G., SMIDSRØD, O., SOON-SHIONG, P. & ESPEVIK, T. 1991. Induction of cytokine production from human monocytes stimulated with alginate. *Journal of Immunotherapy,* 10**,** 286-291.

PATEL, M. M., SMART, J. D., NEVELL, T. G., EWEN, R. J., EATON, P. J. & TSIBOUKLIS, J. 2003. Mucin/Poly(acrylic acid) Interactions: A Spectroscopic Investigation of Mucoadhesion. *Biomacromolecules,* 4**,** 1184-1190.

PATTON, J. S. & BYRON, P. R. 2007. Inhaling medicines: delivering drugs to the body through the lungs. *Nat Rev Drug Discov,* 6**,** 67-74.

PAWAR, S. N. & EDGAR, K. J. 2012. Alginate derivatization: A review of chemistry, properties and applications. *Biomaterials,* 33**,** 3279-3305.

PEREZ-VILAR, J. 2007. Mucin Granule Intraluminal Organization. *American Journal of Respiratory Cell and Molecular Biology,* 36**,** 183-190.

POOLE, C. F. 2003. *The essence of chromatography*, Elsevier.

RAVIV, U., GIASSON, S., KAMPF, N., GOHY, J. F., JEROME, R. & KLEIN, J. 2003. Lubrication by charged polymers. *Nature,* 425**,** 163-5.

ROSS-MURPHY, S. B. & MCEVOY, H. 1986. Fundamentals of Hydrogels and Gelation. *British Polymer Journal,* 18**,** 2-7.

SANDERS, N., RUDOLPH, C., BRAECKMANS, K., DE SMEDT, S. C. & DEMEESTER, J. 2009. Extracellular barriers in respiratory gene therapy. *Adv Drug Deliv Rev,* 61**,** 115-27.

SANDERS, N. N., DE SMEDT, S. C., VAN ROMPAEY, E., SIMOENS, P., DE BAETS, F. & DEMEESTER, J. 2000. Cystic Fibrosis Sputum. *American Journal of Respiratory and Critical Care Medicine,* 162**,** 1905-1911.

SAVAGE, D. C. 2005. Chapter 2 - Mucosal Microbiota. *In:* JIRI, M., MICHAEL, E. L., JERRY, R. M., JOHN, B., LLOYD, M., WARREN STROBERA2 - JIRI MESTECKY, M. E. L. J. R. M. J. B. L. M. & WARREN, S. (eds.) *Mucosal Immunology (Third Edition).* Burlington: Academic Press.

SAXTON, M. J. & JACOBSON, K. 1997. Single-particle tracking: applications to membrane dynamics. *Annu Rev Biophys Biomol Struct,* 26**,** 373-99.

SBALZARINI, I. F. & KOUMOUTSAKOS, P. 2005. Feature point tracking and trajectory analysis for video imaging in cell biology. *Journal of Structural Biology,* 151**,** 182-195.

SCANNELL, J. W., BLANCKLEY, A., BOLDON, H. & WARRINGTON, B. 2012. Diagnosing the decline in pharmaceutical R&D efficiency. *Nat Rev Drug Discov,* 11**,** 191-200.

SELLERS, L. A., ALLEN, A., MORRIS, E. R. & ROSS-MURPHY, S. B. 1988. Mucus glycoprotein gels. Role of glycoprotein polymeric structure and carbohydrate side-chains in gel-formation. *Carbohydrate Research,* 178**,** 93-110.

SELVAGGI, L., SALEMME, M., VACCARO, C., PESCE, G., RUSCIANO, G., SASSO, A., CAMPANELLA, C. & CAROTENUTO, R. 2010. Multiple-Particle-Tracking to investigate viscoelastic properties in living cells. *Methods,* 51**,** 20-26.

SHEEHAN, J. K., KIRKHAM, S., HOWARD, M., WOODMAN, P., KUTAY, S., BRAZEAU, C., BUCKLEY, J. & THORNTON, D. J. 2004. Identification of Molecular Intermediates in the Assembly Pathway of the MUC5AC Mucin. *Journal of Biological Chemistry,* 279**,** 15698-15705.

SHOGREN, R., GERKEN, T. A. & JENTOFT, N. 1989. Role of glycosylation on the conformation and chain dimensions of O-linked glycoproteins: light-scattering studies of ovine submaxillary mucin. *Biochemistry,* 28**,** 5525-36.

SKJÁK-BRÆK, G., SMIDSRØD, O. & LARSEN, B. 1986. Tailoring of alginates by enzymatic modification in vitro. *International Journal of Biological Macromolecules,* 8**,** 330-336.

SMIDSRØD, O., MOE, S. T. & MOE, S. 2008. *Biopolymer chemistry*, Tapir Academic Press.

STANFORD, E. C. C. 1886. Barton. Google Patents.

STARKEY, B. J., SNARY, D. & ALLEN, A. 1974. Characterization of gastric mucoproteins isolated by equilibrium density-gradient centrifugation in caesium chloride. *Biochem J,* 141**,** 633-9.

STROUS, G. J. & DEKKER, J. 1992. Mucin-type glycoproteins. *Critical reviews in biochemistry and molecular biology,* 27**,** 57-92.

SUH, J., DAWSON, M. & HANES, J. 2005. Real-time multiple-particle tracking: applications to drug and gene delivery. *Advanced Drug Delivery Reviews,* 57**,** 63-78.

TAYLOR, C., DRAGET, K. I., PEARSON, J. P. & SMIDSRØD, O. 2005a. Mucous Systems Show a Novel Mechanical Response to Applied Deformation. *Biomacromolecules,* 6**,** 1524-1530.

TAYLOR, C., DRAGET, K. I. & SMIDSROD, O. A. 2007. Use of oligouronates for treating mucus hyperviscosity. Google Patents.

TAYLOR, C., PEARSON, J. P., DRAGET, K. I., DETTMAR, P. W. & SMIDSROD, O. 2005b. Rheological characterization of mixed gels of mucin and alginate. *Carbohydr. Polym.,* 59**,** 189-195.

TAYLOR NORDGÅRD, C. & DRAGET, K. I. 2011. Oligosaccharides As Modulators of Rheology in Complex Mucous Systems. *Biomacromolecules,* 12**,** 3084-3090.

THORNTON, D. J. & SHEEHAN, J. K. 2004. From Mucins to Mucus. *Proceedings of the American Thoracic Society,* 1**,** 54-61.

TIMELL, T. E. 1964. The Acid Hydrolysis of Glycosides: I. General Conditions and the Effect of the Nature of the Aglycone. *Canadian Journal of Chemistry,* 42**,** 1456-1472.

TURNER, B. S., BHASKAR, K. R., HADZOPOULOU-CLADARAS, M. & LAMONT, J. T. 1999. Cysteine-rich regions of pig gastric mucin contain von Willebrand factor and cystine knot domains at the carboxyl terminal. *Biochimica et Biophysica Acta (BBA) - Gene Structure and Expression,* 1447**,** 77-92.

VADER, D. & WYSS, H. Introducion to Rheology. *strain,* 5**,** 0.

VAN KLINKEN, B., DEKKER, J., BULLER, H. & EINERHAND, A. 1995. Mucin gene structure and expression: protection vs. adhesion. *American Journal of Physiology-Gastrointestinal and Liver Physiology,* 269**,** G613-G627.

VÅSET, F. S. 2014. *Biosimilar Mucus as a Model System for Small Intestinal Mucus - Evaluating the Applicability for Nanoparticle Drug Delivery Studies.* Master, NTNU.

WATKINS, J. B., KLAASSEN, C. D. & ACOSTA, D. 2010. *Casarett & Doull's essentials of toxicology*, McGraw-Hill.

WEITZ, D., WYSS, H. & LARSEN, R. 2007. Oscillatory rheology: Measuring the viscoelastic behaviour of soft materials. *GIT laboratory journal Europe,* 11**,** 68-70.

WOODLEY, J. 2001. Bioadhesion: new possibilities for drug administration? *Clin Pharmacokinet,* 40**,** 77-84.

YANG, X., FORIER, K., STEUKERS, L., VAN VLIERBERGHE, S., DUBRUEL, P., BRAECKMANS, K., GLORIEUX, S. & NAUWYNCK, H. J. 2012. Immobilization of pseudorabies virus in porcine tracheal respiratory mucus revealed by single particle tracking. *PLoS One,* 7**,** e51054.

YORK, P. 2013. Design of dosage forms. *Aulton's Pharmaceutics: The Design and Manufacture of Medicines***,** 7.

Appendix A: Bio-similar mucus protocol

The bio-similar mucus consist of a lipid part and a polymer part. This protocol makes 10 mL bio-similar mucus.

Preparation:

1. Make 10 mM isotonic HEPES buffer containing 1.3 mM $CaCl_2$, 1 mM $MgSO_4$ and 137 mM NaCl. HEPES.
2. Make 10 mM non-isotonic HEPES buffer containing 1.3 mM $CaCl_2$ and 1 mM $MgSO_4$.

Lipid solution:

3. Mix 0.0121 g linoleic acid with 0.0396 g cholesterol and 0.033 g phosphatidylcholine in an Eppendorf tube.
4. Add 0.03586 g polysorbate tween 80 and two small magnets.
5. Add 750 µL isotonic 10 mM HEPES buffer and leave the mixture on vigorous magnetic stirring while preparing the polymer solution. The lipid solution must be homogenous before being added to the polymer solution.

Polymer solution:

6. Mix 0.09 g polyacrylic acid with non-isotonic 10 mM HEPES buffer, and leave on vigorous magnetic stirring until dissolved.
7. Add 0.5 g Sigma mucin type II and mix until dissolved.
8. Add 150 µL 5 mM NaOH and make sure the solution is homogenous before proceeding.

Completion:

9. Add 0.682 mL of the lipid solution into the polymer solution. Stir.
10. Add 0.31 g bovine albumin and stir until dissolved.
11. Adjust pH to 7.4 with NaOH.
12. Store the solution cold overnight at ~3 °C before further utilization.

Appendix B: Porcine gastric mucin purification protocol

Porcine gastric mucus gels were removed from the mucosa and immediately transferred into an ice cold cocktail of protease inhibitors (Table B.1) in phosphate buffer (mucus to buffer ratio 1:4 v/v), pH 6.5, to prevent degradation by endogenous proteases. Mucus gel was solubilised in the inhibitor cocktail by high speed homogenisation in a Waring Blender for 1 minute. Soluble material was separated from insoluble cell debris by centrifugation (8000*g*, 1 hour, 4°C). The resulting supernatant was further purified to remove protein and nucleic acid by equilibrium density gradient ultracentrifugation in caesium chloride (CsCl) (Starkey et al., 1974). CsCl was added to give a starting density of 1.42 g/ml, and the solution centrifuged at 100,000*g* for 48 h at 4°C, using a fixed angle rotor.

The contents of each tube were removed as nine equal fractions with care being taken not to disturb the density gradient. The density of each fraction was measured, followed by exhaustive dialysis against distilled water at 4°C. Dialysed fractions were assayed for glycoprotein, protein and nucleic acid. Fractions rich in protein and nucleic acid were discarded, and those rich in glycoprotein were pooled, freeze dried and stored at –20°C.

Table B-1. Concentration and action of protease inhibitors within the proteolytic inhibitor cocktail.

Protease inhibitor	Concentration (mM)	Mode of action
Phenylmethylsulphonyl fluoride	3	Inhibitor of serine proteases, e.g., elastase hydrolyses peptide bond at C-terminal side, and cathepsin and trypsin removes N-terminal dipeptides.
Sodium iodoacetate	1	Inhibitor of thiol-dependent proteases, e.g., cathepsin B and other disulphide dependent enzymes.
Benzamidine Hydrochloride	15	Specific inhibitor of trypsin and trypsin-like serine proteases (hydrolysis of proteins, peptides and amino acids).
Na_2 EDTA	10	Inhibitor of metallo-dependent proteases, e.g., Ca^{2+} dependent enzymes.
N-ethylmaleimide	10	Prevents disulphide group exchange.
ε-amino caproic acid	100	Inhibitor of plasminogen activation to serine protease plasmin (hydrolyses peptide and ester bonds).

Appendix C: SEC-MALLS of alginate LFR 5/60

Below is given the SEC-MALLS chromatogram for alginate LFR 5/60 in Figure C-1 and Fable C-1 shows the analysis of the data using exponential fit.

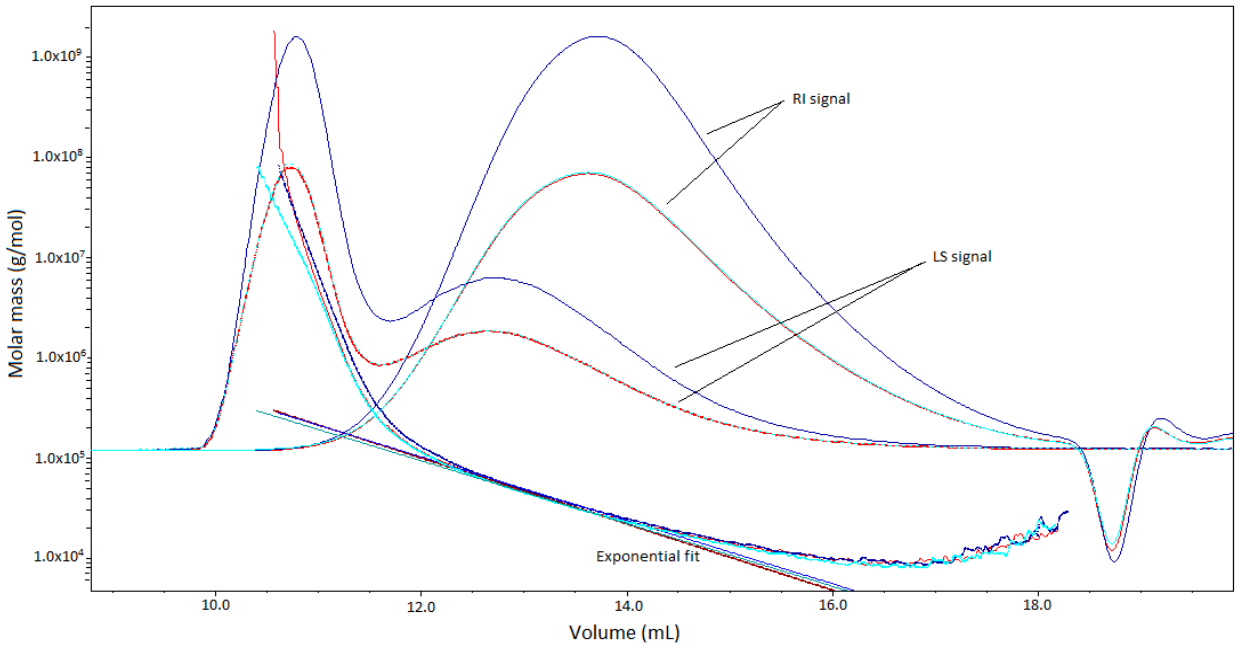

Figure C-1. SEC-MALLS spectra of an alginate LFR 5/60 sample showing both the refractive index (RI) signal which shows the eluted mass of the sample, and the light scattering (LS) signal which shows the molecular sizes. Molar mass (g/mol) is plotted against volume (mL). There were three injections (blue, red and teal colour), with two different volumes.

Table C-1. Data analysis of SEC-MALLS experiment on alginate LFR 5/60 using exponential fit to data. M_n = number-average molecular weight. M_w = weigh-average molecular weight.

Sample	M_n (kDa)		M_w (kDa)		Polydispersity	Injected mass (µg)	Mass recovery (%)
# 1 (red)	11.700 ± 0.008	±	32.800 ± 0.003	±	2.794 ± 0.008	500.000	69.400
# 2 (blue)	12.700 ± 0.006	±	32.900 ± 0.002	±	2.581 ± 0.007	750.000	69.500
# 3 (teal)	12.700 ± 0.006	±	32.000 ± 0.002	±	2.530 ± 0.006	500.000	70.000
Average	12.400		32.600		2.635	583.333	69.600
Standard deviation	0.800		0.700		0.155	144.340	0.300
Standard deviation (%)	6.300		2.100		5.893	24.740	0.500
Minimum	11.700		32.000		2.530	500.000	69.400
Maximum	12.700		32.900		2.794	750.000	70.000

Appendix D: NMR of alginate G-blocks

The ^{1}H NMR spectra from a BRUKER Avance DPX 300 equipped with a 5 mm QNP probe for alginate G-block DP_n 12, G-block DP_n 24 and G-block DP_n 33 are given Figure D-1, D-2 and D-3 respectively.

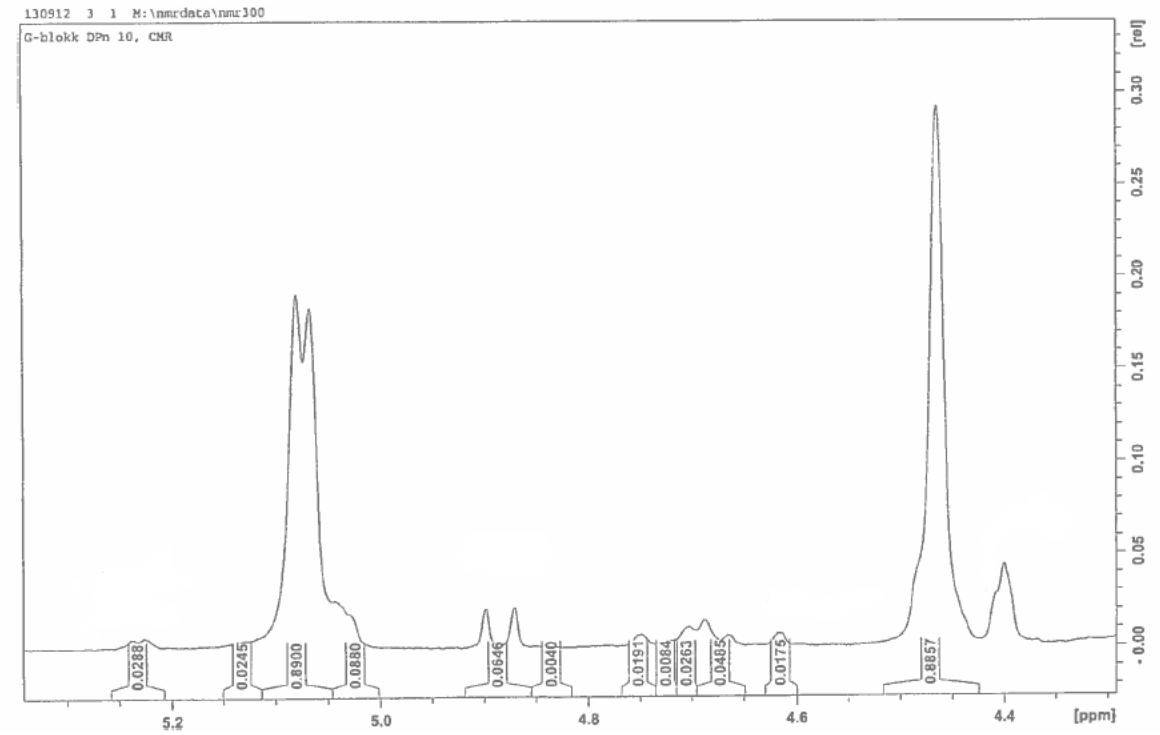

Figure D-1. ^{1}H NMR spectrum of alginate G-block DP_n 12 using a 300 MHz NMR instrument.

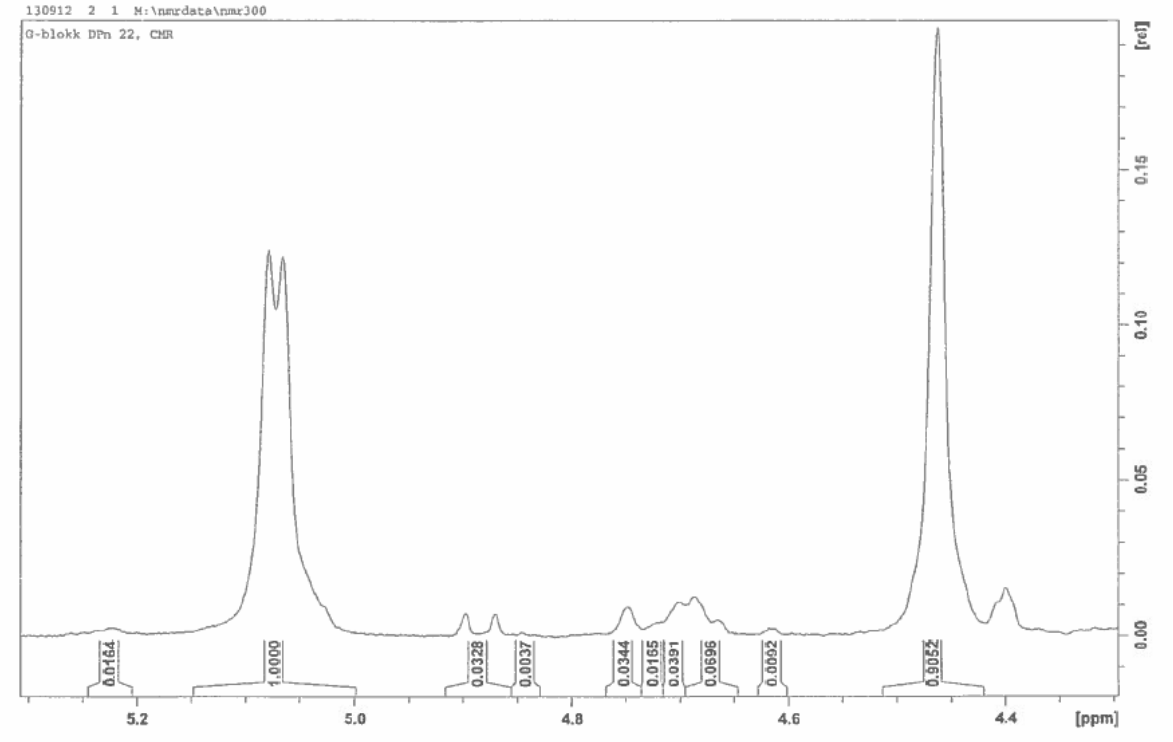

Figure D-2. ^{1}H NMR spectrum of alginate G-block DP_n 24 using a 300 MHz NMR instrument.

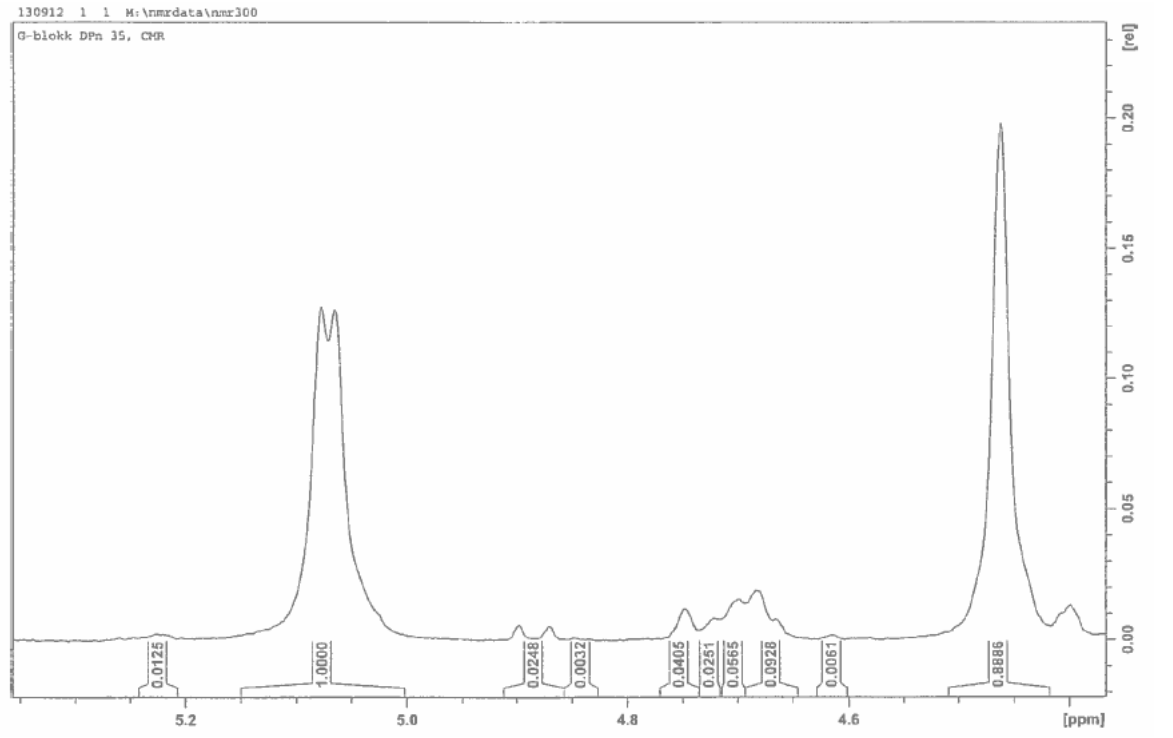

Figure D-3. ^{1}H NMR spectrum of alginate G-block DP_n 33 using a 300 MHz NMR instrument.

All calculations are based on sequential parameter A-C and the different reducing ends, all shown in figure D-4 in the spectrum for the alginate G-block DP_n 12 sample. The method is explained by Grasdalen (Grasdalen, 1983) for G-heavy alginates, who described signal assignments used for determining the sequential parameters shown in the figure.

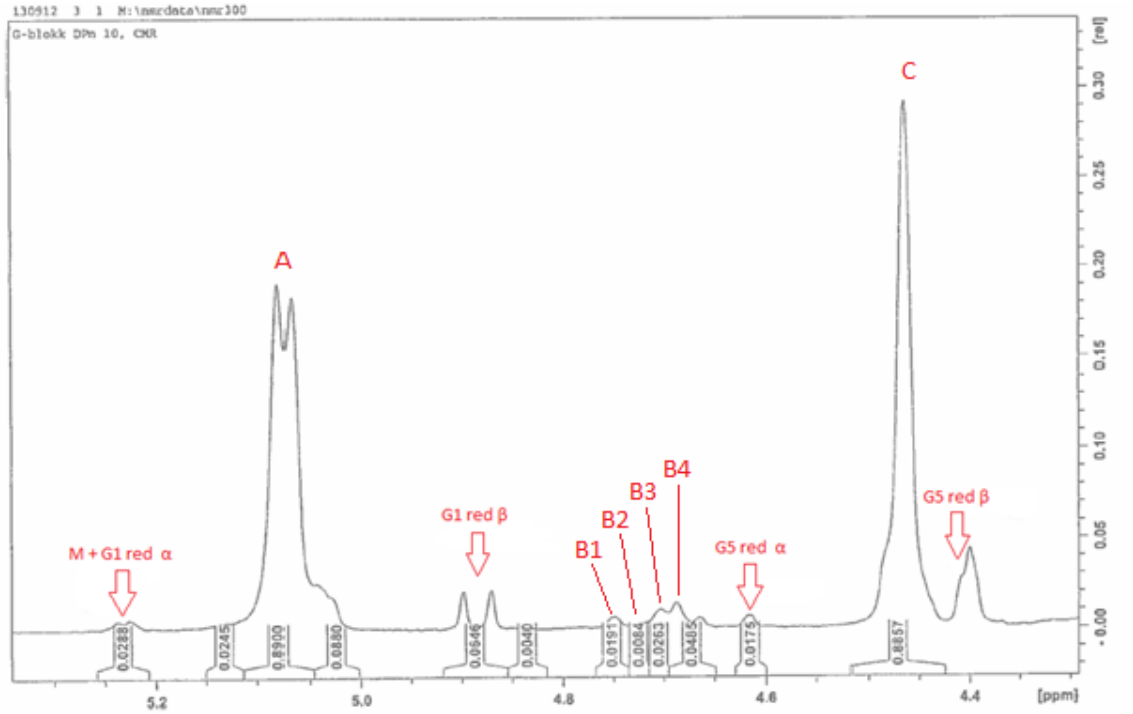

Figure D-4. ^1H NMR spectrum of alginate G-block DP_n 12 on a 300 MHz NMR instrument showing the NMR signals used as basis for the sequential parameters A-C. It also shows the location of the reducing ends of the polysaccharide and their orientation.

A method called "maximum averaging" (Kristiansen) was used to determine the fraction of M and G in the alginate samples. This method uses intermediate values based on the sequential parameters A-C (Figure D-4) that can be calculated according to equation D.1-D.8.

$$I(G) = 0.5 * \big((A + C) + 0.5 * (B1 + B2 + B3)\big) \quad \text{(D.1)}$$

$$I(M) = 0.5 * (B1 + B2 + B3) + B4 \quad \text{(D.2)}$$

$$I(GG) = 0.5 * \big((A + C) - 0.5 * (B1 + B2 + B3)\big) \quad \text{(D.3)}$$

$$I(GM) = 0.5 * (B1 + B2 + B3) \quad \text{(D.4)}$$

$$I(MM) = B4 \quad \text{(D.5)}$$

$$I(GGM) = 0.5 * (B1 + B2 + B3) * \frac{B1}{B1+B2} \quad \text{(D.6)}$$

$$I(MGM) = 0.5 * (B1 + B2 + B3) * \frac{B2}{B1+B2} \quad \text{(D.7)}$$

$$I(GGG) = GG - GGM \quad \text{(D.8)}$$

Because the alginate oligosaccharides are short chains, it is necessary to consider the reducing ends when doing the calculations because the reducing end signals compared to the others signals are higher than they would have been for larger alginate molecules. There are several ways to use the reducing ends, all involving both an alpha oriented and a beta oriented reducing end. The G5 β reducing end is hidden beneath another signal (Figure D-4) and is therefore not used in the calculations. This should theoretically leave two possible ways of doing calculations with the reducing ends –G1 red β + G5 red α and G1 red β + G1 red α. However, the signal for G1 red β has a neighbouring signal (Figure D-4) that is difficult to assess whether or not it is a part of the reducing end signal. Therefore a third possibility for using the reducing ends in the calculations arises, which is using G1 red β↑ + G1 red α. The intermediate values originating from equations D.1-D.8 can be used to calculate fractions of G and M according to equation D.9-D.17. The equation for calculating $\overline{N}_{G>1}$ and DP_n is given in equation D.18 and D.19 respectively. $F(G)_{total}$ is the sum of $F(G)_{internal}$ and $F(G)_{red.ends}$.

$$F(G)_{internal} = \frac{I(G)}{I(M)+I(G)+red.ends} \quad (D.9)$$

$$F(G)_{red.ends} = \frac{red.ends}{I(M)+I(G)+red.ends} \quad (D.10)$$

$$F(M) = \frac{red.ends}{I(M)+I(G)+red.ends} \quad (D.11)$$

$$F(GG)_{internal} = \frac{I(GG)}{I(M)+I(G)+red.ends} \quad (D.12)$$

$$F(GM) = F(MG) = \frac{I(GM)}{I(M)+I(G)+red.ends} \quad (D.13)$$

$$F(MM)_{internal} = \frac{I(MM)}{I(M)+I(G)+red.ends} \quad (D.14)$$

$$F(GGG)_{internal} = \frac{I(GGG)}{I(M)+I(G)+red.ends} \quad (D.15)$$

$$F(GGM) = F(MGG) = \frac{I(GGM)}{I(M)+I(G)+red.ends} \quad (D.16)$$

$$F(MGM) = \frac{I(MGM)}{I(M)+I(G)+red.ends} \quad (D.17)$$

$$\overline{N}_{G>1} = \frac{F(G)-F(MGM)}{F(GGM)} \quad (D.18)$$

$$\overline{DP_n} = \frac{F(G)_{total}+F(M)}{red.ends} \quad (D.19)$$

Appendix E: HPAEC-PAD for alginate G-blocks

The HPAEC-PAD spectra for alginate G-block DP_n 12, 24 and 33 is given in Figure E-1, E-2 and E-3 respectively.

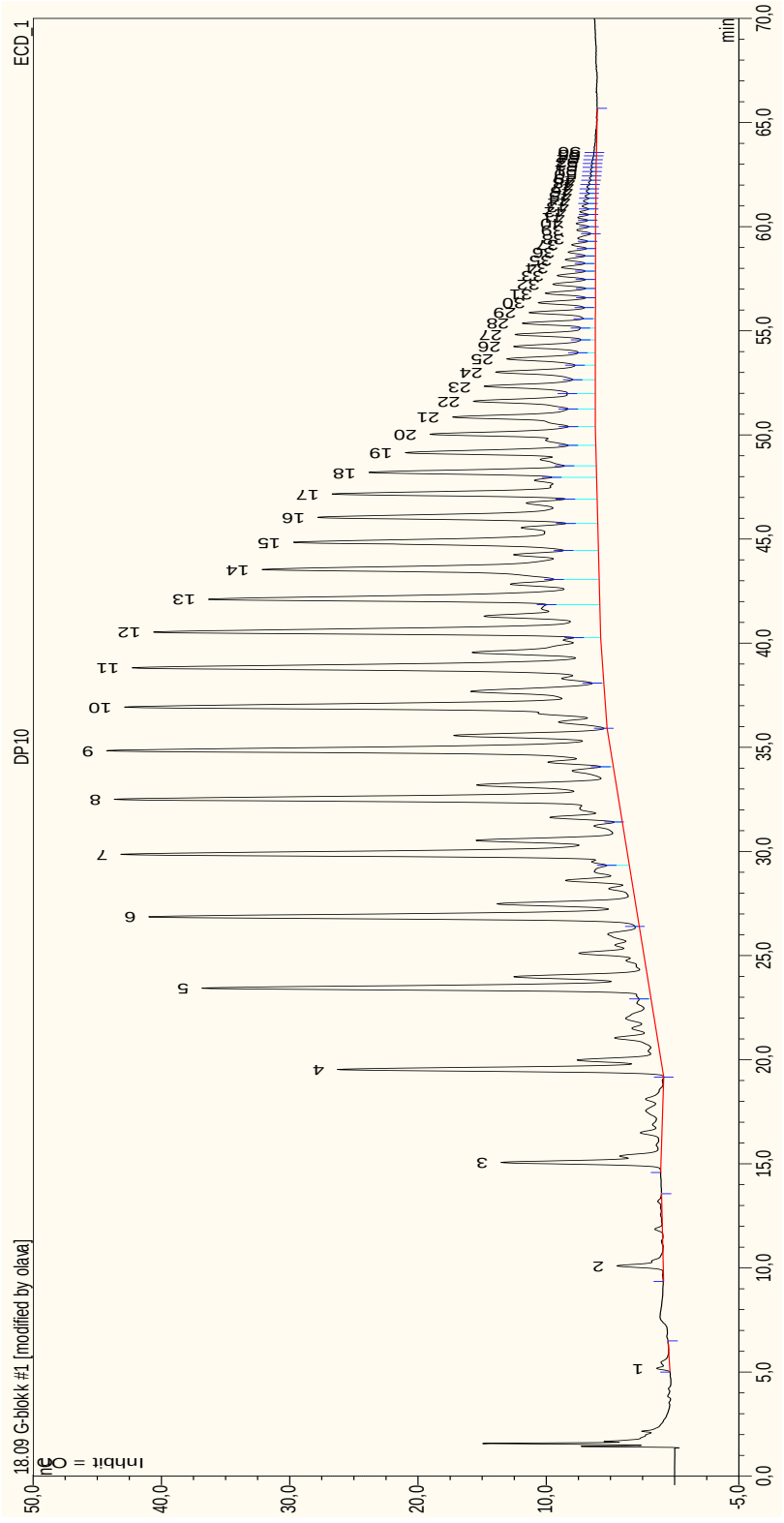

Figure E-1. HPAEC-PAD spectrum of alginate G-block DP_n 12.

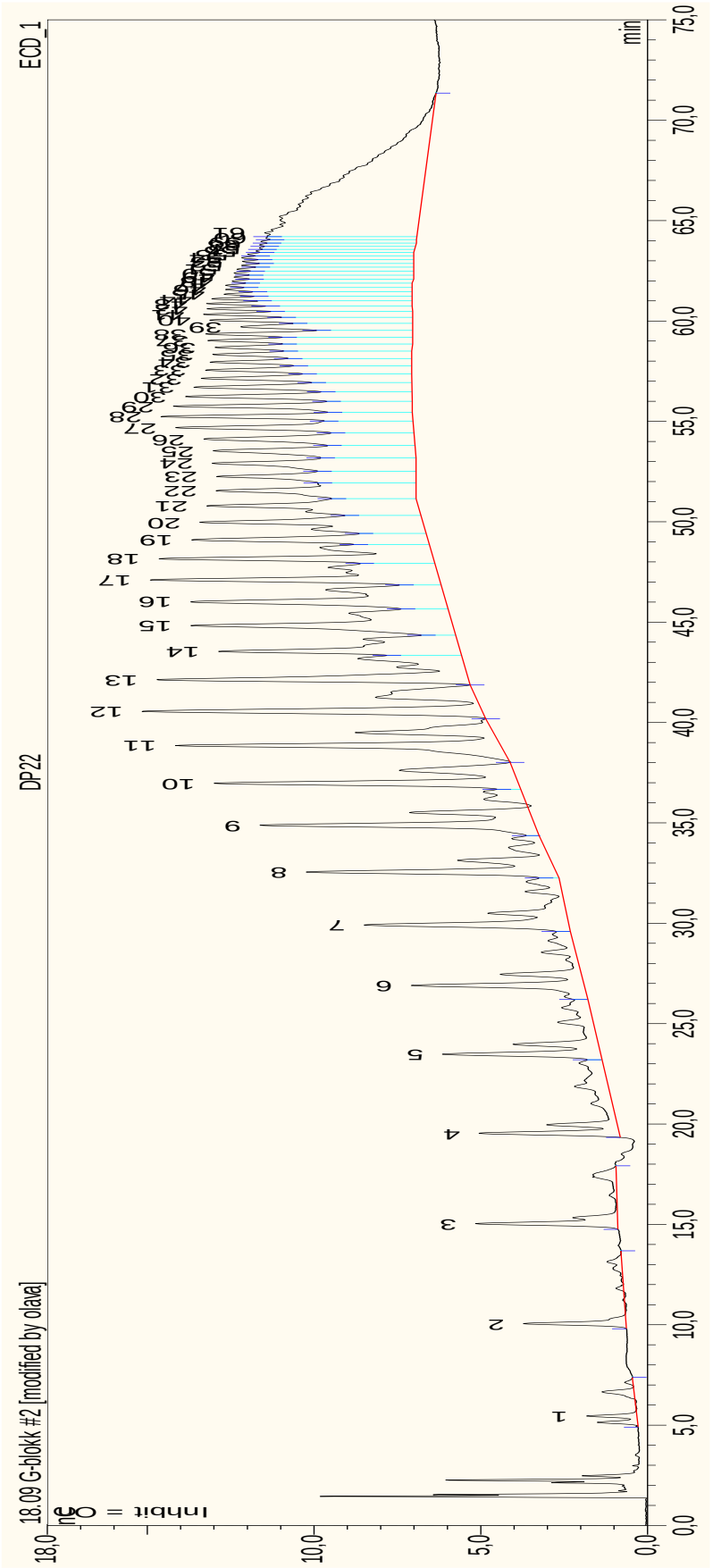

Figure E-2. HPAEC-PAD spectrum of alginate G-block DP_n 24.

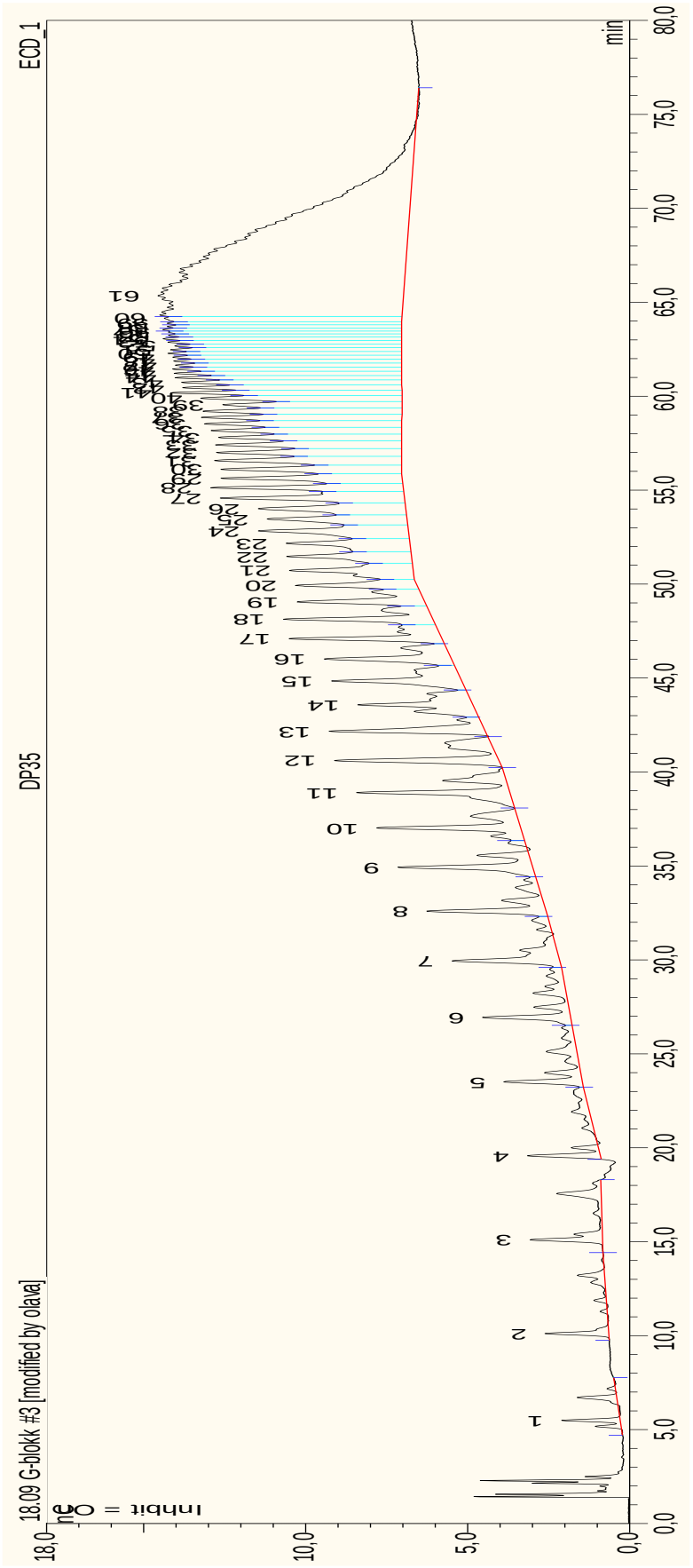

Figure E-3. HPAEC-PAD spectrum of alginate G-block DP_n 33.

In order to quantify of each sample, a molar response factor is required. This factor can be calculated according to equation E.1:

$$Rf_x = (\frac{A_x}{m_x}) \quad \text{(E.1)}$$

where Rf_x is the response factor, A_x is the area of the chromatographic peak and m_x is the concentration of the oligomer. Plotting the molar response factor against DP gives a curve that can be used to calculate molar concentration (C_x), number average (X_n), weight average (W_n) and molecular distribution (DP_n) within the sample through linear regression. For this experiment, the linear regression of the molar response factor is given in equation E.2.

$$Rf = 1.0037 * \ln(DP) + 0.1682 \quad \text{(E2)}$$

Equation E.2 was used to calculate DP_n for all three alginate samples, but example of calculation is only given for the alginate G-block DP_n 12 sample in Table E-1.

Table E-1. Calculated values of molar concentration (C_x), number average (X_n), weight average (W_n) and molecular distribution (DP_n) for alginate DP_n 12 based on the chromatogram in figure F-1. The equations used to calculate the values are given in the bottom of the table.

DP	Peak#	m_x	C_x	W_n	X_n	DP_n
2	1	0.415	146.113	0.001	0.004	0.008
3	2	0.906	478.509	0.002	0.009	0.027
4	3	3.525	2482.661	0.012	0.035	0.142
5	4	6.255	5507.245	0.026	0.063	0.314
6	5	7.972	8423.190	0.040	0.080	0.481
7	6	7.896	9733.420	0.046	0.079	0.556
8	7	7.375	10389.901	0.049	0.074	0.593
9	8	7.917	12547.166	0.059	0.080	0.716
10	9	7.012	12348.996	0.059	0.071	0.705
11	10	6.864	13295.820	0.063	0.069	0.759
12	11	6.582	13909.746	0.066	0.066	0.794
13	12	5.533	12667.427	0.060	0.056	0.723
14	13	4.376	10789.739	0.051	0.044	0.616
15	14	4.224	11158.790	0.053	0.042	0.637
16	15	3.612	10177.474	0.048	0.036	0.581
17	16	2.995	8965.705	0.042	0.030	0.512
18	17	2.468	7822.913	0.037	0.025	0.447
19	18	1.584	5299.609	0.025	0.016	0.303

20	19	1.831	6447.390	0.031	0.018	0.368
21	20	1.508	5575.160	0.026	0.015	0.318
22	21	1.277	4948.588	0.023	0.013	0.283
23	22	1.020	4132.526	0.020	0.010	0.236
24	23	0.854	3609.040	0.017	0.009	0.206
25	24	0.769	3387.051	0.016	0.008	0.193
26	25	0.622	2849.814	0.014	0.006	0.163
27	26	0.550	2615.321	0.012	0.006	0.149
28	27	0.475	2342.623	0.011	0.005	0.134
29	28	0.380	1939.438	0.009	0.004	0.111
30	29	0.362	1913.807	0.009	0.004	0.109
31	30	0.304	1656.958	0.008	0.003	0.095
32	31	0.266	1500.141	0.007	0.003	0.086
33	32	0.226	1311.224	0.006	0.002	0.075
34	33	0.195	1170.315	0.006	0.002	0.067
35	34	0.165	1015.071	0.005	0.002	0.058
36	35	0.148	936.717	0.004	0.001	0.053
37	36	0.129	840.990	0.004	0.001	0.048
38	37	0.112	752.713	0.004	0.001	0.043
39	38	0.089	614.577	0.003	0.001	0.035
40	39	0.079	559.046	0.003	0.001	0.032
41	40	0.082	589.023	0.003	0.001	0.034
42	41	0.067	494.187	0.002	0.001	0.028
43	42	0.060	452.420	0.002	0.001	0.026
44	43	0.056	431.336	0.002	0.001	0.025
45	44	0.048	384.013	0.002	0.000	0.022
46	45	0.040	323.337	0.002	0.000	0.018
47	46	0.034	285.291	0.001	0.000	0.016
48	47	0.032	274.411	0.001	0.000	0.016
49	48	0.025	211.571	0.001	0.000	0.012
50	49	0.021	188.585	0.001	0.000	0.011
51	50	0.020	180.077	0.001	0.000	0.010
52	51	0.018	160.370	0.001	0.000	0.009
53	52	0.014	134.162	0.001	0.000	0.008
54	53	0.013	127.417	0.001	0.000	0.007
55	54	0.011	107.941	0.001	0.000	0.006
56	55	0.008	81.546	0.000	0.000	0.005
57	56	0.040	399.968	0.002	0.000	0.023
Total:		99.463	211088.587	1.000	1.000	**12.052**

Equation:	$m_x = A_x/Rf_x$	$C_x = m_x * M_0 * Peak\#$	$W_n = C_i/C_{total}$	$X_n = m_i/m_{total}$	$DP_n = DPi * X_i$

There are some differences between the results gathered from NMR and HPAEC-PAD. Regarding the shortest alginate G-block sample, the two methods are in full agreement. The medium length G-block sample also show good similarity. However, regarding the longest chained alginate G-block, the two methods do not agree. For this sample, the NMR result was chosen, because the HPAEC-PAD method suffer from poor resolution when the alginate chain lengths become too long. With chains over DP 30-35 (Ballance et al., 2005), base line separation is not good enough, as is seen in Figure E-3.

Appendix F: Confocal laser scanning microscope setup

The parameters used to track Fluospheres ® Carboxylate-modified microspheres (0.2 µm, yellow-green fluorescent (505/515), 2 % solids. Invitrogen, Oregon, USA. Lot#714135) with CLSM Leica SP5 from Leica microsystems (Mannheim, Germany) is given in table F-1.

Table F-1. Parameters used to track Fluospheres ® Carboxylate-modified microspheres (0.2 µm, yellow-green fluorescent (505/515), 2 % solids. Invitrogen, Oregon, USA. Lot#714135) with CLSM Leica SP5 from Leica microsystems (Mannheim, Germany). The particle concentration was 0.0025 % in porcine gastric (PG) mucin sample with concentration of 40 mg/mL.

Parameter	Value
Laser	Argon
Laser power	20 %
Detector	PMT3
Detector spectra	Emission 514 nm
	Excitation 520 – 550 nm
Detector power	5 %
Smart gain	750.2 V
Smart offset	- 1 %
Resolution	512 x 512 pixels
Scan speed	8000 Hz
Image size	65.08 x 65.08 µm
Pixel size	127.35 x 127.35 nm
Acquisition mode	xyt
Time interval	Minimize
Time duration	20.09 s (287 frames)
Objective	HCX PL APO CS 63 x 1.2 water
Zoom	3.78
Pinhole	111.44 (Airy 1)

Appendix G: ImageJ video microscopy analysis

The images captured with CLSM Leica SP5 were loaded into ImageJ as ".lif" files. The particle tracker 2D/3D option under the mosaic plugin was used to locate the fluorescent particles immersed in the mucus. The parameters used is given in Table G-1.

Table G-1. Parameters used to process ".lif" images captured with CLSM Leica SP5 in order to calculate MSD values.

Parameters	Value
Radius	3 pixels
Cut-off	0 pixels
Percentile	0.1 %
Link range	20 frames
Displacement	10 pixels

The radius equals to the approximate particle size in pixels (Levy). The particles were 200 nm in size, so a radius of 3 was used because the microscope resolution makes the particles seem a bit larger than they really are. The particles were measured to appear as approximately 300 nm in size through the microscope. There was an even distribution of particles in most of the samples and the cut-off was consequently set to 0 pixels. The cut-off value is more valuable if the samples were crowded with fluorescent nanoparticles. The percentile value determines the amount of particles based on the particle excited light intensity. The displacement value is the maximum number of pixels a particle can traverse between frames in order to be ascertained as the same particle, while the linking range is the number of subsequent frames a particle must be tracked in order to appear in the analysis screen.

After deciding the parameters, the trajectories for all tracked particles can be visualized and the x- and y- coordinates retrieved. The x- and y- coordinates for each particle is run through a Matlab program to achieve MSD values for each particle (Appendix H).

Appendix H: Matlab program for MSD determination

The Matlab code was created by Astrid Bjørkøy in 2011 in order to translate x- and y- coordinates from ImageJ processing on particles tracked with CLSM Leica SP5 into mean-square displacement (MSD) values. The resulting MSD trajectories were saved as a ".txt" file. The Matlab code is given below.

```
%function ParticleTracker
% Prompt for lag time between frames
% Promt for name of resultfile!
prompt = {'Enter time interval:','Enter name of result file:'};
dlg_title = 'Input for Trajectory Calculations';
num_lines = 1;
def = {'1','results.txt'};
answer = inputdlg(prompt,dlg_title,num_lines,def);
timeinterval = str2double(answer{1});
filnavn = answer{2};
% Open the file with the trajectory data
[File, Path] = uigetfile('*.txt','Open Trajectory file',...
          'M:\Mikroskopi\Catherine Taylor\','MultiSelect','Off')
s1 = char(strcat(Path,File));
fid = fopen(s1);
DELIMITER = ' ';
HEADERLINES = 1;
k = 1;
% Figure out what trajectories are in this file, put the names in
% Nr.Trajectory and the number of frames for particle k in Particles
while 1
    tline = fgetl(fid);
    if ~ischar(tline),   break,   end
    if ~isempty(tline)
        if tline(1) == '%'
            nr = 0;
            Nr(k).Trajectory = tline(4:end);
            k = k+1;
        else nr = nr+1;
        end
    else Particles(k-1) = nr;
    end
end
fclose(fid);
```

```
% Import the trajectory data and put data in newData1
newData1 = importdata(s1, DELIMITER, HEADERLINES);
% Create new variables in the base workspace from those fields.
vars = fieldnames(newData1);
for i = 1:length(vars)
    assignin('base', vars{i}, newData1.(vars{i}));
end
j = 1;
pend = 0;
% For each particle, calculate the msd's for each time step!
% The frame number and (x,y) for each particle are between pstart and pend
% in the data file newData1.
for particle = 1:length(Particles)
    Nr(particle).Trajectory
    pstart = pend + 1;
    pend = pstart + (Particles(particle)-1);
    % p is an array containing the frame numbers
    p = newData1.data(pstart:pend,1);
    x = newData1.data(pstart:pend,2);
    y = newData1.data(pstart:pend,3);
    % maxstep is the maximum lag time possible for the particle
    maxstep = p(end)-p(1);
    for step = 1:maxstep
        ave = [];  % vector of msd's
        i = p(1);  % number of startframe
        while i+step <= p(end)
            % ignore frames missing!
            if ~ismember(i,p) || ~ismember((i+step),p)
            else
                % find the correct position in p, x and y for i and i+step
                i1 = find(p==i);
                i2 = find(p==(i+step));
                new =((x(i1)-x(i2))^2 + (y(i1)-y(i2))^2);
                ave = [new ave];
            end
            i = i+1;
        end
        if ~isempty(ave)
            msd(particle, step) = mean(ave); %mean msd for this step/lag time
        end
    end
```

```
end
% Save the data to a file: lag time in first column, data for the
% particles in the other columns.
 datafile = strcat(Path, filnavn);
 fid = fopen(char(datafile),'a');
 fprintf(fid,'%s', 'Step');
 for i = 1:length(Particles)
     fprintf(fid,'\t %s',Nr(i).Trajectory);
 end
 fprintf(fid,'\n')
 % size(msd,2) is the maximum number of frames for the particles
 % in the data file newData1
 for i = 1:size(msd,2)
     fprintf(fid,'%6.4f \t', i*timeinterval);
     for j = 1:length(Particles)
         % if there's data missing for this lag time, skip info!
         % else save the result
         if msd(j,i) == 0 fprintf(fid,'\t');
         else fprintf(fid,'%6.4f \t',msd(j,i));
         end
     end
     fprintf(fid,'\n');
 end
 fclose(fid);
 clear all
%end
```

Appendix I: Bio-similar mucus treated with alginate G-block DP_n 12 replicates

Replicates of alginate G-block DP_n 12 treated bio-similar mucus is given in Figure I-1 and I-2.

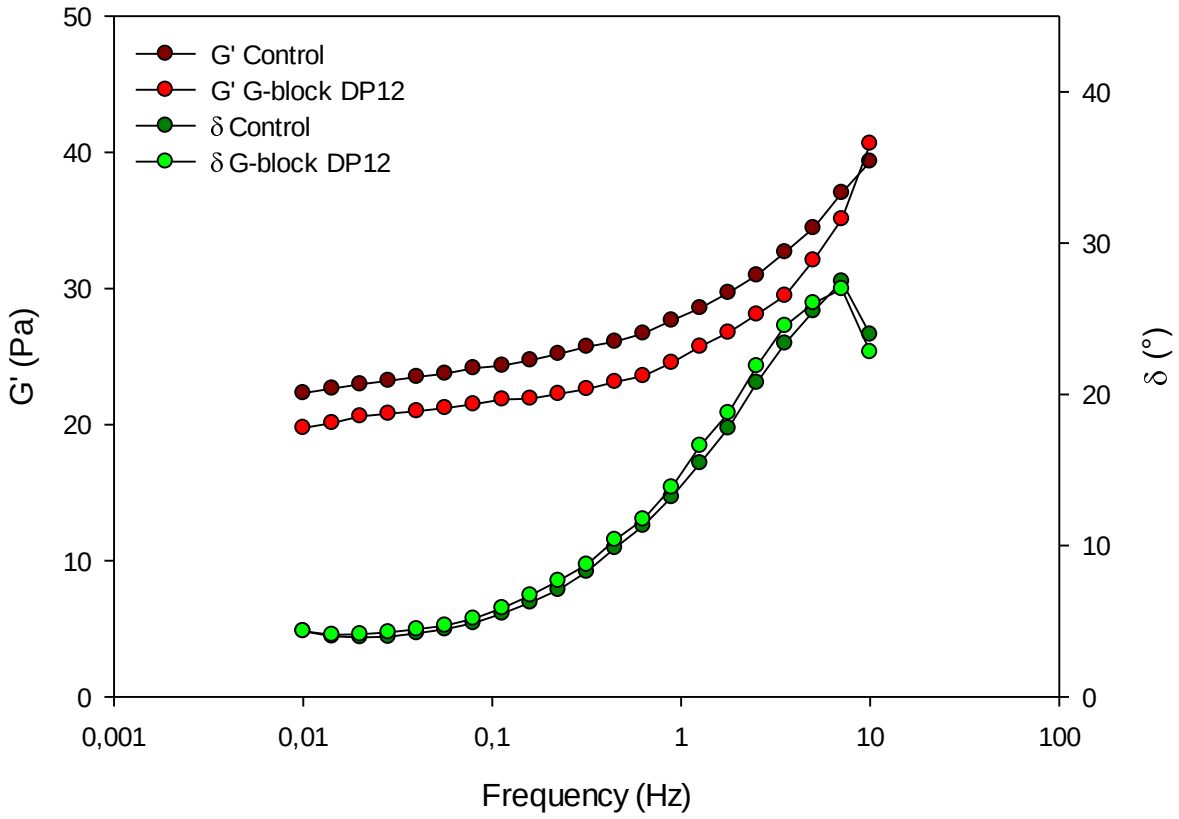

Figure I-1. Elastic modulus (G') and phase angle (δ) values for bio-similar mucus control (saline) and bio-similar mucus treated with alginate G-block DP_n 12 compared. Concentration of alginate was 4.7 mg/mL. Values are from frequency sweeps at 20 °C from low to high frequency with cone dimension C 40 4 ETC. The parameters of the frequency sweep of bio-similar mucus control was a constant strain of 1E-3 and 2E-2 Pa start stress, while the parameters of the treated bio-similar mucus was a constant strain of 9E-4 and 2E-2 Pa start stress.

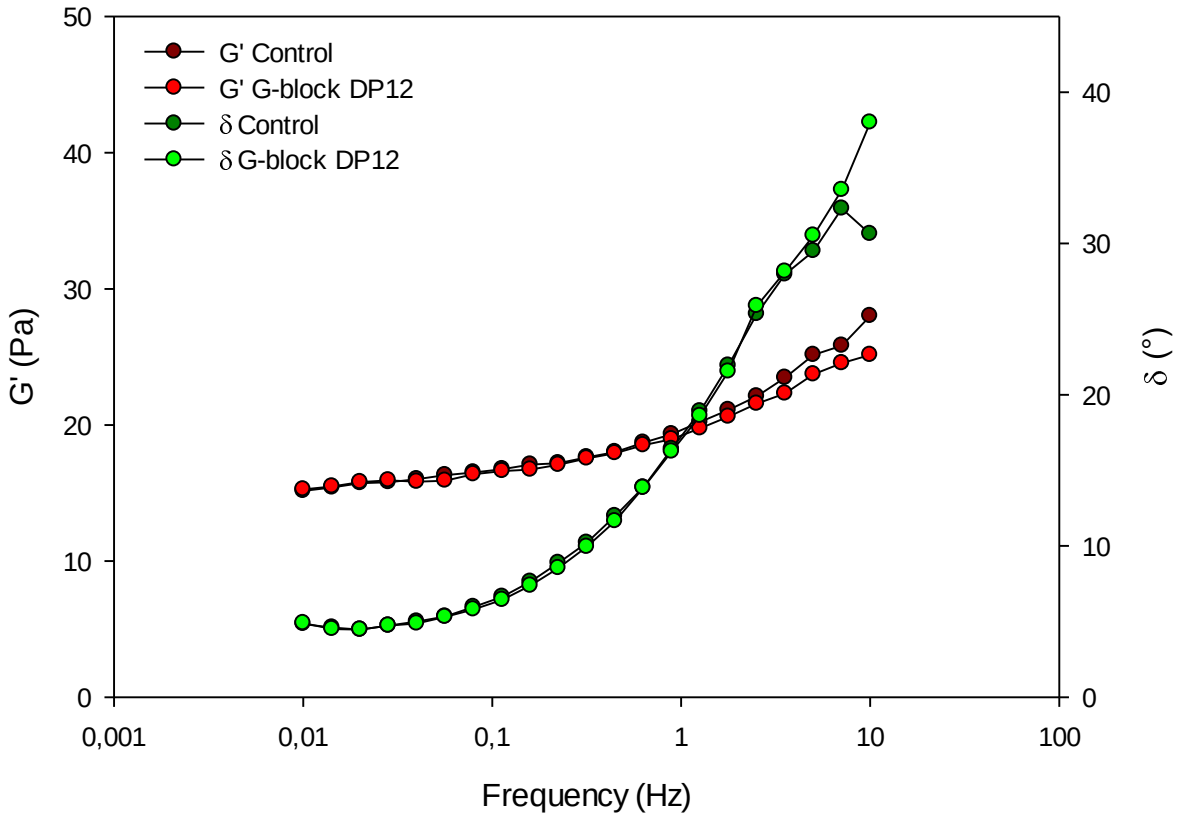

Figure I-2. Elastic modulus (G') and phase angle (δ) values for bio-similar mucus control (saline) and bio-similar mucus treated with alginate G-block DP_n 12 compared. Concentration of alginate was 4.7 mg/mL. Values are from frequency sweeps at 20 °C from low to high frequency with cone dimension C 40 4 ETC. The parameters of the frequency sweep of bio-similar mucus control was a constant strain of 1E-3 and 2E-2 Pa start stress, while the parameters of the treated bio-similar mucus was a constant strain of 6E-4 and 1E-2 Pa start stress.

Appendix J: Frequency sweeps of frozen PG mucin lot#2 samples at 5E-3 and 1E-2 strain

The frequency sweeps of frozen PG mucin lot#2 treated with alginate G-block DP_n 12, DP_n 24, DP_n 33, alginate LFR 5/60 and saline (control) at 5E-3 and 1E-2 strain is given in Figure J-1 and J-2 respectively.

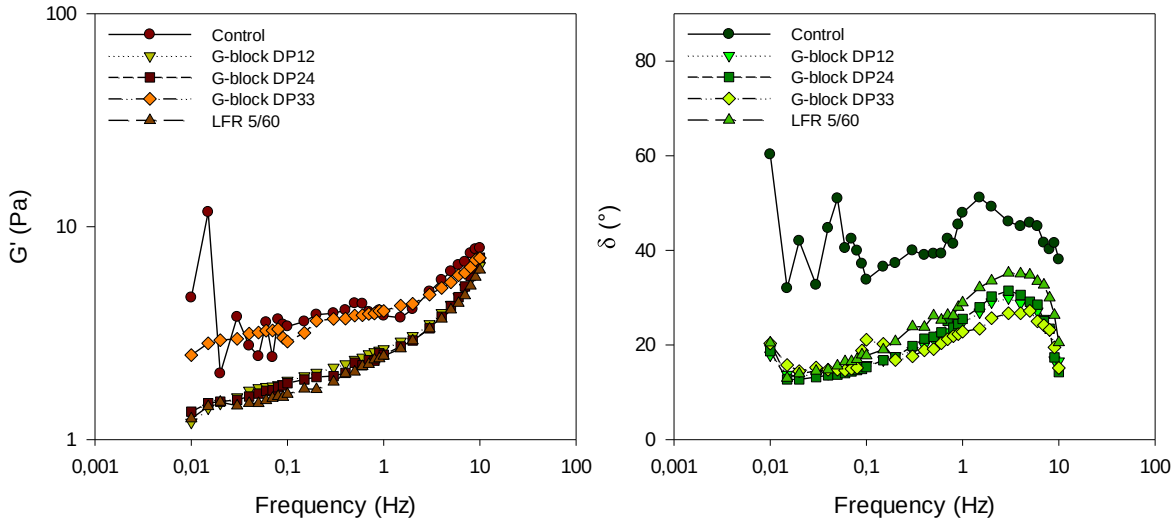

Figure J-1. Elastic modulus (G', left graph) and phase angle (δ, right graph) values for porcine gastric (PG) mucin control (saline) and PG mucin treated with alginate G-block DP_n 12, alginate G-block DP_n 24, alginate G-block DP_n 33 and alginate LFR 5/60 compared. All values are from frequency sweeps at 10 °C from low to high frequency with constant strain 5E-3 and 1E-2 Pa start stress. Cone dimension was C 40 1 ETC. Concentration of PG mucin in MQ-water was 40 mg/mL and concentration of alginate was 4.7 mg/mL.

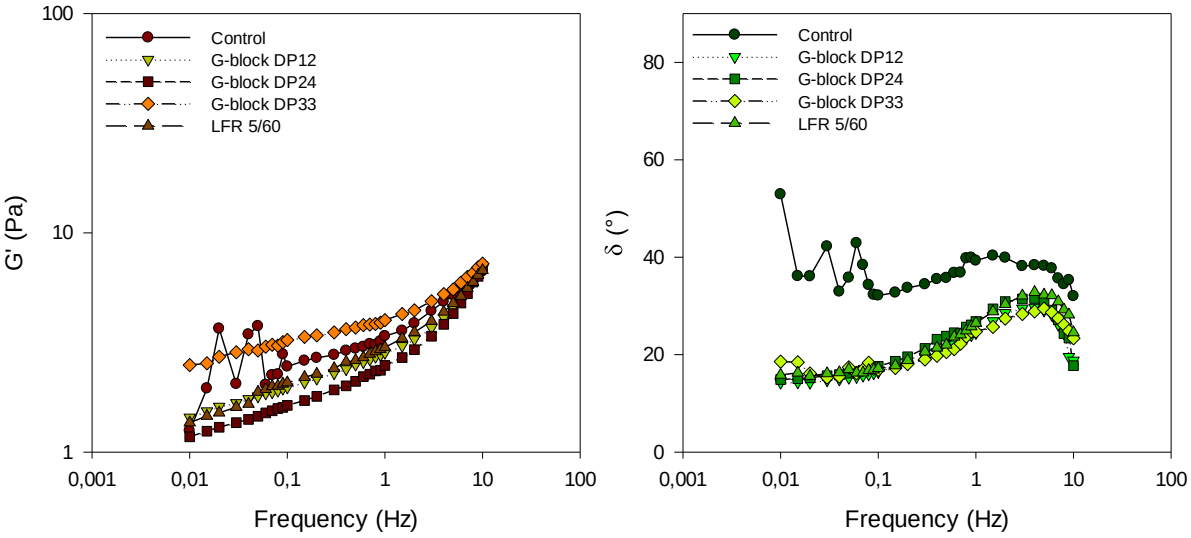

Figure J-2. Elastic modulus (G', left graph) and phase angle (δ, right graph) values for porcine gastric (PG) mucin control (saline) and PG mucin treated with alginate G-block DP_n 12, alginate G-block DP_n 24, alginate G-block DP_n 33 and alginate LFR 5/60 compared. All values are from frequency sweeps at 10 °C from low to high frequency with constant strain 1E-2 and 1E-2 Pa start stress. Cone dimension was C 40 1 ETC. Concentration of PG mucin in MQ-water was 40 mg/mL and concentration of alginate was 4.7 mg/mL.